Energy Finite Element Analysis Developments for High Frequency Vibration Analysis of Composite Structures

by

Xiaoyan Yan

A dissertation submitted in partial fulfillment
of the requirements for the degree of
Doctor of Philosophy
(Naval Architecture and Marine Engineering)
in The University of Michigan
2008

Doctoral Committee:

Professor Nickolas Vlahopoulos, Co-Chair
Assistant Research Scientist Aimin Wang, Co-Chair
Professor Michael M. Bernitsas
Professor Anthony M. Waas
Associate Research Scientist Matthew P. Castanier

To my parents
Baolin Yan and Ruijuan Cao
without whose sacrifices none of this would be possible.

ACKNOWLEDGMENTS

This dissertation is the result of three and half years of work whereby I have been accompanied, supported and encouraged by many people. It is a pleasant aspect that I have now the opportunity to express my gratitude to all of them.

First and foremost, I would like to express my deep and sincere gratitude to my advisor, Professor Nickolas Vlahopoulos, for his support, patience and encourgment throughout my research and study at the University of Michigan. His expertise and technical knowledge is essential to the completion of this dissertation and has taught me innumerable lessons and insights in research.

I would like to sincerely thank Dr. Aimin Wang for giving me consistent guidance and advices to my research and for being the co-chair of my committee. He always finds time to oversee my research and to share his knowledge and expertise with me despite of his busy schedule. This work wouldn’t have been possible without the encourgment and support from him.

I would like to thank Professor Anthony M. Waas for being a member of my committee and for monitoring my work and providing me with valuable comments on my research. I leared a lot of knowledge on composite materials from him.

I appreciate the advice of my other dissertation committee members, Professor Michael M. Bernitsas and Dr. Matthew Castanier. Thank them for giving valuable comments on my dissertation.

I would like to acknowledge a numer of my friends and colleagues, without whom this experience would have been incomplete. First, special thanks to my friends at the University of Michigan, who have made my life and study here an unforgettable

experience. Some of them are: James Bretl, Jim Chang, Jinting Guo, Sina Hassanaliaragh, Elisha Garcia, Zheyu Hong, Jonghun Lee, Yaning Li, Zhen Li, Sai Mohan Majhi, Javid Moraveji, Ellie Nick, Varun Raghunathan, Oscar Tascon, Hui Tang, Zhigang Tian, Wei Wu, Handa Xi, Yanhui Xie. Thanks also due to my colleagues and friends in Houston:, Steven Barras, Nicole Liu, Yang Mu, Xinguo Ning, Jiulong Sun, Jim Wang, Jin Wang, Xiaoning Wang and Lixin Xu. I would also like to thank my best friends, Rong Wu, Ying Jin and Bei Lu, for their continuous encouragement and accompany through the three and half years and for giving me a great time studying in Michigan.

I would like to thank my closest friend Kamaldev Raghavan, who gave me consistent support and encourgment throughout my Ph.D. study.

This research was supported by the Automotive Research Center, a U.S. Army RDECOM center of excellence for modeling and simulation of ground vehicles led by the University of Michigan.

I would also like to thank and the department of Naval Architecture and Marine Engineering, University of Michigan and the Barbour Scholarship for their fellowships and support during my graduate study.

TABLE OF CONTENTS

LIST OF FIGURES

ABSTRACT

Energy finite element analysis (EFEA) has been proven to be an effective and reliable tool for high frequency vibration analysis. It uses the averaged energy density as the primary variable to form the governing differential equations and provides a practical approach to evaluate the structural response at high frequencies, which is hard to reach with conventional finite element analysis because of the computational cost. In the past, EFEA has been applied successfully to different structures, such as beams, rods, plates, curved panels etc. Until recently, however, not much work has been done in the field of composite structures.

Research for developing a new EFEA formulation for modeling composite laminate plates is presented in this dissertation. The EFEA governing differential equation, with the time- and space- averaged energy density as the primary variable, is developed for general composite laminate plates. The power transmission characteristics at plate junctions of non-isotropic materials, including orthotropic plates and composite laminate plates are studied in order to obtain the power transmission coefficients at the junction. These coefficients are utilized to compute the joint matrix that is needed to assemble the global system of EFEA equations. The global system of EFEA equations can be solved numerically and the energy density distribution within the entire system can then be obtained. The results from the EFEA formulation have been validated through comparison with results from very dense FEA models.

Chapter 1

INTRODUCTION

1.1 Research Overview

Composite materials are formed by combining two or more materials that have quite different properties. The different materials work together to give the composite unique properties. The greatest advantage of composite materials is strength and stiffness combined with lightness. Because of these advantages, composite laminate plate and shell structures are being increasingly used as primary structural components in applications where weight saving is of critical concern, such as automotive, aerospace and naval architecture industries.

One of the applications of composite materials is that they can be used for the construction of army vehicles to make them lightweight. However, at the same time, the use of composite materials makes the vehicles structures more vulnerable to dynamic and shock loads. Due to the short duration of shock events, the high frequency content of the loads is responsible for the transfer of power from the location of the excitation to the location where sensitive electronic equipment is mounted. To improve the performance of composite materials under impact and utilize them to their full advantage, it is crucial to have a good understanding of their response under impact loads.

The frequency spectrum where simulation methods can be utilized for vibration analysis can be divided into three regions: low, mid and high frequency. The low frequency region is defined as the frequency range where all components are short compared to the wavelength. Finite Element Analysis (FEA) simulations are used for computing the response of structures at low frequency. In the mid-frequency range, the system is comprised of both long and short members. The method of combining SEA or EFEA with conventional finite element analysis was used to simulate the vibration response at mid frequencies.

The high frequency range is defined as the frequency range where all component member of a system are long compared to the wavelength. At high frequency, conventional FEA methods require a very large number of elements in order to capture the high frequency characteristic of the structures, which results in very high computational costs. Statistical Energy Analysis (SEA) and Energy Finite Element Analysis (EFEA) are the two developments for high frequency vibration analysis.

In SEA, the system is partitioned into coupled “subsystems” of similar modes and the stored and exchanged energies in each “subsystem” are analyzed through a set of linear equations. The primary variable in SEA is the lumped averaged energy in each subsystem. A subsystem can be seen as a part or physical element of the structure that is analyzed. To be modeled as a subsystem, the part or element should be able to vibrate quite independently from other elements and a reverberant sound field should exist with the subsystem. If different wave types exist in the element, then each of the corresponding sound field is modeled as one subsystem. In general, a subsystem is a

group of similar energy storage modes. In SEA, the “statistical” operation is represented by the frequency, spatial and ensemble average over a group of modes.

EFEA is a recently developed finite element approach for high frequency vibration and acoustic analysis. In EFEA, the energy density is defined as the primary variable. The governing differential equation is developed in terms of energy density and numerical solution is employed using finite element approach. It can capture the vibration property of the structure by using a significantly smaller number of elements compared to conventional FEA methods. The EFEA has been utilized in modeling automotives, marine structures and aircrafts etc. It has been validated through comparison to results from very dense FEA models and test data.

Compared to SEA, the advantages of EFEA are that it can provide the detail energy distribution within the subsystems and it can also take into consideration of the local damping effects within the subsystems. Furthermore, it is possible to use the existing models in conventional FEA in the EFEA method.

Until recently, most of the research on EFEA is related to isotropic materials, where the material properties are the same at all the directions. Some work had been done in orthotropic plates where the properties are different in two perpendicular directions. Until recently, not much work has been done in the field of composite plates. In order to extend the EFEA developments for composite materials, it is necessary to derive the more general EFEA differential equations for composite materials.

In this dissertation, the EFEA differential equation for composite laminate plates is developed. The derivation follows the same procedure as the development of EFEA in isotropic materials. First, the equations of motion for composite laminate plate are

obtained. The relationship between the time- and space-averaged energy density and energy intensities are found in order to establish the EFEA governing differential equations for general composite laminate plates. A variational form is employed to solve the EFEA differential equation. The energy density distribution of the composite laminate plates obtained from EFEA formulation is compared and validated with very dense FEA models of the plates. Then, for the coupled composite laminate plates, the power transmission coefficient at the junction is derived by utilizing the wave propagating method. The dynamic stiffness matrix for each plate is derived and the equations of motion of the junction are obtained by applying the appropriate equilibrium and compatibility conditions. The power transmission coefficients are calculated by solving the equations of motion at the junction. At last, the joint matrix at the junction is calculated and the global system of EFEA equation is established. The primary variable of the equation – energy density can then be calculated.

1.2 Literature Review

1.2.1 Finite Element Analysis and composite materials

In the past, conventional finite element analysis has been employed to evaluate the response of the structural system to the dynamic loads. The FEA formulation can be used to analyze arbitrary complex structures. It considers the continuous structures as a number of elements that connected to each other by the compatibility and equilibrium conditions. However, because of the necessity of obtaining the element size much smaller (typically 1/6) than the wavelength, FEA requires small meshes to describe the rapidly changing modes of the structures(Kim, Kang et al. 1994). Thus, FEA is mainly limited to analyzing the vibration at relatively low frequencies.

However, a number of researches have been done on the application of finite element analysis to the high frequency response of composite structures subject to impact/shock loads.

A transient dynamic finite element model was developed to analyze the response of a laminated composite plate subject to a foreign object impact in order to examine the susceptibility to impact of fiber-reinforced laminated composites that have been widely used in aerospace structures (Wu and Chang 1989). Instead of using two-dimensional plate theories, they studied the stress and strain distributions through the laminate thickness during the impact. A correlation was found between the strain energy density distributions and the resultant impact damage from the results.

A super finite element method was employed to predict the transient response of laminated composite plates and cylindrical shells subject to impact loads (Vaziri, Quan et al. 1996). The results were compared with experimental date and theoretical solutions. The super element technique was proved to be a simple and efficient method to predict the response of laminated composite plates and shells under impact loading although its limited applicability due to the linear elastic material behavior assumption.

The response of a fiber-reinforced composite laminate plate subject to central impact was investigated (Oguibe and Webb 1999). The failure mode was approximated by the model combining spring, gap and dashpot elements that account for the energy dissipated during the damage process. The numerical results were compared with the experimental data and good agreements were observed. It was concluded that the coupling between the dynamic response and stiffness degradation due to damage must be considered in order to predict correctly the damage due to impact. This dynamic finite

element model, together with the failure algorithm, can be used as a good numerical tool to predict the response of composite structures under impact loads.

A new weighted homogenization method was introduced for the design analysis of composite laminate structures for light weight armored vehicles (Rostam-Abadi, Chen et al. 2000). The method is modified from the standard homogenization method by applying the weighted material constants of the laminae in order to reflect the nature of beding. Numerical examples were presented using finite element analysis and the method was validated with classical lamination theory and first-order shear deformation theory.

The response of a laminated composite cylindrical shell was calculated by the classical Fourier series and the finite element method (Krishnamurthy, Mahajan et al. 2003). The analytical method provides information to help select appropriate mesh and time step sizes for finite element method. A spectral finite element model was developed to study the effect of wave scattering and power flow in composite beams with general ply stacking sequence (Mahapatra and Gopalakrishnan 2004).

The composite laminate and shell structures subject to low velocity impact were studied by Her and Liang (Her and Liang 2004) using ANSYS/LSDYNA finite element software. The impact force was modeled by the modified Hertz contact law. The effects of various parameters were examined in the parametric study.

The damage of a range of sandwich panels under impact loads was examine using experimental investigation and numerical simulation (Meo, Vignjevic et al. 2005). The numerical simulation was performed using transient dynamic finite element analysis code. The load distribution in the damaged sandwich structure and the failure mechanism under the impact load were examined.

The dynamic analysis of shell structures, with emphasis on application to steel and steel-concrete composite blast resistant door was analyzed by Koh (Koh, Ang et al. 2003). An explicit integration method was adopted considering the short duration and impulsive nature of the blast loading. Composite shell was handled by appropriate integration rule across the thickness. Both material and geometric nonlinearities were considered in the formulation.

The transient response of composite sandwich plates under initial stresses was investigated using a new finite element formulation (Nayakl, Shenoi et al. 2006). The new finite element formulation is based on a nine node assumed strain plate bending element with nine degrees of freedom per node that developed from a refined high order shear deformation theory.

A formulation of asymmetric laminated composite beam element that has super convergence properties was presented (Chakraborty, Mahapatra et al. 2002). The formulation is capable of capturing all the propagating wave modes at high frequencies and can be utilized to solve the free vibration and wave propagation problems in laminated composite beam structures. Qiu (Qiu, Deshpande et al. 2003) used the finite element method to analyze the response of clamped sandwich beams subject to shock loading and compared the results with analytical predictions.

Iannucci and Ankersen (Iannucci and Ankersen 2006) proposed an unconventional energy based composite damage model that has been implemented into the finite element codes for shell elements. In the model, the evolution of damage in each mode (tensile, compressive and shear) was controlled via a set of damage-strain

equations to allow the total energy dissipated for each damage mode to be controlled during impact event.

1.2.2 Statistical Energy Analysis

Statistical Energy Analysis (SEA) is developed based on the idea that at very high frequencies the vibration problem is analogous to a thermal problem in which the vibration energy density and damping are analogous to temperature and heat sinking respectively. SEA has the advantage of reducing the order of governing differential equations in vibratory analysis. In SEA, a large structure is reduced into smaller subsystems which are coupled together through a set of linear equations. SEA is very good in the study of sound and vibration transmission through complex structures at high frequencies. However, it is not reliable at low frequencies due to the statistical uncertainties that occur when there are few resonant modes in each of the subsystems.

The advantage of SEA is that it enables us to describe the subsystems more simply by only a few physical parameters, such as the damping coefficients, modal density, etc. (Lyon 1975). The disadvantage of SEA is that it gives statistical answers, which are subject to some uncertainty. In this case, many of the systems may not have enough modes in certain frequency bands to allow predictions with a high degree of certainty.

The earliest work in the development of SEA were done in 1960s by Lyon and Smith ((Lyon and Maidanik 1962; Smith 1962). In Lyon's work (Lyon and Maidanik 1962), the interaction of a single mode of one system with many modes of another was analyzed and an experimental study of a beam with a sound field was done. It also

showed the basic SEA parameters for the response prediction: modal density, damping and coupling loss factor.

SEA has been applied to different types of systems. Following its initial developments, the systems of plate and beam interaction and two plates connected together were discussed (Lyon and Eichler 1964). The radiation of sound by reinforced plates (Maidanik 1962) and the radiation of sound by cylinders (Manning and Maidanik 1964) were evaluated. SEA is also applied to other structures such as periodically stiffened damped plate structures (Langley, Smith et al. 1997) that are widely used in aerospace and marine vehicles.

Modal density is one of the important parameters in SEA. The development of SEA motivated the effort in the evaluation of modal densities. The modal densities of cylinders (Heckl 1962; Szecheny 1971) and curved panels (Wilkinson 1968) were evaluated. The modal density of composite honeycomb sandwich panels is evaluated (Renji, Nair et al. 1996). In the study, the expression for the modal density of honeycomb sandwich panels with orthotropic face sheets was derived with the consideration of shear flexibility of the core. The expression was verified by experiments and good agreement was observed.

The modal density for the bending of anisotropic structural components was studies by considering the case of periodic boundary conditions initially and then extending to general boundary conditions (Langley 1996). The equation was validated with empirical results.

Another important parameter of SEA is the coupling loss factor. It can be computed using analytical (wave approach) or numerical methods (finite element

method). In the wave approach, the vibration of subsystems are represented by the superposition of travelling waves, and coupling loss factor is evaluated by considering the reflection and transmission at the junction (Fahy 1994).

The coupling loss factor for two coupled beams system was analyzed using two methods: wave-transmission method and natural frequency-shift method (Crandali and Lotz 1971) and the results from two methods are proved same for a particular system. Langley (Langley 1989; Langley 1990) derived the expressions for the coupling loss factor in terms of the frequency and space averaged Green functions on the assumption that the coupling between the subsystems is conservative and weak coupling between the subsystems.

Conventional finite element models were employed to determine the coupling loss factors instead of analytical solutions when the connection between members presents a complexity that cannot be accounted by analytical solutions. It is the only computational option for calculating the power transfer characteristics for complex joints and discontinuous joints. Simmons (Simmons 1991) calculated the SEA coupling loss factors for L- and H- shape plate junctions using finite element methods at discrete frequencies from 10 and 2000 Hz. The vibrational energy of the plates was calculated using FEA instead of the traditional analytical solutions of an infinite junction between semi-infinite plates. The space- and frequency- averaged solutions from FEA were found to be reliable for calculating energy variables, although its calculation of displacement at individual positions frequencies is not meaningful at high frequencies. Such averaged energies of the plates can be used to derive the coupling loss factor of the junction that can be applied to SEA of structures with the same type of junction. In another study (Fredo 1997), FEA

was combined with a SEA-like approach to obtain the power flow coefficients within a system. The advantages of this approach include its ability of dealing with complicated subsystem topologies, complicated joints, narrow bands frequencies and non-resonant transmission mechanisms.

1.2.3 Energy Finite Element Analysis

Energy finite element analysis is an emerging new method for simulating high frequency vibration response. It uses time- and space- averaged energy density as the primary variable in the governing differential equations.

A power flow finite element analysis is presented by Nefske and Sung (Nefske and Sung 1989). In their research, the new method was developed as an alterative to SEA for high frequency vibration analysis. The formulation was based on power flow of a differential control volume considering the conservation of energy. The partial differential equation of the heat conduction type was derived and the finite element approach was employed to solve the differential equation. The power flow finite element model was formed by modifying a standard commercial structural finite element code. It was shown that the same FEA model for predicting the vibration at low frequencies could be modified to form the power flow finite element model for solving the vibration problems at high frequencies for the same structural system.

Wohlever (Wohlever 1988; Wohlever and Bernhard 1992) investigated future the thermal analogy to model mechanical power in structural acoustic systems. Energy density equations were derived from the classical displacement solutions for harmonically excited, hysteretically damped rods and beams. For the lightly damped rod, the relationship between the local power and the local gradient of energy density can be

found. For the beam, however, this relationship can only be found if locally space averaged values of power and energy density were utilized. This relationship, along with the energy balance on a differential control volume, led to the development of a second order equation that models the distribution of energy density in the structure. They also investigated the coupling of energy for rods and beams. Two existing techniques – the wave transmission approach and the receptance method were discussed and a new alternative method in which the upper and lower bounds of power and energy density can be predicted was also introduced.

Bouthier and Bernhard (Bouthier 1992; Bouthier and Bernhard 1992; Bouthier and Bernhard 1995) derived the equations of space- and time- averaged energy density and intensity in the far field and developed a set of equations that govern the space- and time- averaged energy density of plates (Bouthier and Bernhard 1992; Bouthier and Bernhard 1995), membranes (Bouthier and Bernhard 1995) and acoustic spaces. The equations were solved numerically and the results were validated with analytical solutions. The numerical implementation of the energy governing equations allows for some uneven distribution of the damping in the plate and this is one of the advantages of EFEA over SEA.

Cho (Cho 1993; Cho and Bernhard 1998) formulated the EFEA system equations and calculated EFEA power transfer coefficients for coupled structures. The derivation of the partial differential equations that govern the propagation of energy in simple structural elements such as rods, beams, plates and acoustic cavities was first performed and then the derivation of coupling relationships that describes the transfer of energy for

various joints was achieved. The EFEA system equation was formed to solve for the energy densities.

Bitsie and Bernhard (Bitsie and Bernhard 1996) presented the structural-acoustic coupling relationship for energy flow analysis. The coupling relationship based on the principle of conservation of energy flow and the energy superposition principle was formulated. The joint coupling relationship as a function of radiation efficiency and material characteristic impedances was then developed and implemented into the energy finite element formulation or energy boundary element formulation. Some examples of structural-acoustic coupling were performed and the results were compared with the experimental tests.

In another paper by Bernhard and Huff (Bernhard and Huff 1999), the derivation of energy flow analysis techniques were summarized and the cases when discontinuity in either geometric properties or material properties occurs were discussed. The case study was shown to show the utility of the method as a design technique.

In another research (Vlahopoulos, Garza-Rios et al. 1999), the EFEA formulation was applied to marine structures and the first extensive theoretical comparison between SEA and EFEA was presented for complex structures. An algorithm that identifies the locations of joints in the EFEA model was developed and the comparison between SEA solution and EFEA results for a fishing boat was obtained. Both methods were used to analyze a fishing boat and good agreement was observed. Also, the EFEA simulation capabilities for identifying spatially dependent design changes that reduce vibration were demonstrated. In the study, the advantages of EFEA over SEA were also summarized: it can eliminate the uncertainties in defining subsystems and their connections because the

model generation is based on actual geometry; the results can be displayed over the entire system and spatial variation can be assigned to the design variables when studying alternative configurations for performance improvements.

Recently, a Hybrid Finite Element Analysis (hybrid FEA) is also developed to analyze the mid-frequency vibration of structures. Langley and Bremner (Langley and Bremner 1999) presented a hybrid approach based on coupling FEA and SEA methods. The methodology was to use FEA to compute the low frequency global modes of a system and SEA to compute the high frequency local modes of the subsystem. Both low and high frequency global modal degrees of freedom were coupled to each other. The method was validated using an example of two co-linear rod elements.

Vlahopoulos and Zhao (Vlahopoulos and Zhao 1999; Zhao and Vlahopoulos 2000; Vlahopoulos and Zhao 2001; Zhao and Vlahopoulos 2004) did the theoretical derivation of a hybrid finite element method that combines conventional FEA with EFEA to achieve a numerical solution to the vibration at mid-frequencies. In the mid-frequency range, a system has some members that contain several wavelengths (long members) and some members with just a few wavelengths (short members) within their lengths. Long members are modeled by EFEA and short members are modeled by FEA. In the study, the interface conditions at the joints between sections modeled by the EFEA and FEA methods were also derived. The validation was obtained for different configuration of beams.

Since its advent, EFEA has been applied in rods and beams (Wohlever 1988; Wohlever and Bernhard 1992; Cho and Bernhard 1998), isotropic plates (Bouthier and Bernhard 1992; Bouthier and Bernhard 1995; Vlahopoulos, Garza-Rios et al. 1999),

membranes (Bouthier and Bernhard 1995), and structure with heavy fluid loading (Zhang, Wang et al. 2003; Zhang, Vlahopoulos et al. 2005; Zhang, Wang et al. 2005). In the EFEA application, the energy equation of the propagation of both flexural waves (Bouthier and Bernhard 1992; Bouthier and Bernhard 1995) and in-plane waves (Park, Hong et al. 2001) are derived.

Until recently, most of the application of EFEA is related to isotropic materials, where the material property is identical at all the directions. However, as the needs increasing for using different types of materials in the construction of structures, researchers have realized the demand of applying EFEA to other types of materials.

The power flow model was developed for the analysis of flexural waves in orthotropic plates at high frequency (Park, Hong et al. 2003). The energy equation was derived in terms of the time- and space- averaged far-field energy density. The model was validated by comparing the numerical results with classical modal solutions for single orthotropic plate vibrating at different frequencies and with different damping loss factors.

1.2.4 Power transmission through joints

In order to apply the EFEA or SEA to complex structures, it is necessary to obtain the power transmission characteristics at structural joints. In the conventional finite element formulation, the primary variable is continuous between elements at the joints. This continuity is utilized to assemble to global system matrix. In EFEA or SEA, however, the continuity only occurs if the geometry and the material properties do not change. The primary variable - energy density is discontinuous at positions where different member are connected or at locations of discontinuities with a single member.

In order to form the global system of equation at the joints, a special approach based on the continuity of power flow across the joint is developed. This continuity is expressed in terms of power transfer coefficients (in EFEA) or coupling loss factor (in SEA). Usually, the power transfer coefficients or coupling loss factor is determined using either analytical or numerical methods.

The numerical method is based on the concept of employing conventional finite element models to calculate the energy in structural members and then utilizing the energy ratio between members to calculate the coupling loss factors used in SEA (Simmons 1991; Steel and Craik 1994; DeLanghe, Sas et al. 1997; Fredo 1997; Vlahopoulos, Zhao et al. 1999). The finite element method has the flexibility of modeling complex connections which cannot be accounted by analytical solutions. The coupling loss factors were computed through finite element calculations for assemblies of fully connected plates (Simmons 1991; Fredo 1997) and beam junctions (DeLanghe, Sas et al. 1997). The resonant characteristics of coupled systems were also analyzed (Steel and Craik 1994). The power transfer characteristics for spot-welded connections were computed using conventional finite element method (Vlahopoulos, Zhao et al. 1999) in order to apply the EFEA approach to automotive structures.

The wave transmission approach is used extensively in the vibro-acoustic field to estimate the power transmission and reflection coefficients of a joint. The transmission coefficients and coupling loss factors were obtained for two L-junction beams (Sablik 1982). The power transmission from the incident flexural wave was analyzed and it was found that the flexural-torsional transmission can be more efficient than flexural-flexural

transmission for this case. The expression derived in this paper can be used to analyze the beam network in statistical energy analysis.

Sound transmission for thin plate junctions and mode coupling was studied by Craven and Gibbs (Craven and Gibbs 1981; Gibbs and Craven 1981). In the research, both bending and in-plane vibrations for the T-junction of thin plates were presented and results were validated.

Whole and Beckmann (Wohle, Beckmann et al. 1981; Wohle, Beckmann et al. 1981) studied the coupling loss factors for rectangular structural slab junctions with application to the flanking walls in buildings. The method was derived bending, longitudinal and transverse incident waves.

Horner and White (Horner and White 1990) used the expressions of flexural and longitudinal waves and related the time averaged power to travelling wave amplitudes. The continuity and equilibrium at the joint was utilized to yield the solution for power transmission coefficients. The closed-form solutions of the multiple power transmission within finite sections of structures were also derived.

Cho (Cho and Bernhard 1998) described the wave transmission and reflection at a joint by the semi-infinite rod joint model with an incident wave from each rod simultaneously impinges on the joint from each direction. The energy flow boundary condition was applied for all wave components of energy flow and the power carried by each wave type in each of the rod was calculated.

Langley (Langley 1989; Langley 1990) derived the SEA equations for multi-coupled systems with random excitation. The expressions of the coupling loss factors are obtained in terms of the frequency and space averaged Green functions for the coupled

system. Another approach using wave approach was used to derive the wave transmission coefficients (Langley and Heron 1990) for N- plate/beam assembly. The generic plate/beam junctions were considered that consists of an arbitrary number of plates which are either coupled through a beam or directly coupled along a line. The equations of motion of the junction were formulated by deriving the wave dynamic stiffness matrix for each plate and then applying the appropriate equilibrium and compatibility conditions at the junction. This approach minimized the amount of algebraic manipulations that is required for an arbitrary number of plate assembly.

In another study of Langley (Langley 1994), the coupling loss factor for the junction at which an arbitrary number of curved panels are connected were derived using the similar procedure. In this paper, the method of deriving the wave dynamic stiffness matrix for the calculation of coupling loss factors was extended to the case of non-isotropic components such as a curved panel by providing a definition of a diffuse wave field that is appropriate to non-isotropic components.

The in-plane power flow analysis for coupled thin finite plates were analyzed (Park, Hong et al. 2001). The longitudinal and in-plane shear energy equations were derived for two plates connected at a certain angle. The computation was performed by using single Fourier series approximation and the equations were established from the equilibrium of energy flow and the continuity of energy flow between the plates.

The power transmission between non-isotropic materials was also investigated (Langley 1994; Bosmans, Mees et al. 1996; Bosmans and Nightinghale 1999; Bosmans, Vermeir et al. 2002). The analytical solution of structure-borne sound transmission between thin orthotropic plates was obtained (Bosmans, Mees et al. 1996). Two models

were presented for predicting the power transmission characteristics of two orthotropic plates connected by a rigid junction. One was based on the solution for the wave propagation in semi-infinite plates. Another model was based on modal summation solution for finite-size plates. Numerical results were obtained for the bending wave transmission between an L-junction of two orthotropic plates using both methods and compared with the results from equivalent isotropic junction.

The theory presented above was modified in order to calculate the coupling loss factor of an orthotropic stiffening rib at the joint (Bosmans and Nightinghale 1999). The stiffening rib is modeled as an orthotropic plate strip of eccentric beam using concepts of plate strip theory and plate/beam joint modeling (Langley and Heron 1990). Two typical features of wave propagation in orthotropic plates were proposed: the structural intensity is not parallel to the direction of wave propagation; the vibrational energy is not distributed uniformly over all directions in a reverberant field. These two features require new derivation of the coupling loss factors for orthotropic and anisotropic materials.

The derivation of coupling loss factor for coupled anisotropic plates was also presented recently (Bosmans, Vermeir et al. 2002). The angle dependence of the wavenumber was taken into consideration during the derivation. It was shown that the general expression for the coupling loss factor applicable to anisotropic components that was first derived by Langley (Langley 1994) for junction of curved panels is identical to the derivation by Bosmans (Bosmans, Mees et al. 1996). In Langley's expression, the coupling loss factor was written in terms of the wave transmission coefficient, the group velocity and the phase velocity on the source plate. In Bosmans's expression, however, the coupling loss factor can be directly calculated from the transmission coefficient

without requiring the calculation of group velocity. These two expressions were shown to be identical and one can be derived from another.

1.3 Dissertation Contribution

In this dissertation, the developments of energy finite element analysis to composite laminate plates are presented in order to simulate the high frequency response of composite laminate plates subject to impact loading. The EFEA differential equation, in which the energy density is the primary variable, is developed for the general composite laminate plates. After that, the power transmission coefficients are derived for coupled orthotropic plates and coupled composite laminate plates. The joint matrix is then derived to obtain the global system EFEA equation. The system equation can be solved to yield the energy distribution in the different components within the entire composite structure.

The equations of motion for composite laminate plates are different from the equations of motion governing the vibration of isotropic plates. The equations have more terms and they also involve the coupling between the bending and in-plane motions. A convergence study, however, shows that at high frequencies, the coupling between bending and in-plane terms becomes insignificant and can be neglected in our research.

In order to obtain the EFEA differential equation in composite laminate plates, the far field wave solution was first obtained. The time- and space-averaged energy density and energy intensities can be expressed in terms of the wave solution of displacement and the relationship between the energy density and energy intensities is obtained. This relationship, together with the relationship of dissipated power with energy density, and the power balance at the steady-state, can be utilized to get the EFEA differential

equation, in which energy density is the primary variable. The differential equation can be solved numerically using a finite element approach. The EFEA differential equation for composite laminate plate is derived for the bending and in-plane motions respectively.

In the research, an alternative approach for obtaining the EFEA differential equations in composite laminate plates is also presented. The group velocity for non-isotropic materials is found to be angle-dependent and the heading of group velocity is different from the heading of wave propagation in these materials. The averaged group velocity for composite laminate plate is obtained by integrating the value over all the angles of wave propagation. An equivalent homogenized isotropic material can then be found for the composite laminate plate, on the condition that the group velocity remains the same for two cases. An alternate EFEA differential equation for the composite laminate plate can then be formed by using the EFEA differential equation for equivalent isotropic plate.

The power transmission mechanism for orthotropic plate junctions and general composite laminate plate junctions is studies in order to analyze the power transmitted from the excitation location to the other components within the composite structure. The approach that has been adopted in this research is to consider the vibrations of the structure in terms of elastic waves propagating through the structure and are partially reflected and partially transmitted at the junctions. The derivation of power transmission coefficients is achieved by deriving a “wave dynamic stiffness matrix” for each plate first and then applying the appropriate equilibrium and compatibility conditions at the junction. The joint matrix is derived from the power transmission coefficients at the

junction and the global matrix of coupled orthotropic/composite laminate plates is assembled.

Some examples are presented as validation for the derivation. First, the energy density distribution of two types of single composite laminate plates was calculated and the results are compared with the results from very dense FEA models. Second, the power transmission of four types of L-junction of two identical orthotropic plates is calculated using the EFEA formulation. The first plate is given excitation at several randomly selected locations and the energy density level in the two plates is calculated using both EFEA and very dense FEA models. At last, the power transmission of an L-junction of two general composite laminate plates is examined. In the two cases, the second plate is connected to the different edge of the first plate. Again, the energy density level in the two plates is computed and compared with FEA model. In all the case studies, good agreements between EFEA results and the results from very dense FEA model are observed.

1.4 Dissertation Overview

In Chapter 2, the background information of EFEA is introduced and the formulation associated with the flexural energy of isotropic plates is overviewed. First, the EFEA derivation for single isotropic is presented. Then, the information of EFEA development at isotropic plate junctions is provided. This chapter gives the basic concept of EFEA formulation and the procedure of formulation development of EFEA.

In Chapter 3, the EFEA development in single composite laminate plate is presented. First, the stress-strain relation for generally orthotropic lamina is expressed and the synthesized stiffness matrix of composite laminate plate is obtained from the

properties of each lamina. Second, the governing equations for the vibration of composite laminate plate are given and a convergence study is presented to show that the coupling between bending and in-plane terms in the equations of motion can be neglected for high frequency analysis. Third, the time- and space- averaged energy density and energy intensities are derived and the relationship between the energy density and energy intensities and the EFEA differential equation is obtained using this relationship and the power balance at a steady state over a differential control volume of the plate. Then, the differential equation is solved numerically using a finite element approach and two numerical examples are presented. In both examples, the energy density distribution in the mid-span of the plate is calculated from 1000 Hz to 5000 Hz. The results obtained from EFEA are compared with the results from very dense FEA model in both examples and good agreement is observed. Finally, an alternative approach to derive the EFEA differential equation in composite laminate plate is presented. The approach is based on finding the averaged group velocity of the composite laminate plate and finding the equivalent homogenized isotropic plate to represent the composite plate while forming the EFEA different equation. Some validation is also given for this approach.

In Chapter 4, the power transmission characteristics of coupled orthotropic plates are studied. The approach is to consider the elastic waves propagating in the excited plate and are partially reflected and partially transmitted to other plates through the junction. The power transmission coefficients can be calculated by deriving the wave dynamic stiffness matrix for each plate and utilizing the appropriate equilibrium and compatibility conditions at the joint. First, the in-plane wavenumbers for orthotropic plate is derived and the wave dynamic stiffness matrix is obtained. The complete equations are assembled

and the power transmission coefficients are calculated. Second, the joint matrix is expressed in terms of the power transmission coefficients. Then, the global matrix for coupled orthotropic plate is formed using the joint matrix to connect the elements at structural or material discontinuities. Finally, the formulation is validated through a set of numerical examples in which four cases of an L-junction of two orthotropic plates are considered. The energy density level in two plates is calculated using both EFEA and FEA model and the results are compared.

In Chapter 5, the power transmission through coupled composite laminate plates is studied following the same procedure as Chapter 4. The numerical example is given for two general composite laminate plates connected at a rectangular angle. Again, good agreement is shown between the EFEA results and results from very dense FEA model.

Finally, conclusions and recommendations for future work are presented in Chapter 6.

Chapter 2

BACKGROUND OF ENERGY FINITE ELEMENT ANALYSIS

2.1 Introduction

In order to present the current Energy Finite Element Analysis (EFEA) development of composite structures, some background information will be given about the EFEA method in this chapter. EFEA has been applied successfully to a variety of member such as rods and beams (Wohlever 1988; Wohlever and Bernhard 1992; Cho and Bernhard 1998), isotropic plates (Bouthier and Bernhard 1992; Bouthier and Bernhard 1995; Vlahopoulos, Garza-Rios et al. 1999), membranes (Bouthier and Bernhard 1995) etc. To given a general idea of its methodology and derivation procedure, the EFEA formulation associated with the flexural energy in isotropic plates is overviewed in this chapter. The EFEA development for single isotropic plates is presented first, and then the EFEA formulations at plate junctions are introduced.

2.2 EFEA Developments for a Single Isotropic Plate

The EFEA development in a single isotropic plate consists of the following steps:

1. Find the governing differential equation of the vibration of the plate.
2. Find the wave solution of the displacement to the governing differential equation and the dispersion relationship.

3. Express energy density and energy intensities in terms of the wave solution of the displacement.
4. Find the relationship between the time- and space- averaged energy density and energy intensities.
5. Establish the EFEA differential equation for the plate using the power balance over a differential control volume of the plate and the relationship between energy density and energy intensities, as long as the relationship between the dissipated power and the energy density.
6. Solve the system of EFEA differential equations numerically.

The EFEA governing differential equation associated with the flexural wave is developed by considering the wave solution to the governing differential equation of the plate bending. The equation of motion for a thin, transversely vibrating isotropic plate excited by a point force at (x_0, y_0) can be expressed as (Bouthier and Bernhard 1992):

$$D(1+i\eta)\nabla^4 w + \rho h \frac{\partial^2 w}{\partial t^2} = F\delta(x-x_0)(y-y_0)e^{i\omega t} \quad (2.1)$$

where $D = Eh^3/[12(1-\nu^2)]$ is the rigidity of the plate, η is the structural damping loss factor, ρ is the mass density, h is the thickness of the plate, $(x_0, y_0)$is the location where the excitation force is added.

The general form of the far-field solution can be expressed as the following where the bending displacement within the plate is considered as a linear superposition of waves associated with two orthogonal directions x and y (Bouthier and Bernhard 1992; Bouthier and Bernhard 1995).

$$w_{ff}(x,y,t) = \left\{Ae^{-i(k_x x+k_y y)} + Be^{i(k_x x-k_y y)} + Ce^{-i(k_x x-k_y y)} + De^{i(k_x x+k_y y)}\right\}e^{i\omega t} \quad (2.2)$$

where A, B, C, D are the constants associated with the amplitudes of propagating wave in the positive and negative x and y directions respectively, k_x and k_y are complex wave numbers associated with the damped frequency of oscillation in the x and y directions (Bouthier and Bernhard 1992).

$$k_x = k_{xl}(1 - i\frac{\eta}{4}) \text{ , } k_y = k_{yl}(1 - i\frac{\eta}{4}) \text{ and } k_{xl} = k_{yl} = \sqrt[4]{\frac{\rho h}{D}\omega^2} \tag{2.3}$$

The energy density is the primary variable in formulating the governing differential equation and the energy density averaged over a period can be expressed in terms of the far-field displacement solution (Bouthier and Bernhard 1992) as:

$$\langle e \rangle = \langle \frac{D}{4}\left[\frac{\partial^2 w}{\partial x^2}\left(\frac{\partial^2 w}{\partial x^2}\right)^* + \frac{\partial^2 w}{\partial y^2}\left(\frac{\partial^2 w}{\partial y^2}\right)^* + 2\nu\frac{\partial^2 w}{\partial x^2}\left(\frac{\partial^2 w}{\partial y^2}\right)^* + 2\nu(1-\nu)\frac{\partial^2 w}{\partial x \partial y}\left(\frac{\partial^2 w}{\partial x \partial y}\right)^*\right] + \frac{\rho h}{4}\frac{\partial w}{\partial t}\left(\frac{\partial w}{\partial t}\right)^* \rangle \tag{2.4}$$

where ν is the Poisson ratio, h is the thickness of the plate, $\langle\ \rangle$ indicates time averaging over a period, $\langle\ \rangle^*$ indicates the complex conjugate.

The two energy intensity components averaged over a period can also be expressed in terms of the far-field displacement solution as:

$$\langle I_x \rangle = \langle D\left[\frac{\partial^2 w}{\partial x^2} + \nu\frac{\partial^2 w}{\partial y^2}\right]\left(\frac{\partial^2 w}{\partial x \partial t}\right)^* + D(1-\nu)\frac{\partial^2 w}{\partial x \partial y}\left(\frac{\partial^2 w}{\partial y \partial t}\right)^* - D\frac{\partial}{\partial x}\nabla^2 w\left(\frac{\partial w}{\partial t}\right)^* \rangle \tag{2.5}$$

$$\langle I_y \rangle = \langle D\left[\frac{\partial^2 w}{\partial y^2} + \nu\frac{\partial^2 w}{\partial x^2}\right]\left(\frac{\partial^2 w}{\partial y \partial t}\right)^* + D(1-\nu)\frac{\partial^2 w}{\partial x \partial y}\left(\frac{\partial^2 w}{\partial x \partial t}\right)^* - D\frac{\partial}{\partial y}\nabla^2 w\left(\frac{\partial w}{\partial t}\right)^* \rangle \tag{2.6}$$

The far-field displacement solution can be substituted into the above expressions for energy density and intensities. The time- and space- averaged energy density and intensities $\langle \underline{e} \rangle, \langle \underline{I_x} \rangle, \langle \underline{I_y} \rangle$ can be obtained by integrating the expressions over one wavelength. After some algebraic manipulations, the expressions for the space- averaged

over a wave length and time- averaged over a period energy density and energy intensity are derived:

$$\langle \underline{e} \rangle = \frac{D}{2}\left[k_{xl}^4\left(A_x^2 e^{-\frac{\eta}{2}k_{xl}x} + B_x^2 e^{\frac{\eta}{2}k_{xl}x}\right) + k_{yl}^4\left(A_y^2 e^{-\frac{\eta}{2}k_{yl}y} + B_y^2 e^{\frac{\eta}{2}k_{yl}y}\right)\right] \quad (2.7)$$

$$\langle \vec{I} \rangle = \langle \overrightarrow{I_x} \rangle + \langle \overrightarrow{I_y} \rangle = D\omega\left[k_{xl}^3\left(A_x^2 e^{-\frac{\eta}{2}k_{xl}x} - B_x^2 e^{\frac{\eta}{2}k_{xl}x}\right)\vec{\imath} + k_{yl}^3\left(A_y^2 e^{-\frac{\eta}{2}k_{yl}y} - B_y^2 e^{\frac{\eta}{2}k_{yl}y}\right)\vec{\jmath}\right] \quad (2.8)$$

By observing the similarities between equations (2.7) and (2.8), a relationship between the energy density and the intensity can be derived (Bouthier and Bernhard 1992):

$$\langle \vec{I} \rangle = -\frac{c_g^2}{\eta\omega}\nabla\langle \underline{e} \rangle \quad (2.9)$$

where $c_g = 2\sqrt[4]{\frac{D\omega^2}{\rho h}}$ is the group speed, η is the hysteresis damping factor, ω is the radian frequency.

The time and space averaged dissipated power $\langle \underline{\Pi}_{diss} \rangle$ is associated to the corresponding energy density and the relationship between them can be expressed as (Cremer, Heckl et al. 1973) :

$$\langle \underline{\Pi}_{diss} \rangle = \eta\omega\langle \underline{e} \rangle \quad (2.10)$$

The power balance at steady-state gives:

$$\langle \underline{\Pi}_{in} \rangle = \langle \underline{\Pi}_{diss} \rangle + \nabla\langle \vec{I} \rangle \quad (2.11)$$

where $\langle \underline{\Pi}_{in} \rangle$ is the input power.

Thus, the EFEA differential equation for a plate can be derived by considering a power balance at the steady state over a differential control volume of the plate and the relationship between the dissipated power and energy density (Bouthier and Bernhard 1992):

$$-\frac{c_g^2}{\eta\omega}\nabla^2\langle \underline{e}\rangle + \eta\omega\langle \underline{e}\rangle = \langle \underline{\Pi}_{in}\rangle \quad (2.12)$$

And a finite element formulation (Cho 1993) can be employed to solve equation (2.12) numerically. The weak variational form of equation (2.12) for each element can be expressed as (Vlahopoulos, Garza-Rios et al. 1999):

$$-\int_{C_e} \emptyset\hat{n}\frac{c_g^2}{\eta\omega}\nabla\langle \underline{e}\rangle dC_e + \int_{S_e}\frac{c_g^2}{\eta\omega}\nabla\emptyset\nabla\langle \underline{e}\rangle dS + \int_{S_e}\eta\omega\,\emptyset\langle \underline{e}\rangle dS - \int_{S_e}\emptyset\,\langle \underline{\Pi}_{in}\rangle\, dS = 0 \quad (2.13)$$

where $\emptyset$ is an arbitrary function, C_e is the boundary of the element, S_e is the surface of the element, $\hat{n}$ is the unit vector normal to the element boundary.

The system of linear equations can be obtained by using the shape functions within each element and representing all variables as a linear superposition of the shape functions and the nodal values (Vlahopoulos, Garza-Rios et al. 1999):

$$[K^e]\{e^e\} = \{F^e\} + \{Q^e\} \quad (2.14)$$

where $\{e^e\}$ is the vector of nodal values for the time- and space- averaged energy density, $[K^e]$ is the system matrix for each element, $\{F^e\}$ is the excitation vector which represents the energy input at each node, $\{Q^e\}$ is the power flow across the element boundary.

2.3 EFEA Developments for Isotropic Plate Junctions

In the conventional finite element formulations, the primary variable (displacement, stress or strain) is continuous between elements and the global system matrix is assembled based on this continuity. In EFEA, however, at positions where different members are connected, or at positions the material properties change, the primary variable (energy density) is discontinuous. The assembly of the global system matrix is based on the continuity of power flow $\{Q^e\}$ across the joint. The power flow

can be expressed in terms of energy density at two adjacent element and joint matrix (Vlahopoulos, Garza-Rios et al. 1999).

$$\begin{Bmatrix} Q_n^i \\ Q_{n+1}^i \\ Q_m^j \\ Q_{m+1}^j \end{Bmatrix} = [JC]_j^i \begin{Bmatrix} e_n^i \\ e_{n+1}^i \\ e_m^j \\ e_{m+1}^j \end{Bmatrix} \tag{2.15}$$

where n and $n+1$ represents the two nodes of the i element at the joint, m and $m+1$ represents the two nodes of the j element at the joint, the joint matrices $[JC]_j^i$ define the power transfer across elements at the joints and are derived from the power transfer coefficients:

$$[J] = ([I] - [\tau])([I] + [\tau])^{-1} \int_B \phi_i \, \phi_j \, dB \tag{2.16}$$

where ϕ_i , ϕ_j are Lagrangian basis functions, B is the boundary area between elements i and j at the joint, $[\tau]$ is the matrix of power transmission coefficient, which are evaluated from analytical solutions of semi-infinite members (Langley and Heron 1990).

The final assembled system of EFEA equations can be expressed as (Vlahopoulos, Garza-Rios et al. 1999):

$$\left(\begin{bmatrix} [K^e]_i & \\ & [K^e]_j \end{bmatrix} + [JC]_j^i \right) \begin{Bmatrix} \{e^i\} \\ \{e^j\} \end{Bmatrix} = \begin{Bmatrix} \{F^e\}_i \\ \{F^e\}_j \end{Bmatrix} \tag{2.17}$$

where $[K^e]_i$ and $[K^e]_j$ are the element matrix for the i and j element, $\{e^i\}$ and $\{e^j\}$ are the vectors containing all the nodal degrees of freedom for elements i and j.

The global system of equations can be solved to obtain the energy density distribution within the entire system.

2.4 Example of Previous EFEA Applications

The EFEA method has been employed in the past during one of the case studies developed by the Automotive Research Center in order to assess the high frequency vibration of a conventional vehicle due to track excitation (Pierre, Vlahopoulos et al. 2004; Pierre, Vlahopoulos et al. 2004). EFEA results for the flexural energy for the vehicle is shown in Figure 2.1.

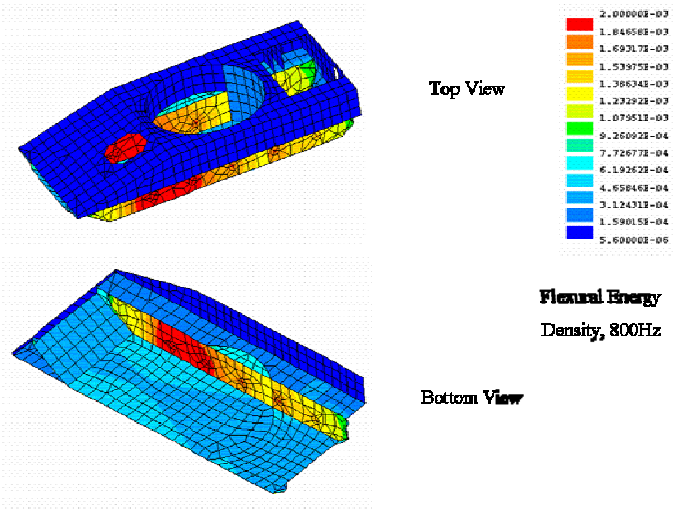

Figure 2.1.EFEA results for the flexural energy in a vehicle due to track excitation

In order to demonstrate the significant savings in computational resources achieved by the EFEA method, a conventional FEA model and the EFEA model for the same vehicle are presented in Figure 2.2. It can be observed that many more elements are required by the conventional FEA. It is also important to notice that although many more elements are present in the FEA model the frequency range of its validity is much lower than the frequency range which can be covered by the EFEA model because of the different primary variables employed by the two methods.

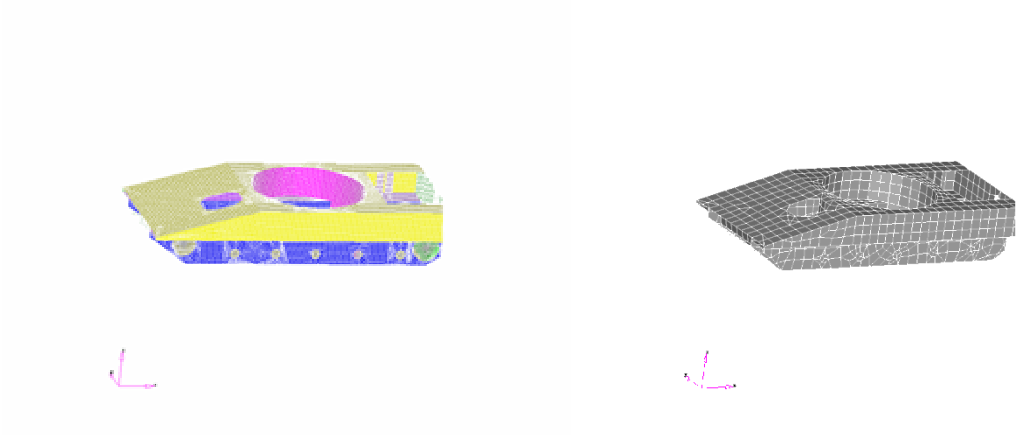

Figure 2.2 Conventional FEA and EFEA model for an Army vehicle

Chapter 3

EFEA DEVELOPMENTS IN SINGLE COMPOSITE LAMINATE PLATE

3.1 Introduction

In this chapter, the EFEA formulation for general composite laminate plates is derived. First, some background of composite laminate plates is introduced and the synthesis of the stiffness matrix is presented. Second, the EFEA differential equation in composite laminate plates is derived. Third, some numerical examples are given and the results from EFEA are compared with very dense FEA model. Finally, an alternative approach for forming the EFEA differential equation is given.

Composite laminate plates are formed from two or more laminae bonded together to act as an integral structural element. The property of the laminate plate is determined by the different property and orientation of each lamina. Different theories have been used to analyze composite laminate plates, such as 2-D and 3-D theories (Agarwal and Broutman 1990). In the 2-D theory, the laminate plate is simplified as an equivalent single-layer plate, so this theory is also called Equivalent Single-Layer (ESL) Laminate Theory. The common approaches used in the 2-D theory include the Classical Laminate Plate Theory (CLPT) and shear deformation laminate theory. In our work, the Classical

Laminate Plate Theory is employed to develop the EFEA formulations in composite laminate plates.

The Classical Laminated Plate Theory is an extension of the classical plate theory to composite laminates. In the CLPT, it is assumed that the Kirchhoff hypothesis holds (Reddy 1997):

(1) Straight lines perpendicular to the mid-surface before deformation remain straight after deformation.

(2) The transverse normals do not experience elongation.

(3) The transverse normals rotate such that they remain perpendicular to the mid-surface after deformation.

In addition, perfect bonding between layers is assumed (Agarwal and Broutman 1990):

(1) The bonding itself is infinitesimally small; there is no flaw or gap between layers.

(2) The bonding is non-shear-deformable, which means that no lamina can slip relative to another.

(3) The strength of bonding is as strong as it needs to be; the laminate acts as a single lamina with special integrated properties.

Classical laminate theory applies to the plate over which forces and moments are assumed constant, and in which the shear strains through thickness are ignored. This assumption is not accurate enough for thick composite plates. In that case, the shear deformation theory or the layer by layer theory, which account for the transverse shear

deformation and the shear discontinuity through the plate thickness, can be used and some of the restrictions of the classical laminate theory can be relaxed.

3.2 Synthesis of Stiffness Matrix for Composite Laminate Plates

3.2.1 Stress-strain relation for generally orthotropic lamina

A single layer of a laminated composite material is generally referred to as a ply or lamina. A composite laminate plate is constructed by stacking several unidirectional laminae in a specified sequence of orientation as shown in Figure 3.1. Properties of the laminate can be predicted by knowing the properties of its constituent laminae. The principal material directions of each lamina make a different angle with a common set of reference axis. Each lamina is orthotropic and obeys the stress-strain relations referred to its principle material axes. Thus, in order to get the properties of the laminate, it is necessary to refer the stress-strain relationship in the lamina to a common reference coordinate system. A lamina referred to arbitrary axes is called a generally orthotropic lamina (Agarwal and Broutman 1990).

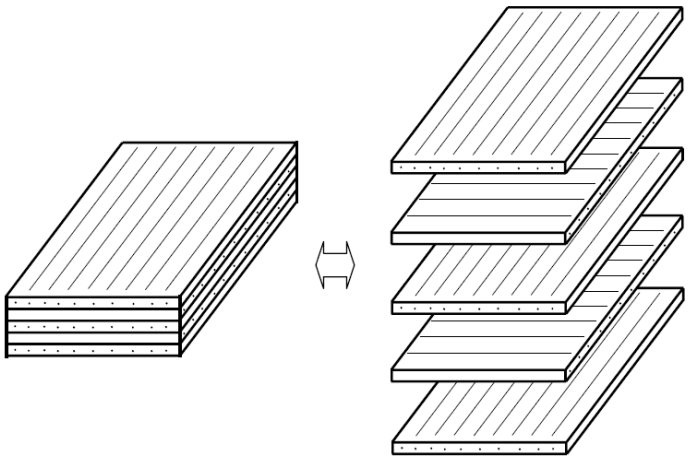

Figure 3.1 Construction of composite laminate plate

The principal material axes of an orthotropic lamina are orientated at an angle θ with the reference coordinate axes. The principal material axes of the lamina are referred as $L-T$ axes and the reference coordinate axes are referred as $x-y$ axes. Stresses and strains can be transformed from one set of axes to another.

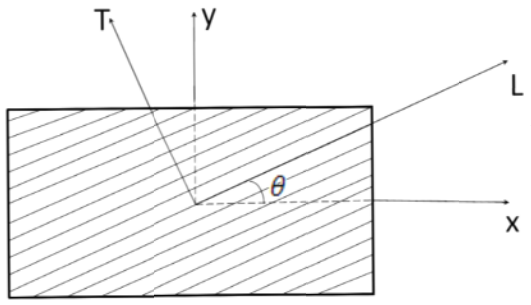

Figure 3.2 Two coordinates of a generally orthotropic lamina

$$\begin{Bmatrix}\sigma_L\\ \sigma_T\\ \tau_{LT}\end{Bmatrix} = [T]\begin{Bmatrix}\sigma_x\\ \sigma_y\\ \tau_{xy}\end{Bmatrix} \tag{3.1}$$

$$\begin{Bmatrix}\varepsilon_L\\ \varepsilon_T\\ \frac{1}{2}\gamma_{LT}\end{Bmatrix} = [T]\begin{Bmatrix}\varepsilon_x\\ \varepsilon_y\\ \frac{1}{2}\gamma_{xy}\end{Bmatrix} \tag{3.2}$$

where the transformation matrix can be expressed as (Agarwal and Broutman 1990):

$$[T] = \begin{bmatrix}\cos^2\theta & \sin^2\theta & 2\sin\theta\cos\theta\\ \sin^2\theta & \cos^2\theta & -2\sin\theta\cos\theta\\ -\sin\theta\cos\theta & \sin\theta\cos\theta & \cos^2\theta-\sin^2\theta\end{bmatrix} \tag{3.3}$$

The stress-strain relation in the $L-T$ axes is given by:

$$\begin{Bmatrix}\sigma_L\\ \sigma_T\\ \tau_{LT}\end{Bmatrix} = \begin{bmatrix}Q_{11} & Q_{12} & 0\\ Q_{12} & Q_{22} & 0\\ 0 & 0 & 2Q_{66}\end{bmatrix}\begin{Bmatrix}\varepsilon_L\\ \varepsilon_T\\ \frac{1}{2}\gamma_{LT}\end{Bmatrix} \tag{3.4}$$

where

$$Q_{11} = \frac{E_L}{1-\nu_{LT}\nu_{TL}}$$

$$Q_{22} = \frac{E_T}{1-\nu_{LT}\nu_{TL}} \tag{3.5}$$

$$Q_{12} = \frac{\nu_{LT}E_T}{1-\nu_{LT}\nu_{TL}} = \frac{\nu_{TL}E_L}{1-\nu_{LT}\nu_{TL}}$$

$$Q_{66} = G_{LT}$$

where E_L and E_T are the elastic moduli in the longitudinal and transverse directions respectively, G_{LT} is the shear modulus, ν_{LT} and ν_{TL} are the major and minor Poisson ratios.

The similar stress-strain relation for an orthotropic lamina referred to arbitrary axes can be expressed as:

$$\begin{Bmatrix}\sigma_x\\ \sigma_y\\ \tau_{xy}\end{Bmatrix} = \begin{bmatrix}\overline{Q}_{11} & \overline{Q}_{12} & \overline{Q}_{16}\\ \overline{Q}_{12} & \overline{Q}_{22} & \overline{Q}_{26}\\ \overline{Q}_{16} & \overline{Q}_{26} & \overline{Q}_{66}\end{bmatrix}\begin{Bmatrix}\varepsilon_x\\ \varepsilon_y\\ \frac{1}{2}\gamma_{xy}\end{Bmatrix} = [\mathrm{T}]^{-1}\begin{bmatrix}Q_{11} & Q_{12} & 0\\ Q_{12} & Q_{22} & 0\\ 0 & 0 & 2Q_{66}\end{bmatrix}[\mathrm{T}]\begin{Bmatrix}\varepsilon_x\\ \varepsilon_y\\ \frac{1}{2}\gamma_{xy}\end{Bmatrix} \tag{3.6}$$

Thus, the relationship between $[\overline{Q}]$ and $[Q]$ matrix can be expressed as (Agarwal and Broutman 1990):

$$\overline{Q}_{11} = Q_{11}\cos^4\theta + Q_{22}\sin^4\theta + 2(Q_{12}+2Q_{66})\sin^2\theta\cos^2\theta$$

$$\overline{Q}_{22} = Q_{11}\sin^4\theta + Q_{22}\cos^4\theta + 2(Q_{12}+2Q_{66})\sin^2\theta\cos^2\theta$$

$$\overline{Q}_{12} = (Q_{11}+Q_{22}-4Q_{66})\sin^2\theta\cos^2\theta + Q_{12}(\cos^4\theta+\sin^4\theta)$$

$$\overline{Q}_{66} = (Q_{11}+Q_{22}-2Q_{12}-2Q_{66})\sin^2\theta\cos^2\theta + Q_{66}(\cos^4\theta+\sin^4\theta)$$

$$\overline{Q}_{16} = (Q_{11}-Q_{12}-2Q_{66})\cos^3\theta\sin\theta - (Q_{22}-Q_{12}-2Q_{66})\cos\theta\sin^3\theta$$

$$\overline{Q}_{26} = (Q_{11}-Q_{12}-2Q_{66})\cos\theta\sin^3\theta - (Q_{22}-Q_{12}-2Q_{66})\cos^3\theta\sin\theta \tag{3.7}$$

3.2.2 Synthesis of stiffness matrix for composite laminate plates

The synthesis of the stiffness matrix for composite laminate plate is achieved by considering the equivalent system of forces and moments acting on the laminate cross

section. The equivalent system of forces and moments are obtained by integrating the corresponding stress and the stress times the moment arm through the laminate thickness h.

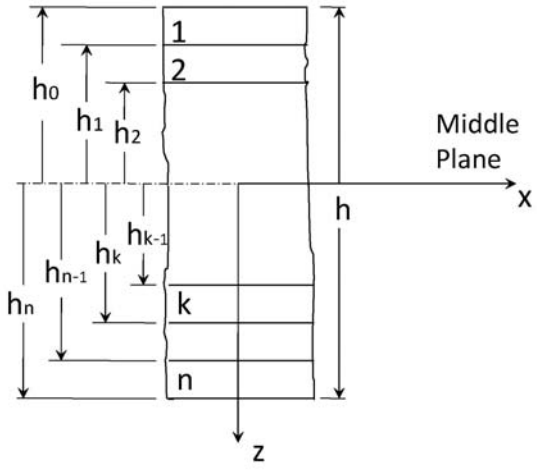

Figure 3.3 Geometry of multilayered laminate

The synthesized stiffness matrices can be obtained as (Agarwal and Broutman 1990):

$$A_{ij} = \sum_{k=1}^{n} \left(\overline{Q}_{ij}\right)_k (h_k - h_{k-1})$$

$$B_{ij} = \frac{1}{2}\sum_{k=1}^{n} \left(\overline{Q}_{ij}\right)_k (h_k^2 - h_{k-1}^2) \qquad (3.8)$$

$$D_{ij} = \frac{1}{3}\sum_{k=1}^{n} \left(\overline{Q}_{ij}\right)_k (h_k^3 - h_{k-1}^3)$$

The three matrices $[A]$, $[B]$ and $[D]$ are called the extensional stiffness matrix, coupling stiffness matrix and bending stiffness matrix. The forces and moments can be expressed as (Agarwal and Broutman 1990; Reddy 1997):

$$\begin{Bmatrix} N \\ M \end{Bmatrix} = \begin{bmatrix} A & B \\ B & D \end{bmatrix} \begin{Bmatrix} \varepsilon^0 \\ k \end{Bmatrix} \qquad (3.9)$$

where $\varepsilon^0 = \begin{Bmatrix} \varepsilon_x^0 \\ \varepsilon_y^0 \\ \gamma_{xy}^0 \end{Bmatrix}$ are the mid plane strains, $k = \begin{Bmatrix} k_x \\ k_y \\ k_{xy} \end{Bmatrix}$ are the plate curvatures, $N = \begin{Bmatrix} N_x \\ N_y \\ N_{xy} \end{Bmatrix}$ are the resultant forces and $M = \begin{Bmatrix} M_x \\ M_y \\ M_{xy} \end{Bmatrix}$ are the resultant moments.

The extensional stiffness matrix$[A]$ relates the resultant forces to the mid-plane strains, and the bending stiffness matrix $[D]$ relates the resultant moments to the plate curvatures. The coupling matrix $[B]$ implies the coupling between bending and extension of the plate, which means, the normal and shear forces acting at the mid-plane of the plate result in not only the in-plane deformations, but also twisting and bending motions.

3.3 Governing Equations for the Vibration of Composite Laminate Plates

If the thickness of the laminate is very small compared to the dimension of the plate, the classical laminated theory can be used to simplify the composite laminate plate as a single-layer anisotropic plate. The material properties, orientation, thickness of each plate can be taken into consideration in the stiffness matrices of the plate. The equations of motion of the composite laminate plate are coupled and thus very difficult to solve for the general solution of the displacements. However, at the high frequency, the following convergence study shows that the coupling can be neglected.

In the following convergence study, we take the angle-ply plates as an example. The equations of motion for free vibration of angle-ply plates with in-plane inertia neglected can be expressed as (Whitney and Ashton 1987):

$$A_{11}\frac{\partial^2 u}{\partial x^2} + A_{66}\frac{\partial^2 u}{\partial y^2} + (A_{12} + A_{66})\frac{\partial^2 v}{\partial x \partial y} - 3B_{16}\frac{\partial^3 w}{\partial x^2 \partial y} - B_{26}\frac{\partial^3 w}{\partial y^3} = 0$$

$$(A_{12} + A_{66})\frac{\partial^2 u}{\partial x \partial y} + A_{66}\frac{\partial^2 v}{\partial x^2} + A_{22}\frac{\partial^2 v}{\partial y^2} - B_{16}\frac{\partial^3 w}{\partial x^3} - 3B_{26}\frac{\partial^3 w}{\partial x \partial y^2} = 0$$

$$D_{11}\frac{\partial^4 w}{\partial x^4} + 2(D_{12} + 2D_{66})\frac{\partial^4 w}{\partial x^2 \partial y^2} + D_{22}\frac{\partial^4 w}{\partial y^4} - B_{16}\left(3\frac{\partial^3 u}{\partial x^2 \partial y} + \frac{\partial^3 v}{\partial x^3}\right)$$

$$-B_{26}\left(\frac{\partial^3 u}{\partial y^3} + 3\frac{\partial^3 v}{\partial x \partial y^2}\right) - \rho\omega^2 w = 0 \quad (3.10)$$

The frequency equation for the vibration of angle-ply laminate plate can be expressed as the following (Whitney and Ashton 1987):

$$\omega_{mn}^2 = \frac{\pi^4}{\rho R^4 b^4}\Big\{D_{11}m^4 + 2(D_{12} + 2D_{66})m^2 n^2 R^2 + D_{22}n^4 R^4 - \frac{1}{J_3}[m(B_{16}m^2 +$$

$$3B_{26}n^2 R^2)J_1 + nR(3B_{16}m^2 + B_{26}n^2 R^2)J_2]\Big\} \quad (3.11)$$

where:

$$J_1 = (A_{11}m^2 + A_{66}n^2 R^2)(B_{16}m^2 + 3B_{26}n^2 R^2)$$

$$- n^2 R^2 (A_{12} + A_{66})(3B_{16}m^2 + B_{26}n^2 R^2)$$

$$J_2 = (A_{66}m^2 + A_{22}n^2 R^2)(3B_{16}m^2 + B_{26}n^2 R^2)$$

$$- n^2 R^2 (A_{12} + A_{66})(B_{16}m^2 + 3B_{26}n^2 R^2)$$

$$J_3 = (A_{11}m^2 + A_{66}n^2 R^2)(A_{66}m^2 + A_{22}n^2 R^2) - (A_{12} + A_{66})m^2 n^2 R^2$$

$R = a/b$ is the ratio of the length and the width of the plate,

D_{ij} and B_{ij} are the bending and coupling stiffness of the plate.

When the effect of coupling is neglected, equation (10) becomes (Whitney and Ashton 1987):

$$\omega_{mn}^2 = \frac{\pi^4}{\rho R^4 b^4}[D_{11}m^4 + 2(D_{12} + 2D_{66})m^2 n^2 R^2 + D_{22}n^4 R^4] \quad (3.12)$$

A two-layer, square angle-ply plate is used to implement the convergence study. The properties of the laminate plate are as follows:

$$E_L = 25Gpa, E_L/E_T = 40;\ G_{LT}/E_T = 0.6, \nu_{LT} = 0.25 \quad (3.13)$$

The exact frequency and the frequency with the coupling effect neglected are calculated and plotted with respect to the increase of mode number for three different angles of angle-ply laminate plates. The results are show in Figure 3.4.

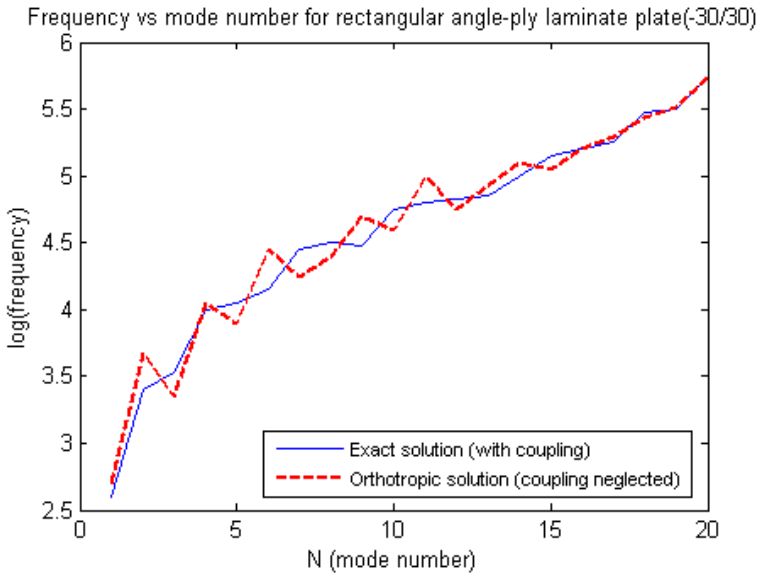

(a) -30/30 angle-ply

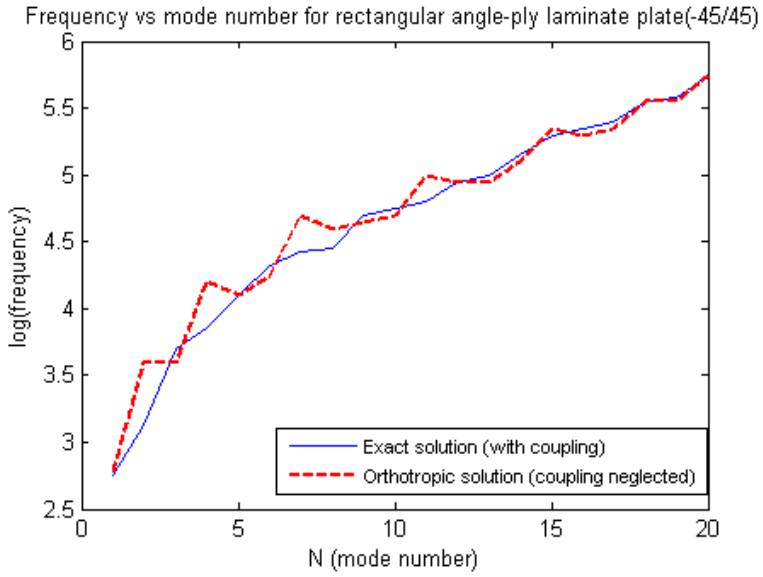

(b) -45/45 angle-ply

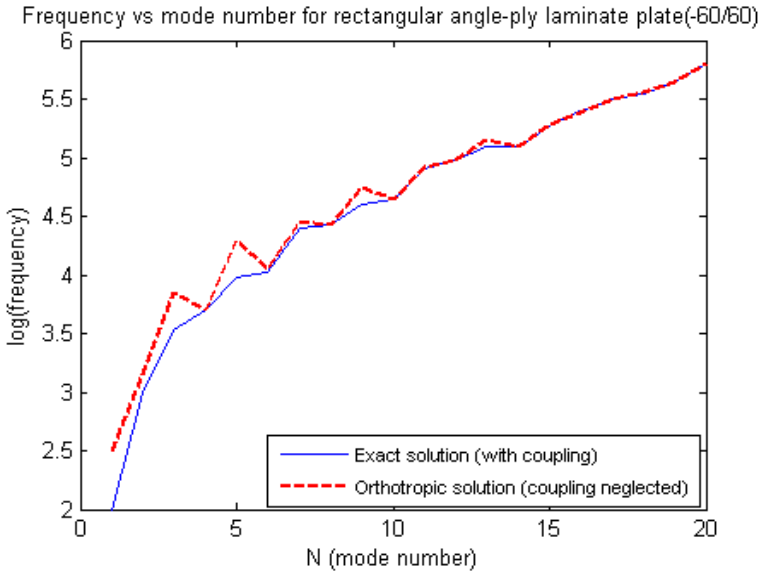

(c) -60/60 angle-ply

Figure 3.4 Exact and approximate frequencies for the angle-ply laminate plate

From Figure 3.4, we can see that with the increasing of mode number, the difference of the frequency between the exact (with coupling) and approximate (coupling neglected) solution becomes insignificant. The similar tendency is also found for the other types of laminate plates. Thus, the coupling terms are neglected at high frequency for the following derivations of EFEA formulations.

After dropping the non-linear and coupling terms, the general equation governing the out-of-plane and in-plane vibration of a composite laminated plate can be expressed as the following (Reddy 1997; Reddy 2004):

$$D_{11}\frac{\partial^4 w}{\partial x^4} + 4D_{16}\frac{\partial^4 w}{\partial x^3 \partial y} + 2(D_{12} + 2D_{66})\frac{\partial^4 w}{\partial x^2 \partial y^2} + 4D_{26}\frac{\partial^4 w}{\partial x \partial y^3} + D_{22}\frac{\partial^4 w}{\partial y^4} + m\frac{\partial^2 w}{\partial t^2}$$

$$= F\delta(x - x_0)(y - y_0)e^{i\omega t} \qquad (3.14)$$

$$A_{11}\frac{\partial^2 u}{\partial x^2} + 2A_{16}\frac{\partial^2 u}{\partial x \partial y} + A_{66}\frac{\partial^2 u}{\partial y^2} + A_{16}\frac{\partial^2 v}{\partial x^2} + (A_{12} + A_{66})\frac{\partial^2 v}{\partial x \partial y} + A_{26}\frac{\partial^2 v}{\partial y^2} = \rho\frac{\partial^2 u}{\partial t^2} \qquad (3.15)$$

$$A_{16}\frac{\partial^2 u}{\partial x^2}+(A_{12}+A_{66})\frac{\partial^2 u}{\partial x\partial y}+A_{26}\frac{\partial^2 u}{\partial y^2}+A_{66}\frac{\partial^2 v}{\partial x^2}+2A_{26}\frac{\partial^2 v}{\partial x\partial y}+A_{22}\frac{\partial^2 v}{\partial y^2}=\rho\frac{\partial^2 v}{\partial t^2} \quad (3.16)$$

where D_{ij} are the bending stiffness, A_{ij} are the extensional stiffness, they can both be obtained from the properties of each ply in the laminate, w is the transverse displacement of the plate, u, v are the x and y components of in-plane displacement in the middle plane of the plate.

3.4 EFEA Development for the Flexural Waves in Composite Laminate Plates

3.4.1 Wave solution of displacement and the dispersion relation for flexural waves

The general form of the far-field solution of the equation of motion can be obtained by considering the plane wave motion (Langley 1996):

$$w_{ff}(x,y,t)=Ae^{-i(k_x x+k_y y)}e^{i\omega t} \quad (3.17)$$

where A is the constant associated with the amplitude of propagating wave, k_x and k_y are complex wave numbers associated with the damped frequency of oscillation in the x and y directions.

$$k_x=k_{xl}(1-i\tfrac{\eta}{4}),\ k_y=k_{yl}(1-i\tfrac{\eta}{4}) \quad (3.18)$$

where k_{xl} and k_{yl} are the real parts of wave numbers k_x and k_y.

Substituting the far-field solution to the equation of motion, we can get the dispersion relation as follows (Langley 1996):

$$D_{11}k_{xl}^4+4D_{16}k_{xl}^3k_{yl}+2(D_{12}+2D_{66})k_{xl}^2k_{yl}^2+4D_{16}k_{xl}k_{yl}^3+D_{22}k_{yl}^4=m\omega^2 \quad (3.19)$$

Let k be the total wave number in the plate, k_{xl} and k_{yl} can be expressed as the x and y components of k as:

$$k_{xl} = k\cos\theta$$

$$k_{yl} = k\sin\theta \tag{3.20}$$

where θ is the angle of wave propagation.

Substituting the above relationship into the dispersion relationship (3.19) yields the expression of total wave number k in terms of the wave propagation angle θ.

$$k = \left[\frac{m\omega^2}{D_{11}\cos^4\theta + 4D_{16}\cos^3\theta\sin\theta + 2(D_{12}+2D_{66})\cos^2\theta\sin^2\theta + 4D_{16}\cos\theta\sin^3\theta + D_{22}\sin^4\theta}\right]^{1/4} \tag{3.21}$$

Because of the anisotropy of the composite laminate plate, the wave numbers in the composite laminate plate depend on the direction of the wave propagation. In the EFEA, the diffuse wave fields are assumed to exist in the plate. Thus, we need to take the average of wave numbers by integrating it from 0 to 2π.

Integrate them over θ, and we can obtain the averaged wave numbers.

$$k_{xl}^* = \frac{1}{2\pi}\int_0^{2\pi} k\cos\theta d\theta$$

$$k_{yl}^* = \frac{1}{2\pi}\int_0^{2\pi} k\sin\theta d\theta \tag{3.22}$$

At small damping, averaged complex wave numbers k_x^* and k_y^* can be expressed approximated by the averaged wave numbers as (Bouthier and Bernhard 1992; Park, Hong et al. 2003):

$$k_x^* = k_{xl}^*\left(1 - i\frac{\eta}{4}\right)$$

$$k_y^* = k_{yl}^*\left(1 - i\frac{\eta}{4}\right) \tag{3.23}$$

3.4.2 Derivation of time- and space- averaged energy density and intensities

Energy density is the amount of energy stored in a given system or region of space per unit volume. Energy intensity is known as the amount of energy transported past a given area of the medium per unit of time.

The total energy density is the sum of the kinetic and potential energy densities. The time-averaged total energy density of the laminated plate can be expressed in terms of the displacement as (Jones 1999):

$$\langle e \rangle = \frac{1}{4} Re \left\{ D_{11} \frac{\partial^2 w}{\partial x^2} \left(\frac{\partial^2 w}{\partial x^2} \right)^* + 2D_{12} \frac{\partial^2 w}{\partial x^2} \left(\frac{\partial^2 w}{\partial y^2} \right)^* + D_{22} \frac{\partial^2 w}{\partial y^2} \left(\frac{\partial^2 w}{\partial y^2} \right)^* + 4D_{66} \frac{\partial^2 w}{\partial x \partial y} \left(\frac{\partial^2 w}{\partial x \partial y} \right)^* + 4D_{16} \frac{\partial^2 w}{\partial x^2} \left(\frac{\partial^2 w}{\partial x \partial y} \right)^* + 4D_{26} \frac{\partial^2 w}{\partial y^2} \left(\frac{\partial^2 w}{\partial x \partial y} \right)^* + m \frac{\partial w}{\partial t} \left(\frac{\partial w}{\partial t} \right)^* \right\} \quad (3.24)$$

The x and y components of the time-averaged intensity of a laminated plate can be expressed by the forces and moments of the plate (Park, Hong et al. 2003):

$$\langle I_x \rangle = \frac{1}{2} Re \left\{ -Q_{xz} \left(\frac{\partial w}{\partial t} \right)^* + M_x \left(\frac{\partial^2 w}{\partial x \partial t} \right)^* + M_{xy} \left(\frac{\partial^2 w}{\partial y \partial t} \right)^* \right\} \quad (3.25)$$

$$\langle I_y \rangle = \frac{1}{2} Re \left\{ -Q_{yz} \left(\frac{\partial w}{\partial t} \right)^* + M_y \left(\frac{\partial^2 w}{\partial y \partial t} \right)^* + M_{yx} \left(\frac{\partial^2 w}{\partial x \partial t} \right)^* \right\} \quad (3.26)$$

For the laminate plate, the bending moments, twisting moments and the shear forces can be expressed in terms of the displacement as the following (Whitney and Ashton 1987):

$$M_x = -\left(D_{11} \frac{\partial^2 w}{\partial x^2} + D_{12} \frac{\partial^2 w}{\partial y^2} + 2D_{16} \frac{\partial^2 w}{\partial x \partial y} \right)$$

$$M_y = -\left(D_{12} \frac{\partial^2 w}{\partial x^2} + D_{22} \frac{\partial^2 w}{\partial y^2} + 2D_{26} \frac{\partial^2 w}{\partial x \partial y} \right)$$

$$M_{xy} = M_{xy} = -\left(D_{16} \frac{\partial^2 w}{\partial x^2} + D_{26} \frac{\partial^2 w}{\partial y^2} + 2D_{66} \frac{\partial^2 w}{\partial x \partial y} \right) \quad (3.27)$$

$$Q_{xz} = -\left(D_{11} \frac{\partial^3 w}{\partial x^3} + (D_{12} + 2D_{66}) \frac{\partial^3 w}{\partial x \partial y^2} + 3D_{16} \frac{\partial^3 w}{\partial x^2 \partial y} + D_{26} \frac{\partial^3 w}{\partial y^3} \right)$$

$$Q_{yz} = -\left(D_{22}\frac{\partial^3 w}{\partial y^3} + (D_{12} + 2D_{66})\frac{\partial^3 w}{\partial x^2 \partial y} + 3D_{26}\frac{\partial^3 w}{\partial x \partial y^2} + D_{16}\frac{\partial^3 w}{\partial x^3}\right) \tag{3.28}$$

Substituting the far-field displacement solution into the expressions and taking the spatial average of the time-averaged energy density and intensities yield the time- and space- averaged energy density and energy intensities (Fahy 1982):

$$\langle \underline{e} \rangle = \frac{k_{xl}^* k_{yl}^*}{\pi^2} \int_0^{\pi/k_{yl}^*} \int_0^{\pi/k_{xl}^*} \langle e \rangle dx dy \tag{3.29}$$

$$\langle \underline{I_x} \rangle = \frac{k_{xl}^* k_{yl}^*}{\pi^2} \int_0^{\pi/k_{yl}^*} \int_0^{\pi/k_{xl}^*} \langle I_x \rangle dx dy \tag{3.30}$$

$$\langle \underline{I_y} \rangle = \frac{k_{xl}^* k_{yl}^*}{\pi^2} \int_0^{\pi/k_{yl}^*} \int_0^{\pi/k_{xl}^*} \langle I_y \rangle dx dy \tag{3.31}$$

The time-averaged energy density and intensities are taken averaged over a half wavelength for the above expressions. When the damping is small, all of the second order and higher terms of the damping loss factor are neglected. After some manipulations, the simplified expressions for the time- and space- averaged energy density and intensities can be found as the following (see Appendix):

$$\begin{aligned}\langle \underline{e} \rangle = {} & \frac{1}{4}\left[D_{11}{k_{xl}^*}^4 + 2(D_{12} + 2D_{66}){k_{xl}^*}^2{k_{yl}^*}^2 + D_{22}{k_{yl}^*}^4 + m\omega^2\right](|A|^2 e^{--} + |B|^2 e^{+-} + \\ & |C|^2 e^{-+} + |D|^2 e^{++}) \\ & + \left(D_{16}{k_{xl}^*}^3 k_{yl}^* + D_{26} k_{xl}^* {k_{yl}^*}^3\right)(|A|^2 e^{--} - |B|^2 e^{+-} - |C|^2 e^{-+} + |D|^2 e^{++}) \\ = {} & \langle \underline{e} \rangle_1 + \langle \underline{e} \rangle_2 \end{aligned} \tag{3.32}$$

$$\begin{aligned}\langle \underline{I_x} \rangle = {} & \omega\left[D_{11}{k_{xl}^*}^3 + (D_{12} + 2D_{66})k_{xl}^*{k_{yl}^*}^2\right](|A|^2 e^{--} - |B|^2 e^{+-} + |C|^2 e^{-+} - |D|^2 e^{++}) \\ & + \omega\left[3D_{16}{k_{xl}^*}^2 k_{yl}^* + D_{26}{k_{yl}^*}^3\right](|A|^2 e^{--} + |B|^2 e^{+-} - |C|^2 e^{-+} - |D|^2 e^{++}) \\ = {} & \langle \underline{I_x} \rangle_1 + \langle \underline{I_x} \rangle_2 \end{aligned} \tag{3.33}$$

$$\begin{aligned}\langle \underline{I_y} \rangle = {} & \omega\left[D_{22}{k_{yl}^*}^3 + (D_{12} + 2D_{66}){k_{xl}^*}^2 k_{yl}^*\right](|A|^2 e^{--} + |B|^2 e^{+-} - |C|^2 e^{-+} - |D|^2 e^{++}) \\ & + \omega\left[3D_{26}k_{xl}^*{k_{yl}^*}^2 + D_{16}{k_{xl}^*}^3\right](|A|^2 e^{--} - |B|^2 e^{+-} + |C|^2 e^{-+} - |D|^2 e^{++})\end{aligned}$$

$$= \langle \underline{I}_y \rangle_1 + \langle \underline{I}_y \rangle_2 \tag{3.34}$$

where $e^{\pm\pm}$ represents $exp\left\{\pm\frac{\eta}{2}k_{xl}^{*}x \pm \frac{\eta}{2}k_{yl}^{*}y\right\}$, $\langle \underline{e} \rangle, \langle \underline{I}_x \rangle$ and $\langle \underline{I}_y \rangle$ represent the time- and space-averaged energy density and energy intensities.

3.4.3 Derivation of EFEA differential equation and its variational statement

By observing the expressions of time- and space- averaged energy density and intensities, we can find that the two parts of the x and y components of the time- and space-averaged intensities are proportional to the first derivatives of two parts of the time- and space-averaged energy density with respect to x and y:

$$\langle \underline{I}_x \rangle_1 = \alpha_1 \frac{\partial \langle \underline{e} \rangle_1}{\partial x},\ \langle \underline{I}_y \rangle_1 = \beta_1 \frac{\partial \langle \underline{e} \rangle_1}{\partial y} \tag{3.35}$$

$$\langle \underline{I}_x \rangle_2 = \alpha_2 \frac{\partial \langle \underline{e} \rangle_2}{\partial x},\ \langle \underline{I}_y \rangle_2 = \beta_2 \frac{\partial \langle \underline{e} \rangle_2}{\partial y} \tag{3.36}$$

where $\alpha_1, \beta_1, \alpha_2, \beta_2$ are the four coefficients that can be expressed in terms of the stiffness, frequency and wave numbers:

$$\alpha_1 = \frac{-8\omega\left[D_{11}{k_{xl}^{*}}^2 + (D_{12}+2D_{66}){k_{yl}^{*}}^2\right]}{\eta\left[D_{11}{k_{xl}^{*}}^4 + 2(D_{12}+2D_{66}){k_{xl}^{*}}^2{k_{yl}^{*}}^2 + D_{22}{k_{yl}^{*}}^4 + m\omega^2\right]}$$

$$\beta_1 = \frac{-8\omega\left[D_{22}{k_{yl}^{*}}^2 + (D_{12}+2D_{66}){k_{xl}^{*}}^2\right]}{\eta\left[D_{11}{k_{xl}^{*}}^4 + 2(D_{12}+2D_{66}){k_{xl}^{*}}^2{k_{yl}^{*}}^2 + D_{22}{k_{yl}^{*}}^4 + m\omega^2\right]}$$

$$\alpha_2 = \frac{-8\omega\left(3D_{16}{k_{xl}^{*}}^2 k_{yl}^{*} + D_{26}{k_{yl}^{*}}^3\right)}{\eta k_{xl}^{*}\left(D_{16}{k_{xl}^{*}}^3 k_{yl}^{*} + D_{26}k_{xl}^{*}{k_{yl}^{*}}^3\right)}$$

$$\beta_2 = \frac{-8\omega\left(3D_{26}k_{xl}^{*}{k_{yl}^{*}}^2 + D_{16}{k_{xl}^{*}}^3\right)}{\eta k_{yl}^{*}\left(D_{16}{k_{xl}^{*}}^3 k_{yl}^{*} + D_{26}k_{xl}^{*}{k_{yl}^{*}}^3\right)}$$

Considering the isotropic plate case, the bending stiffness can be expressed as:

$$D_{11} = D_{22} = \frac{Et^3}{12(1-\nu^2)} = D,\ D_{12} = \frac{E\nu t^3}{12(1-\nu^2)},\ D_{66} = \frac{Et^3}{24(1+\nu)},\ D_{16} = D_{26} = 0 \tag{3.37}$$

where E is the Young's modulus and t is the thickness of the plate.

Thus, for isotropic plate, the four coefficients can be simplified as:

$$\alpha_1 = \beta_1 = -\frac{C_g^2}{\eta\omega},\ \alpha_2 = \beta_2 = 0$$

where $C_g = 2\left(\frac{\omega^2 D}{m}\right)^{1/4}$ is the group speed of the isotropic plate.

Therefore, for the isotropic plate, the following relationship can be obtained:

$$\langle \vec{\underline{I}} \rangle = -\frac{C_g^2}{\eta\omega}\nabla\langle \underline{e} \rangle \tag{3.38}$$

Equation (3.38) is the relationship between the time- and space- energy density and intensities of isotropic plates; it appears same as equation (2.9). It is obtained as a special case in our derivation and it appeared same as in (Bouthier and Bernhard 1992).

Considering a power balance at a steady state over a differential control volume of the plate, the power balance equation can be written as (Bouthier and Bernhard 1992; Bouthier and Bernhard 1995):

$$\langle \underline{\Pi}_{in} \rangle = \langle \underline{\Pi}_{diss} \rangle + \nabla\langle \vec{\underline{I}} \rangle \tag{3.39}$$

where the dissipated power and energy density can be expressed in the following relationship (Cremer, Heckl et al. 1973):

$$\langle \underline{\Pi}_{diss} \rangle = \eta\omega\langle \underline{e} \rangle \tag{3.40}$$

Using the relationship between the dissipated power and energy density and the relationship between energy density and energy intensity, the EFEA differential equation with energy density as the primary variable can be obtained for the bending wave motion of composite laminate plates:

$$\left(\alpha_1 \frac{\partial^2}{\partial x^2} + \beta_1 \frac{\partial^2}{\partial y^2}\right)\langle \underline{e} \rangle_1 + \left(\alpha_2 \frac{\partial^2}{\partial x^2} + \beta_2 \frac{\partial^2}{\partial y^2}\right)\langle \underline{e} \rangle_2 + \eta\omega\left(\langle \underline{e} \rangle_1 + \langle \underline{e} \rangle_2\right)$$
$$= \langle \underline{\Pi}_{in} \rangle_1 + \langle \underline{\Pi}_{in} \rangle_2 \tag{3.41}$$

In the EFEA differential equation, we made the assumption that the input power splits into two parts. The subscript 1 corresponds to the stiffness coefficients $D_{11}, D_{22}, D_{12}, D_{66}$, which correspond to the orthotropic plate, and the subscripts 2 corresponds to the stiffness $D_{16}$and D_{26}.

In order to prove the above assumption of input power, we did the following validation. A NASTRAN model is used to obtain the results in FEA model and a Fourier expansion method is employed to obtain the results from EFEA formulation.

The analytic solution is obtained from the double Fourier series solution (Park, Hong et al. 2003) to the out-of-plane equation of motion of a finite composite laminate plate (3.14). It can be expresses as:

$$w(x,y,t) = \sum_{m=0}^{\infty}\sum_{n=0}^{\infty} W_{mn} \sin\left(\frac{m\pi x}{L_x}\right)\cos\left(\frac{n\pi y}{L_y}\right)e^{i\omega t} \tag{3.42}$$

where W_{mn} is the coefficient of (m,n) mode of the displacement, L_x, L_y are the dimension of the finite composite laminate plate. W_{mn} can be solved by substituting equation (3.42) into equation (3.14).

$$W_{mn} = \frac{\frac{4}{L_x L_y} F \sin\left(\frac{m\pi x_0}{L_x}\right)\cos\left(\frac{n\pi y_0}{L_y}\right)}{D_{11}\left(\frac{m\pi}{L_x}\right)^4 + 4D_{16}\left(\frac{m\pi}{L_x}\right)^3\left(\frac{n\pi}{L_y}\right) + 2(D_{12}+2D_{66})\left(\frac{m\pi}{L_x}\right)^2\left(\frac{n\pi}{L_y}\right)^2 + 4D_{26}\left(\frac{m\pi}{L_x}\right)\left(\frac{n\pi}{L_y}\right)^3 + D_{22}\left(\frac{n\pi}{L_y}\right)^4 - m\omega^2} \tag{3.43}$$

The input power can be expressed in terms of the force and the velocity as (Cremer, Heckl et al. 1973):

$$\Pi_{in} = \frac{1}{2}\mathrm{Re}\left\{\left(Fe^{i\omega t}\right) \times \left(\frac{\partial w(x_0,y_0,t}{\partial t}\right)^*\right\} \tag{3.44}$$

From equation (3.44), the input power for the composite laminate plate and the corresponding orthotropic plate is calculated and the results are compared with the ones obtained from very dense FEA model. Figure 3.5 presents the comparison of the input power computed by the FEA model and the input power derived from the EFEA

formulation for the same laminate plate. Very good agreement is observed between the two sets of results.

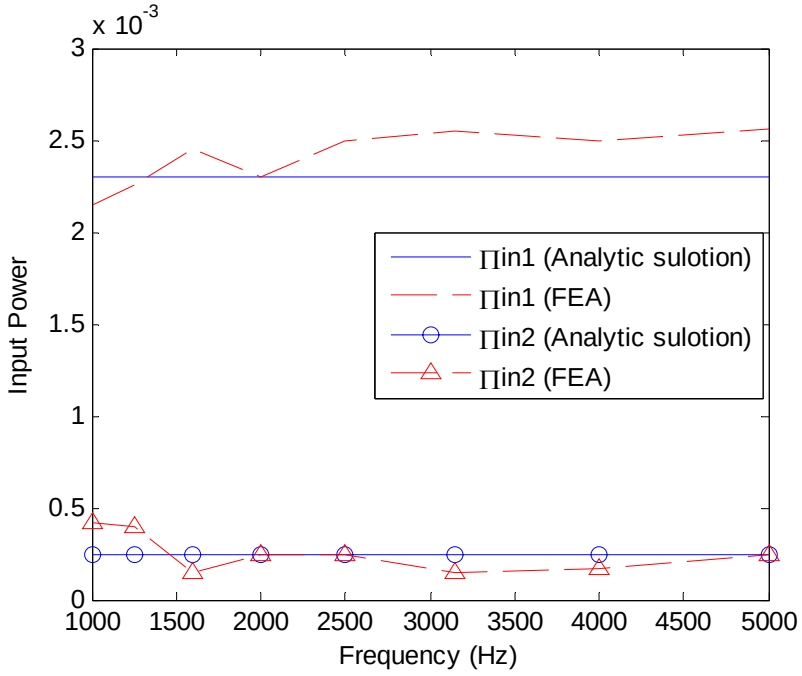

Figure 3.5 Input power comparison between FEA and analytic solutions

To develop a variational statement of the energy density differential equation (3.41), we get the linear equation:

$$P_i^1 + \sum\langle \underline{e}_j \rangle_1 K_{ij}^1 + \sum\langle \underline{e}_j \rangle_1 M_{ij}^1 - F_i^1 = 0 \tag{3.45}$$

$$P_i^2 + \sum\langle \underline{e}_j \rangle_2 K_{ij}^2 + \sum\langle \underline{e}_j \rangle_2 M_{ij}^2 - F_i^2 = 0 \tag{3.46}$$

The terms are:

$$P_i^{1,2} = \int_\Gamma \Phi_\mathrm{i} \left(\alpha_{1,2} \frac{\partial \langle \underline{e} \rangle_{1,2}}{\partial x} \vec{\imath} + \beta_{1,2} \frac{\partial \langle \underline{e} \rangle_{1,2}}{\partial y} \vec{\jmath}\right) \cdot \vec{n} d\Gamma$$

$$K_{ij}^{1,2} = -\int_D \left(\alpha_{1,2} \frac{\partial \Phi_\mathrm{i}}{\partial x} \frac{\partial \Phi_\mathrm{j}}{\partial x} + \beta_{1,2} \frac{\partial \Phi_\mathrm{i}}{\partial y} \frac{\partial \Phi_\mathrm{j}}{\partial y}\right) dD$$

$$M_{ij}^{1,2} = \int_D \eta\omega\left(\Phi_\mathrm{i} \Phi_\mathrm{j}\right) dD$$

$$F_i^{1,2} = \int_D \Phi_\mathrm{i} \langle \underline{\Pi}_{in} \rangle_{1,2} dD$$

A linear matrix equation can be developed as:

$$[K^{1,2} + M^{1,2}]\langle \underline{e} \rangle_{1,2} + P^{1,2} - F^{1,2} = 0 \quad (3.47)$$

The subscript 1 corresponds to the stiffness coefficients $D_{11}, D_{22}, D_{12}, D_{66}$, which correspond to the orthotropic plate, and the subscripts 2 corresponds to the stiffness $D_{16}$and D_{26}. After getting the matrix formulation of the EFEA differential equation, we are able to solve the differential equation numerically.

3.5 EFEA Development for the In-plane Waves in Composite Laminate Plates

3.5.1 Displacement solution the dispersion relationship for in-plane waves

The equations governing the in-plane vibration of the composite laminate plate have been expressed in equations (3.15) and (3.16). Since the two displacement components u and v are coupled with each other in the equations, it is difficult to obtain the general displacement solution of the equations. However, the solution can be obtained by using a displacement vector (Park, Hong et al. 2001):

$$\vec{d}(x, y, t) = \nabla\varphi(x, y, t) + \nabla \times \psi(x, y, t) \quad (3.48)$$

where $\varphi(x, y, t)$ is a scalar quantity that represents the displacement potential which corresponding to the dilational motion of the plate, $\psi(x, y, t)$ is the a vector quantity that represents the displacement potential which corresponds to the rotational motion of the plate.

Substituting equation (3.48) into the plate's in-plane equations of motion, we can obtain the solution of the two displacement potentials and thus get the expression of u and v from equation (3.48).

$\varphi(x, y, t)$ can be expressed as (Park, Hong et al. 2001):

$$\varphi(x,y,t) = \left\{A_l e^{-i(k_{lx}x+k_{ly}y)} + B_l e^{i(k_{lx}x-k_{ly}y)} + C_l e^{-i(k_{lx}x-k_{ly}y)} + D_l e^{i(k_{lx}x+k_{ly}y)}\right\} e^{i\omega t} \tag{3.49}$$

where k_{lx}, k_{ly} are the x and y components of the complex longitudinal wavenumber k_l.

The longitudinal wave component u_l and v_l of the in-plane displacements u and v can be written as:

$$u_l(x,y,t) = \frac{\partial \varphi}{\partial x} = \cos\theta_l \left\{Ae^{-i(k_{lx}x+k_{ly}y)} - Be^{i(k_{lx}x-k_{ly}y)} + Ce^{-i(k_{lx}x-k_{ly}y)} - De^{i(k_{lx}x+k_{ly}y)}\right\} e^{i\omega t} \tag{3.50}$$

$$v_l(x,y,t) = \frac{\partial \varphi}{\partial y} = \sin\theta_l \left\{Ae^{-i(k_{lx}x+k_{ly}y)} + Be^{i(k_{lx}x-k_{ly}y)} - Ce^{-i(k_{lx}x-k_{ly}y)} - De^{i(k_{lx}x+k_{ly}y)}\right\} e^{i\omega t} \tag{3.51}$$

where $A = -ik_lA_l, B = -ik_lB_l, C = -ik_lC_l, D = -ik_lD_l, \cos\theta_l = k_{lx}/k_l$ and $\sin\theta_l = k_{ly}/k_l$.

$\psi(x,y,t)$ can be expressed as (Park, Hong et al. 2001):

$$\psi(x,y,t) = \left\{A_s e^{-i(k_{sx}x+k_{sy}y)} + B_s e^{i(k_{sx}x-k_{sy}y)} + C_s e^{-i(k_{sx}x-k_{sy}y)} + D_s e^{i(k_{sx}x+k_{sy}y)}\right\} e^{i\omega t} \tag{3.52}$$

where k_{sx}, k_{sy} are the x and y components of the complex in-plane shear wavenumber k_s.

Thus, the in-plane shear wave components u_s and v_s of the in-plane displacements shear u and v can be written as:

$$u_s(x,y,t) = -\frac{\partial \psi}{\partial y} = \sin\theta_s \left\{-Ae^{-i(k_{sx}x+k_{sy}y)} - Be^{i(k_{sx}x-k_{sy}y)} + Ce^{-i(k_{sx}x-k_{sy}y)} + De^{i(k_{sx}x+k_{sy}y)}\right\} e^{i\omega t} \tag{3.53}$$

$$v_s(x,y,t) = \frac{\partial \psi}{\partial x} = \cos\theta_s \left\{Ae^{-i(k_{sx}x+k_{sy}y)} - Be^{i(k_{sx}x-k_{sy}y)} + Ce^{-i(k_{sx}x-k_{sy}y)} - De^{i(k_{sx}x+k_{sy}y)}\right\} e^{i\omega t} \tag{3.54}$$

where $A = -ik_s A_s, B = -ik_s B_s, C = -ik_s C_s, D = -ik_s D_s, \cos\theta_s = k_{sx}/k_s$ and $\sin\theta_s = k_{sy}/k_s$.

3.5.2 Derivation of time- and space- averaged energy density and intensities

The time-averaged total energy density of the in-plane vibration of thin composite laminate plates can be written as:

$$\langle e \rangle = \frac{1}{4} Re\left\{\left[A_{11}\frac{\partial u}{\partial x} + A_{12}\frac{\partial v}{\partial y} + A_{16}\left(\frac{\partial u}{\partial y} + \frac{\partial v}{\partial x}\right)\right]\left(\frac{\partial u}{\partial x}\right)^* + \left[A_{12}\frac{\partial u}{\partial x} + A_{22}\frac{\partial v}{\partial y} + A_{26}\left(\frac{\partial u}{\partial y} + \frac{\partial v}{\partial x}\right)\right]\left(\frac{\partial v}{\partial y}\right)^* + \left[A_{16}\frac{\partial u}{\partial x} + A_{26}\frac{\partial v}{\partial y} + A_{66}\left(\frac{\partial u}{\partial y} + \frac{\partial v}{\partial x}\right)\right]\left(\frac{\partial u}{\partial y} + \frac{\partial v}{\partial x}\right) + \rho h\left[\left(\frac{\partial u}{\partial t}\right)\left(\frac{\partial u}{\partial t}\right)^* + \left(\frac{\partial v}{\partial t}\right)\left(\frac{\partial v}{\partial t}\right)^*\right]^*\right\} \quad (3.55)$$

The x and y components of the time-averaged in-plane vibration energy intensities of the composite laminate plate can be expressed as:

$$\langle I_x \rangle = -\frac{1}{2} Re\left\{\left[A_{11}\frac{\partial u}{\partial x} + A_{12}\frac{\partial v}{\partial y} + A_{16}\left(\frac{\partial u}{\partial y} + \frac{\partial v}{\partial x}\right)\right]\left(\frac{\partial u}{\partial t}\right)^* + \left[A_{16}\frac{\partial u}{\partial x} + A_{26}\frac{\partial v}{\partial y} + A_{66}\left(\frac{\partial u}{\partial y} + \frac{\partial v}{\partial x}\right)\right]\left(\frac{\partial v}{\partial t}\right)^*\right\} \quad (3.56)$$

$$\langle I_y \rangle = -\frac{1}{2} Re\left\{\left[A_{12}\frac{\partial u}{\partial x} + A_{22}\frac{\partial v}{\partial y} + A_{26}\left(\frac{\partial u}{\partial y} + \frac{\partial v}{\partial x}\right)\right]\left(\frac{\partial v}{\partial t}\right)^* + \left[A_{16}\frac{\partial u}{\partial x} + A_{26}\frac{\partial v}{\partial y} + A_{66}\left(\frac{\partial u}{\partial y} + \frac{\partial v}{\partial x}\right)\right]\left(\frac{\partial u}{\partial t}\right)^*\right\} \quad (3.57)$$

Substituting equations (3.50) and (3.51) into equations (3.55)-(3.57), and taking the spatial average of the time-averaged energy density and intensities over a half wavelength yield the time- and space- averaged energy density and energy intensities for the longitudinal motion of the plate.

$$\langle \underline{e} \rangle_l = \frac{1}{4}\Big\{\Big[(A_{11}+A_{22}-2A_{12})k_{xl}^2k_{yl}^2 + A_{66}\big(k_{xl}^2-k_{yl}^2\big)+\rho h\omega^2k^2\Big](|A|^2e^{--}+ |B|^2e^{+-}+\ |C|^2e^{-+}+|D|^2e^{++}) + \Big[2(A_{26}-A_{16})k_{xl}k_{yl}\big(k_{xl}^2-k_{yl}^2\big)\Big](|A|^2e^{--}- |B|^2e^{+-}-\ |C|^2e^{-+}+|D|^2e^{++})\Big\} \quad (3.58)$$

$$\langle \underline{I}_x \rangle_l = \frac{\omega}{2}\Big[k_{xl}\big(A_{11}k_{xl}^2+A_{12}k_{yl}^2\big)(|A|^2e^{--}-|B|^2e^{+-}+\ |C|^2e^{-+}-|D|^2e^{++}) + 2A_{16}k_{xl}^2k_{yl}(|A|^2e^{--}+|B|^2e^{+-}-\ |C|^2e^{-+}-|D|^2e^{++})\Big] \quad (3.59)$$

$$\langle \underline{I}_y \rangle_l = \frac{\omega}{2}\Big[k_{yl}\big(A_{12}k_{xl}^2+A_{22}k_{yl}^2\big)(|A|^2e^{--}+|B|^2e^{+-}-\ |C|^2e^{-+}-|D|^2e^{++}) + 2A_{26}k_{xl}k_{yl}^2(|A|^2e^{--}-|B|^2e^{+-}+\ |C|^2e^{-+}-|D|^2e^{++})\Big] \quad (3.60)$$

Similarly, the time- and space- averaged energy density and energy intensities for the in-plane shear waves can be derived by substituting equations (3.53) and (3.54) into equations (3.55)-(3.57):

$$\langle \underline{e} \rangle_s = \frac{1}{4}\Big\{\Big[(A_{11}+A_{22}-2A_{12}-2A_{66})k_{xl}^2k_{yl}^2 + A_{66}\big(k_{xl}^4+k_{yl}^4\big)+\rho h\omega^2k^2\Big](|A|^2e^{--}+ |B|^2e^{+-}+\ |C|^2e^{-+}+|D|^2e^{++}) + \Big[2(A_{16}-A_{26})k_{xl}k_{yl}\big(k_{yl}^2-k_{xl}^2\big)\Big](|A|^2e^{--}- |B|^2e^{+-}-\ |C|^2e^{-+}+|D|^2e^{++})\Big\} \quad (3.61)$$

$$\langle \underline{I}_x \rangle_s = -\frac{\omega}{2}\Big\{\Big[(-A_{11}+A_{12}+A_{66})k_{xl}k_{yl}^2 - A_{66}k_{xl}^3\Big](|A|^2e^{--}-|B|^2e^{+-}+\ |C|^2e^{-+}- |D|^2e^{++}) + \Big[(2A_{16}-A_{26})k_{xl}^2k_{yl} - A_{16}k_{yl}^3\Big](|A|^2e^{--}+|B|^2e^{+-}-\ |C|^2e^{-+}- |D|^2e^{++})\Big\} \quad (3.62)$$

$$\langle \underline{I}_y \rangle_s = -\frac{\omega}{2}\Big\{\Big[(A_{12}-A_{22}+A_{66})k_{xl}^2k_{yl} - A_{66}k_{yl}^3\Big](|A|^2e^{--}+|B|^2e^{+-}-\ |C|^2e^{-+}- |D|^2e^{++}) + \Big[(2A_{26}-A_{16})k_{xl}k_{yl}^2 - A_{26}k_{xl}^3\Big](|A|^2e^{--}-|B|^2e^{+-}+\ |C|^2e^{-+}- |D|^2e^{++})\Big\} \quad (3.63)$$

where $e^{\pm\pm}$ represents $exp\left\{\pm\frac{\eta}{2}k_{xl}^*x \pm \frac{\eta}{2}k_{yl}^*y\right\}$, $\langle \underline{e} \rangle$, $\langle \underline{I}_x \rangle$ and $\langle \underline{I}_y \rangle$ represent the time- and space-averaged energy density and energy intensities.

3.5.3 Derivation of EFEA differential equations for in-plane motions

Similar to section 3.4.3, we can find that for both longitudinal and in-plane shear wave motions, the two parts of the x and y components of the time- and space-averaged intensities are proportional to the first derivatives of two parts of the time- and space-averaged energy density with respect to x and y. The relationship similar to equations (3.35) and (3.36) can be found for the longitudinal and in-plane shear wave motions respectively.

For the longitudinal wave motion:

$$\langle \underline{I}_x \rangle_{l1} = \alpha_{l1} \frac{\partial \langle \underline{e} \rangle_{l1}}{\partial x},\ \langle \underline{I}_y \rangle_{l1} = \beta_{l1} \frac{\partial \langle \underline{e} \rangle_{l1}}{\partial y} \tag{3.64}$$

$$\langle \underline{I}_x \rangle_{l2} = \alpha_{l2} \frac{\partial \langle \underline{e} \rangle_{l2}}{\partial x},\ \langle \underline{I}_y \rangle_{l2} = \beta_{l2} \frac{\partial \langle \underline{e} \rangle_{l2}}{\partial y} \tag{3.65}$$

where $\alpha_{l1}, \beta_{l1}, \alpha_{l2}, \beta_{l2}$ are the four coefficients that can be expressed in terms of the stiffness, frequency and wave numbers:

$$\alpha_{l1} = \frac{-4\omega\left(A_{11}k_{xl}^2 + A_{12}k_{yl}^2\right)}{\eta\left[(A_{11}+A_{22}-2A_{12})k_{xl}^2k_{yl}^2 + A_{66}\left(k_{xl}^2 - k_{yl}^2\right) + \rho h\omega^2 k^2\right]}$$

$$\beta_{l1} = \frac{-4\omega\left(A_{12}k_{xl}^2 + A_{22}k_{yl}^2\right)}{\eta\left[(A_{11}+A_{22}-2A_{12})k_{xl}^2k_{yl}^2 + A_{66}\left(k_{xl}^2 - k_{yl}^2\right) + \rho h\omega^2 k^2\right]}$$

$$\alpha_{l2} = \frac{-8\omega A_{16}k_{xl}k_{yl}}{\eta\left[2(A_{26}-A_{16})k_{xl}k_{yl}\left(k_{xl}^2 - k_{yl}^2\right)\right]}$$

$$\beta_{l2} = \frac{-8\omega A_{26}k_{xl}k_{yl}}{\eta\left[2(A_{26}-A_{16})k_{xl}k_{yl}\left(k_{xl}^2 - k_{yl}^2\right)\right]}$$

For the in-plane shear wave motion:

$$\langle \underline{I}_x \rangle_{s1} = \alpha_{s1} \frac{\partial \langle \underline{e} \rangle_{s1}}{\partial x},\ \langle \underline{I}_y \rangle_{s1} = \beta_{s1} \frac{\partial \langle \underline{e} \rangle_{s1}}{\partial y} \tag{3.66}$$

$$\langle \underline{I}_x \rangle_{s2} = \alpha_{s2} \frac{\partial \langle \underline{e} \rangle_{s2}}{\partial x},\ \langle \underline{I}_y \rangle_{s2} = \beta_{s2} \frac{\partial \langle \underline{e} \rangle_{s2}}{\partial y} \tag{3.67}$$

where $\alpha_{s1}, \beta_{s1}, \alpha_{s2}, \beta_{s2}$ can be expressed as follows:

$$\alpha_{s1} = \frac{4\omega\left[(-A_{11}+A_{12}+A_{66})k_{yl}^2 - A_{66}k_{xl}^2\right]}{\eta\left[(A_{11}+A_{22}-2A_{12}-2A_{66})k_{xl}^2k_{yl}^2 + A_{66}\left(k_{xl}^4+k_{yl}^4\right)+\rho h\omega^2k^2\right]}$$

$$\beta_{s1} = \frac{4\omega\left[(A_{12}-A_{22}+A_{66})k_{xl}^2 - A_{66}k_{yl}^2\right]}{\eta\left[(A_{11}+A_{22}-2A_{12}-2A_{66})k_{xl}^2k_{yl}^2 + A_{66}\left(k_{xl}^4+k_{yl}^4\right)+\rho h\omega^2k^2\right]}$$

$$\alpha_{s2} = \frac{2\omega\left[(2A_{16}-A_{26})k_{xl}^2 - A_{16}k_{yl}^2\right]}{\eta k_{xl}^2(A_{16}-A_{26})\left(k_{yl}^2-k_{xl}^2\right)}$$

$$\beta_{s2} = \frac{2\omega\left[(2A_{26}-A_{16})k_{yl}^2 - A_{26}k_{xl}^2\right]}{\eta k_{yl}^2(A_{16}-A_{26})\left(k_{yl}^2-k_{xl}^2\right)}$$

Using the relationship between the dissipated power and energy density and the relationship between energy density and energy intensity, the EFEA differential equation with energy density as the primary variable can be obtained for the in-plane wave motion of composite laminate plates.

For longitudinal wave motion:

$$\left(\alpha_{l1}\frac{\partial^2}{\partial x^2} + \beta_{l1}\frac{\partial^2}{\partial y^2}\right)\langle \underline{e}\rangle_{l1} + \left(\alpha_{l2}\frac{\partial^2}{\partial x^2} + \beta_{l2}\frac{\partial^2}{\partial y^2}\right)\langle \underline{e}\rangle_{l2} + \eta\omega\left(\langle \underline{e}\rangle_{l1} + \langle \underline{e}\rangle_{l2}\right)$$
$$= \langle \underline{\Pi}_{in}\rangle_{l1} + \langle \underline{\Pi}_{in}\rangle_{l2} \tag{3.68}$$

For in-plane shear wave motion:

$$\left(\alpha_{s1}\frac{\partial^2}{\partial x^2} + \beta_{s1}\frac{\partial^2}{\partial y^2}\right)\langle \underline{e}\rangle_{s1} + \left(\alpha_{s2}\frac{\partial^2}{\partial x^2} + \beta_{s2}\frac{\partial^2}{\partial y^2}\right)\langle \underline{e}\rangle_{s2} + \eta\omega\left(\langle \underline{e}\rangle_{s1} + \langle \underline{e}\rangle_{s2}\right)$$
$$= \langle \underline{\Pi}_{in}\rangle_{s1} + \langle \underline{\Pi}_{in}\rangle_{s2} \tag{3.69}$$

3.6 Numerical Examples and Validation

In order to demonstrate the validity of the new EFEA formulation in composite laminate plates, the results from very dense FEA models are used to compare the results from the EFEA model of two types of laminate plates. In both examples, the bending motion of the plate is studied.

3.6.1 Two-layer cross-ply laminate plate

In this example, the vibration of a two-layer cross-ply composite laminate plate with several excitations on the plate is analyzed using FEA and EFEA models respectively at several different frequencies. The plate is a 1m×1m square cross-ply (0/90) plate with two layers of equal thickness. Layers with the following engineering constants are used:

$$E_L = 25Gpa, E_L = 40E_T, G_{LT} = 0.6E_T, \nu_{LT} = 0.25 \tag{3.70}$$

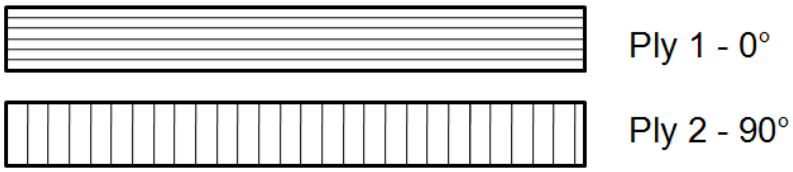

Figure 3.6 Configuration of two-layer cross-ply laminate plate

The thickness of each layer is 0.0025m. The bending stiffness matrix can be obtained from the properties, thickness and orientation of the two layers and they are expressed in the D matrix.

$$D = \begin{bmatrix} 134.0 & 1.63 & 0 \\ 1.63 & 134.0 & 0 \\ 0 & 0 & 3.91 \end{bmatrix} Gpa \cdot m^3 \tag{3.71}$$

Figure 3.7 presents the laminate plate models in FEA and EFEA respectively. To capture the response of the plate at high frequencies, the conventional FEA model has 10,000 elements. The EFEA model has only 100 elements.

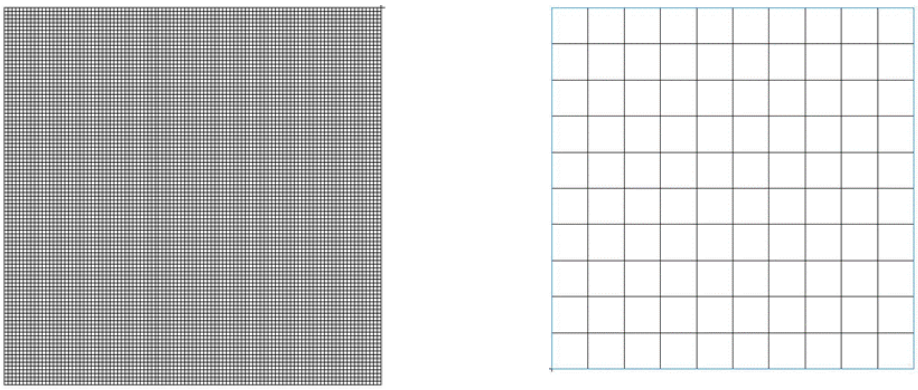

Figure 3.7 Conventional FEA model (left) and EFEA model (right)

The distribution of energy density along the mid-span of the plate is evaluated by the FEA and the EFEA for 1/3 octave bands of the frequencies from 1000Hz to 5000Hz. In the FEA model, the plate is excited at several randomly selected locations and the velocity at each node can be computed. First, the input power at each excitation location is computed and it becomes the input power in the EFEA matrix. The energy density distribution within the plate can be calculated and the results are averaged over the 1/3 octave bands for each central frequency in order to compare the results with EFEA model. The comparisons of the energy density distribution at several frequencies are presented in Figure 3.8 and differences smaller than 0.5dB are observed.

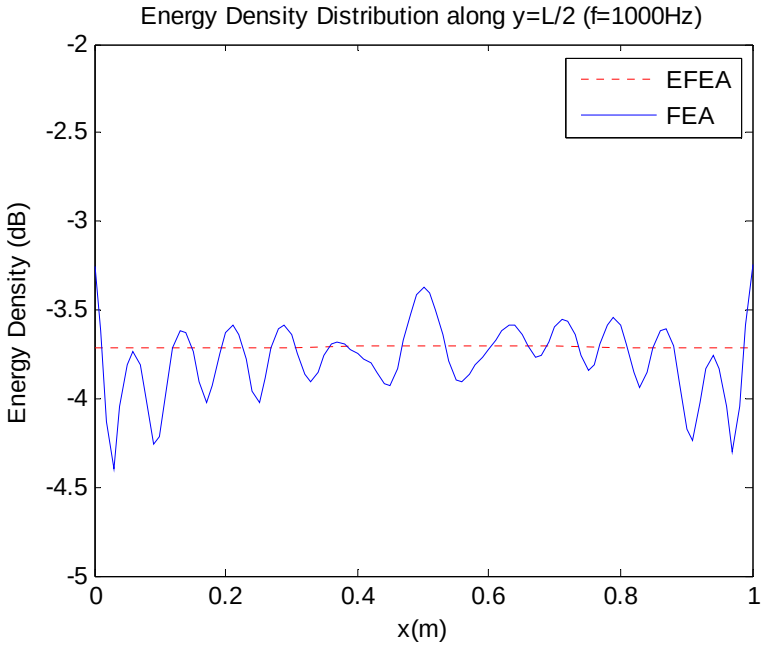
Energy Density Distribution along y=L/2 (f=1000Hz)
EFEA
FEA
Energy Density (dB)
x(m)
-2
-2.5
-3
-3.5
-4
-4.5
-5
0
0.2
0.4
0.6
0.8
1

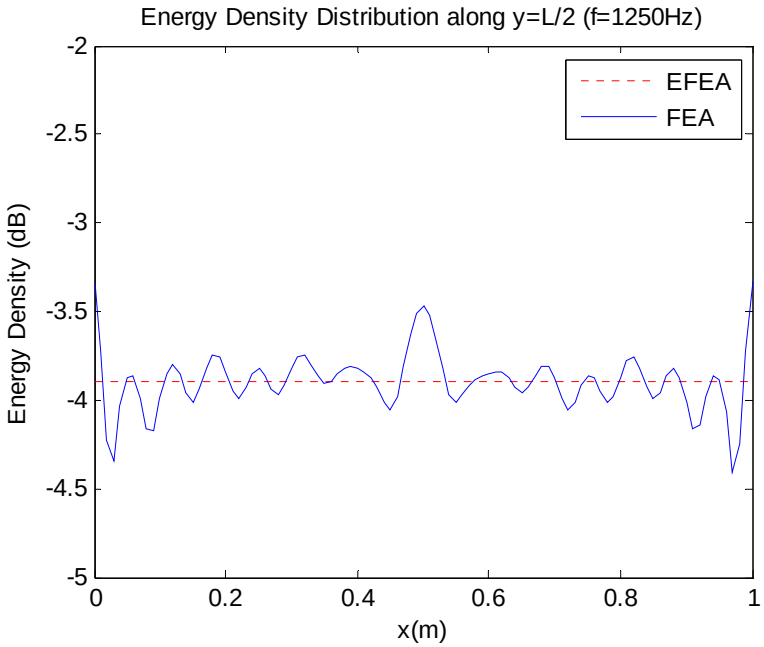
Energy Density Distribution along y=L/2 (f=1250Hz)
EFEA
FEA
Energy Density (dB)
x(m)
-2
-2.5
-3
-3.5
-4
-4.5
-5
0
0.2
0.4
0.6
0.8
1

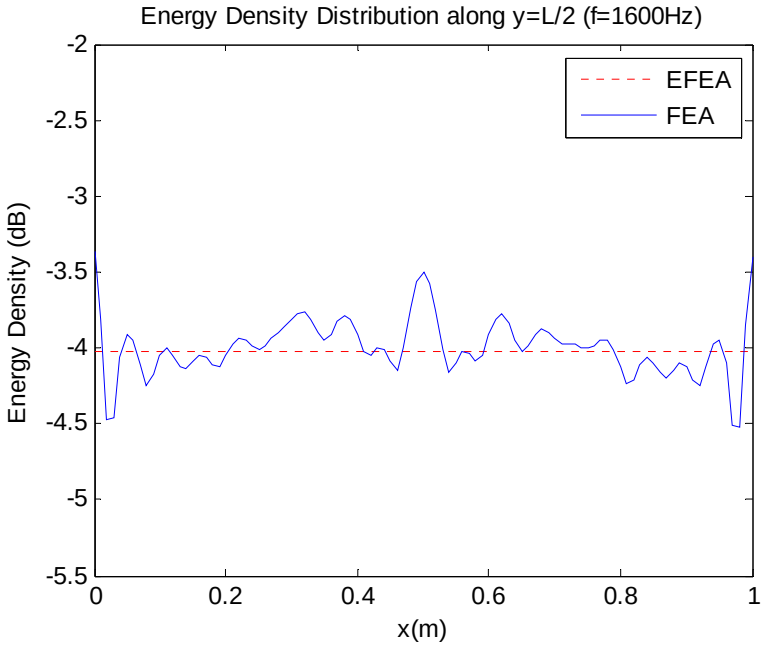
Energy Density Distribution along y=L/2 (f=1600Hz)
EFEA
FEA
Energy Density (dB)
x(m)
-2
-2.5
-3
-3.5
-4
-4.5
-5
-5.5
0
0.2
0.4
0.6
0.8
1

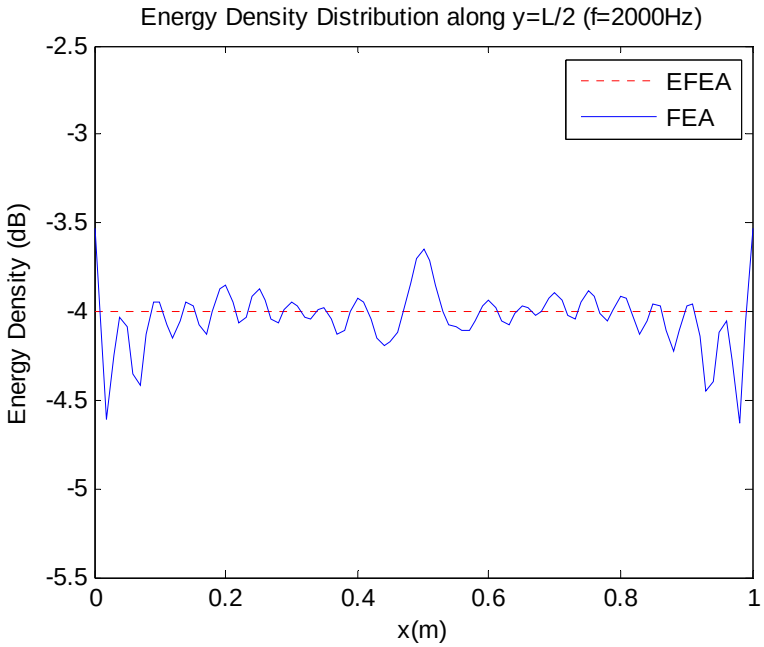
Energy Density Distribution along y=L/2 (f=2000Hz)
EFEA
FEA
Energy Density (dB)
x(m)
-2.5
-3
-3.5
-4
-4.5
-5
-5.5
0
0.2
0.4
0.6
0.8
1

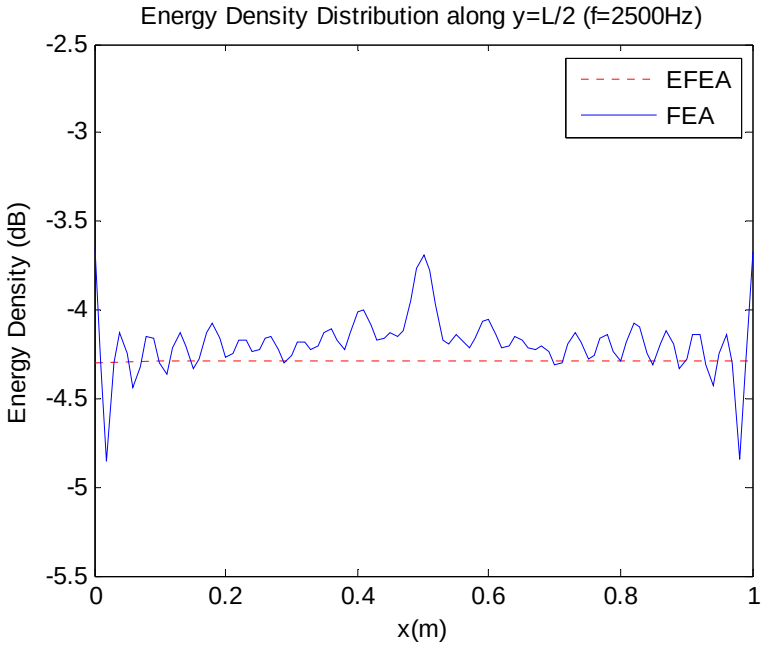
Energy Density Distribution along y=L/2 (f=2500Hz)
EFEA
FEA
Energy Density (dB)
x(m)
-2.5
-3
-3.5
-4
-4.5
-5
-5.5
0
0.2
0.4
0.6
0.8
1

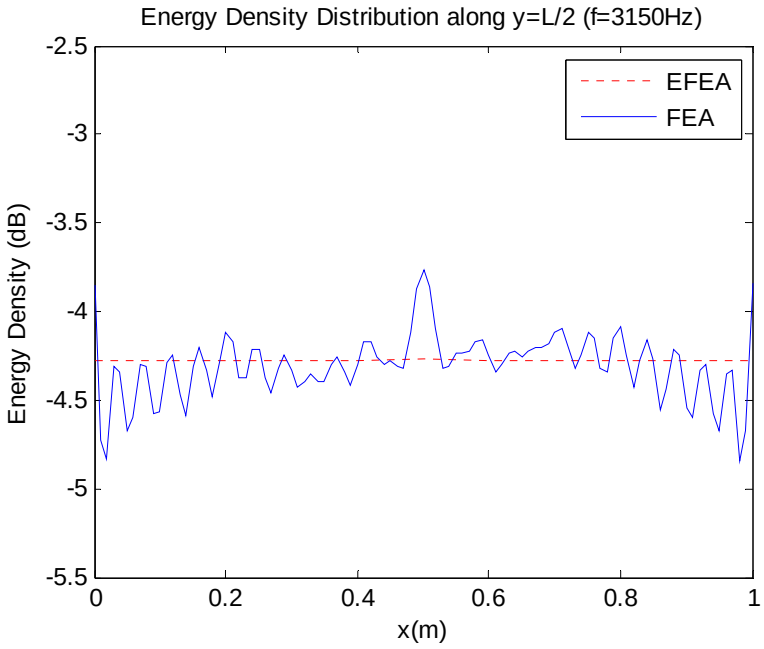
Energy Density Distribution along y=L/2 (f=3150Hz)
EFEA
FEA
Energy Density (dB)
x(m)
-2.5
-3
-3.5
-4
-4.5
-5
-5.5
0
0.2
0.4
0.6
0.8
1

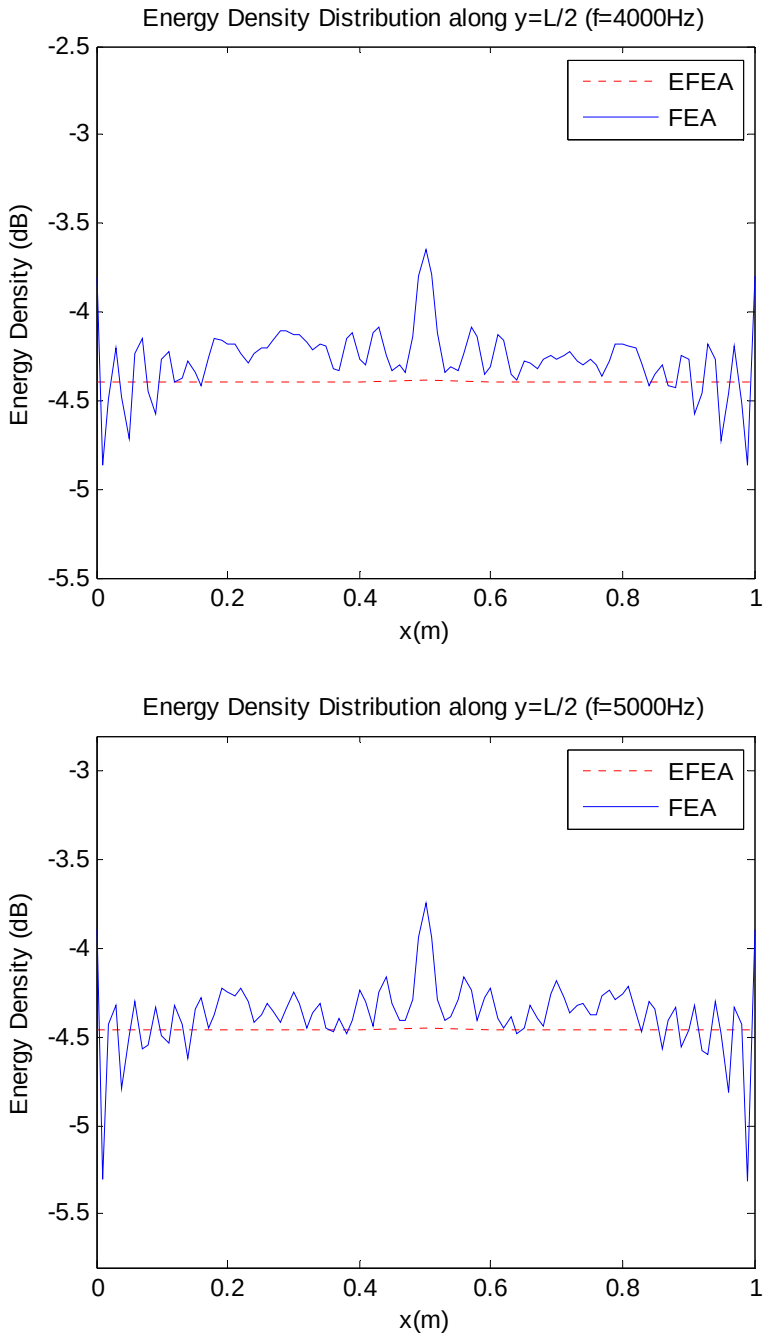

Figure 3.8 Distribution of energy density along the mid-span of the cross-ply laminate plate computed by the dense FEA and EFEA models at 1000Hz-5000Hz 1/3 octave bands

3.6.2 Two-layer general laminate plate

In this part, the example of a more general composite laminate plate is calculated in conventional EFA and EFEA models. The plate is a 1m×1m square laminated plate with two layers of equal thickness. The two layers are at 0 and 45 degree orientation. Layers with the following engineering constants are used:

$$E_L = 20Gpa, E_T = 2\ Gpa, G_{LT} = 0.7Gpa, \nu_{LT} = 0.35 \tag{3.72}$$

The configuration of the laminate is illustrated in the following Figure 3.9.

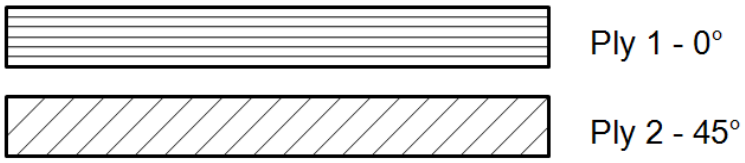

Figure 3.9 Configuration of composite laminate plate

The thickness of each layer is 0.0025m. The bending stiffness matrix can be calculated as:

$$D = \begin{bmatrix} 140.0 & 30.9 & 23.7 \\ 30.9 & 45.0 & 23.7 \\ 23.7 & 23.7 & 30.8 \end{bmatrix} Gpa \cdot m^3 \tag{3.73}$$

The comparisons of the energy density distribution at mid-span of the plate at several frequencies are presented in Figure 3.10. Similar to the example of cross-ply laminate plate, very good agreement can be observed from the comparison between EFEA and FEA results. EFEA captures the energy distribution level in the plate well while using a significantly smaller number of elements.

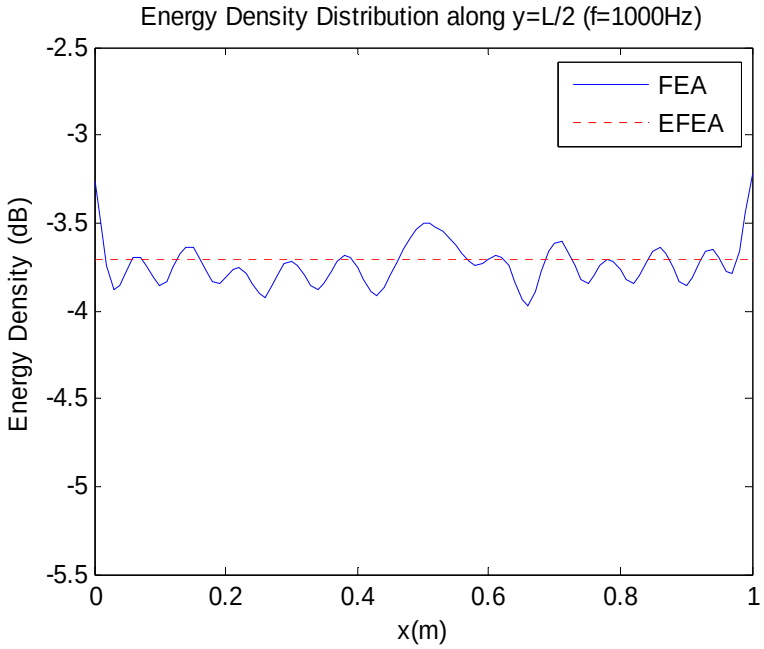
Energy Density Distribution along y=L/2 (f=1000Hz)
FEA
EFEA
Energy Density (dB)
x(m)
-2.5
-3
-3.5
-4
-4.5
-5
-5.5
0
0.2
0.4
0.6
0.8
1

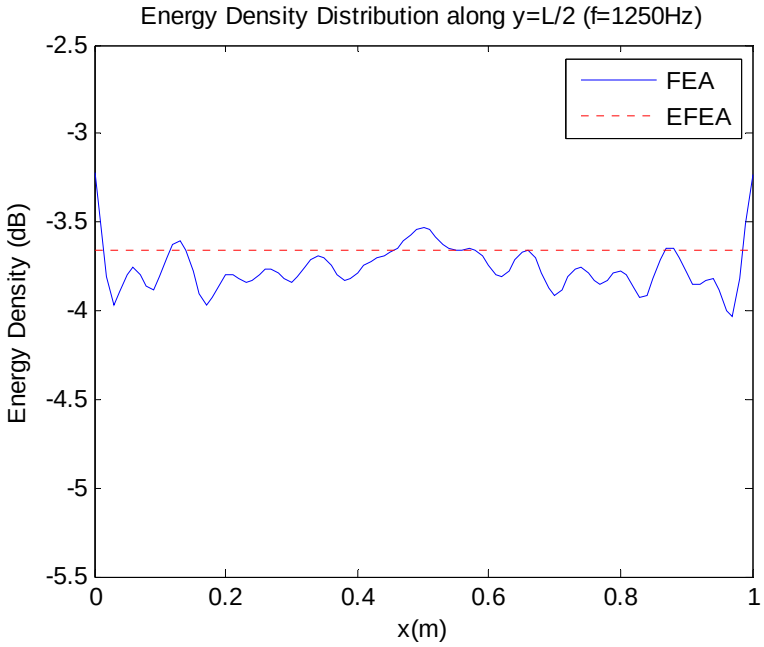
Energy Density Distribution along y=L/2 (f=1250Hz)
FEA
EFEA
Energy Density (dB)
x(m)
-2.5
-3
-3.5
-4
-4.5
-5
-5.5
0
0.2
0.4
0.6
0.8
1

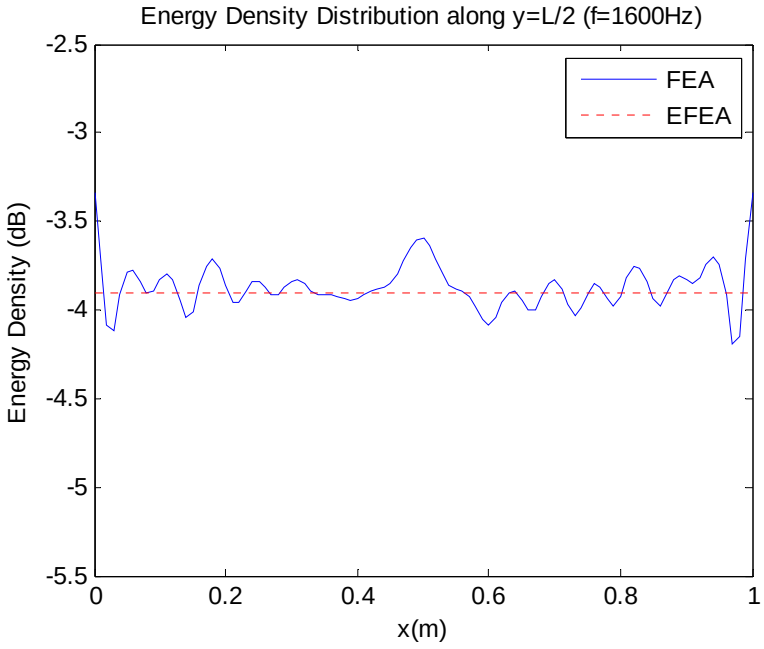
Energy Density Distribution along y=L/2 (f=1600Hz)
FEA
EFEA
Energy Density (dB)
-2.5
-3
-3.5
-4
-4.5
-5
-5.5
0
0.2
0.4
0.6
0.8
1
x(m)

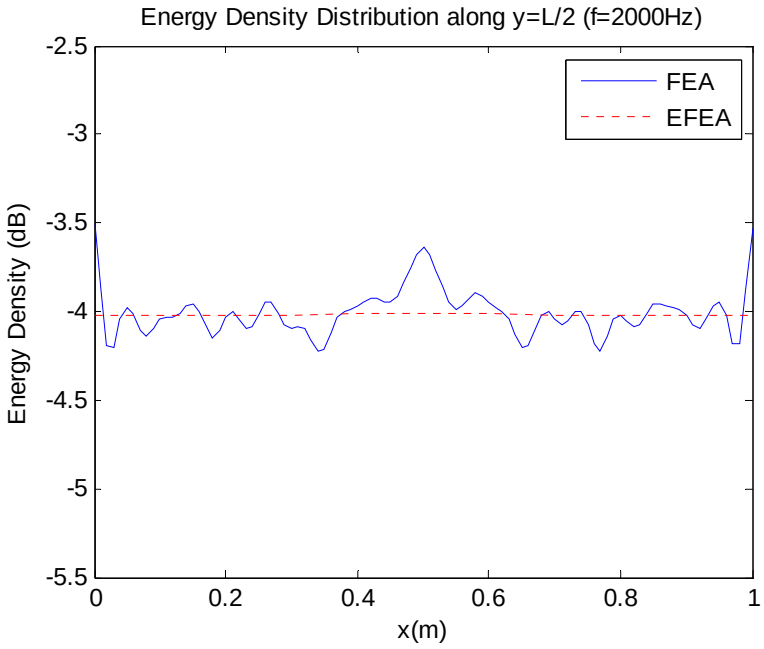
Energy Density Distribution along y=L/2 (f=2000Hz)
FEA
EFEA
Energy Density (dB)
-2.5
-3
-3.5
-4
-4.5
-5
-5.5
0
0.2
0.4
0.6
0.8
1
x(m)

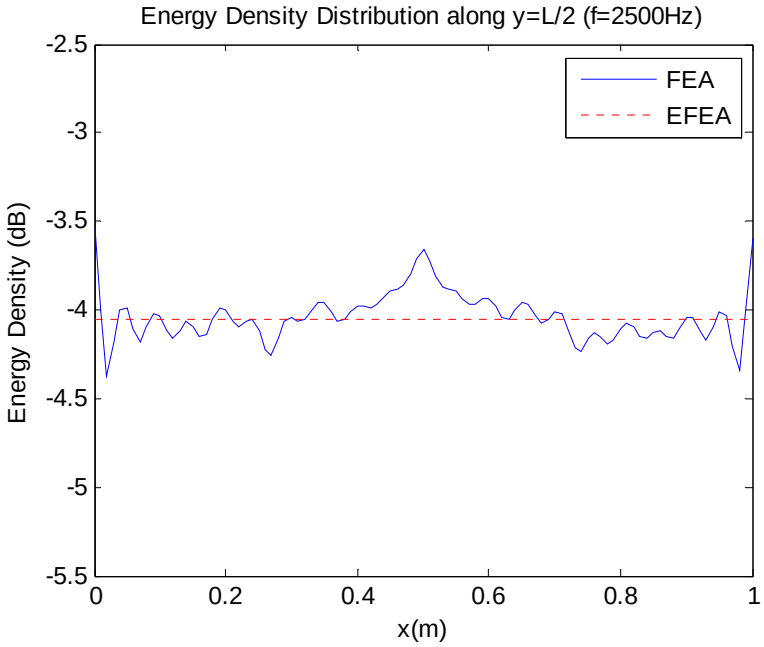
Energy Density Distribution along y=L/2 (f=2500Hz)
FEA
EFEA
Energy Density (dB)
-2.5
-3
-3.5
-4
-4.5
-5
-5.5
0
0.2
0.4
0.6
0.8
1
x(m)

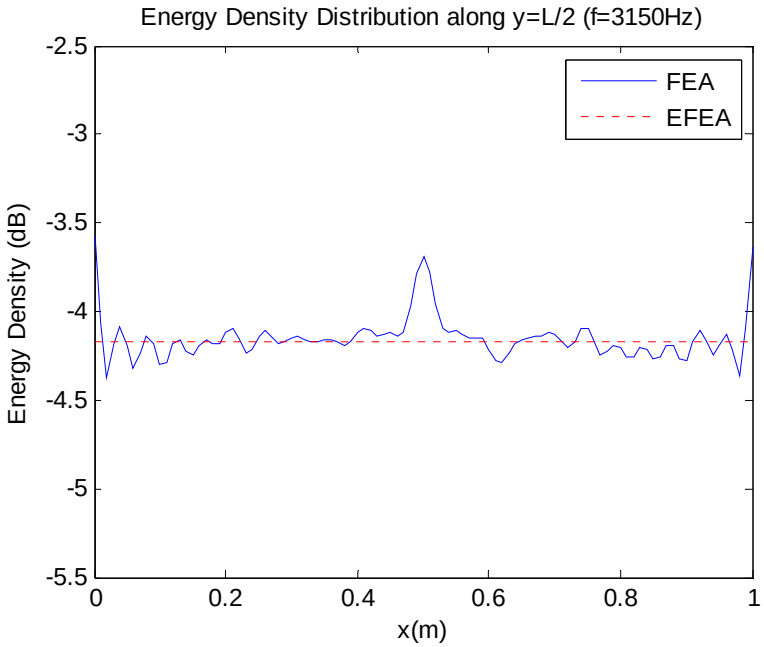
Energy Density Distribution along y=L/2 (f=3150Hz)
FEA
EFEA
Energy Density (dB)
-2.5
-3
-3.5
-4
-4.5
-5
-5.5
0
0.2
0.4
0.6
0.8
1
x(m)

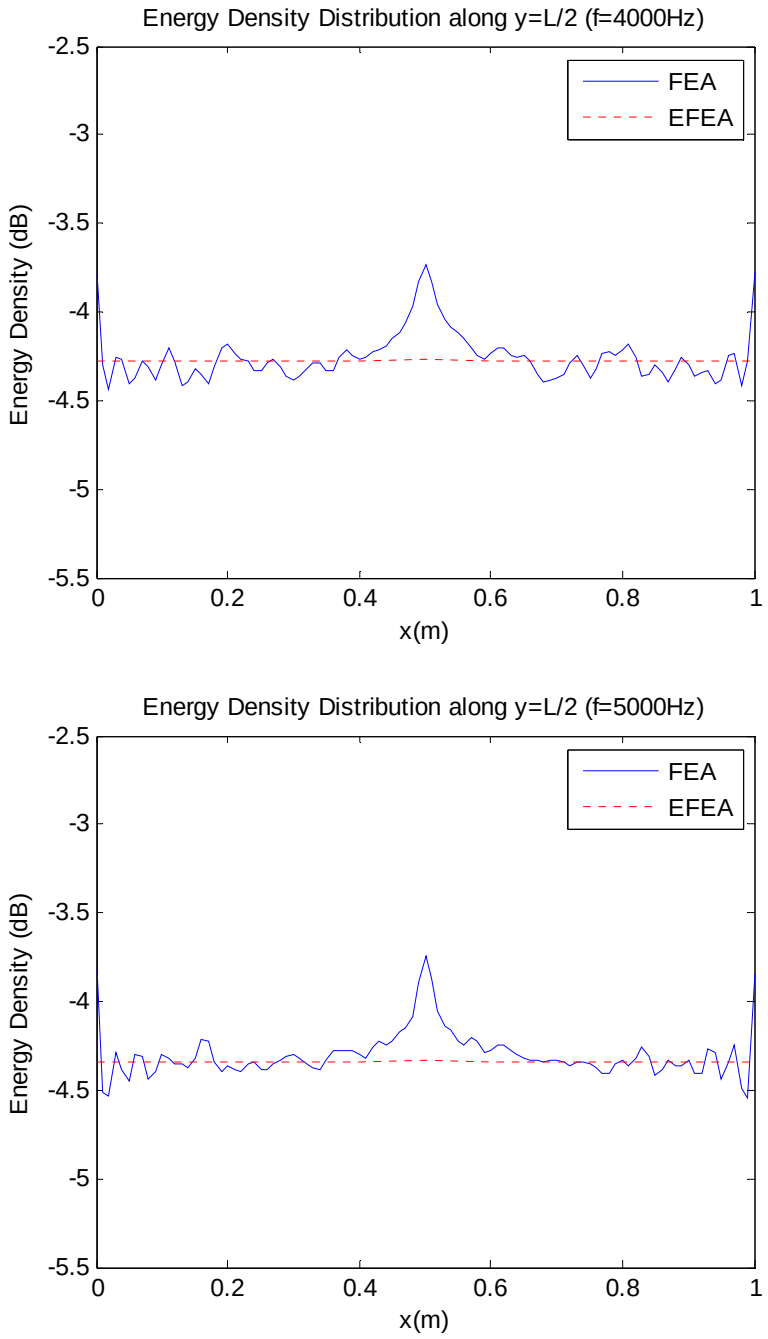

Figure 3.10 Distribution of energy density along the mid-span of the general laminate plate computed by the dense FEA and EFEA models at 1000Hz-5000Hz 1/3 octave bands

3.7 An Alternative Method to Derive the EFEA Differential Equation for Composite Laminate Plates

3.7.1Group velocity for composite laminate plates

From the classical laminate theory, composite laminate plate can be considered as an anisotropic plate. The wavenumber has angle dependence in anisotropic media (Bosmans, Mees et al. 1996; Bosmans, Vermeir et al. 2002). The energy distribution and the direction of energy flow in anisotropic media are affected by the angle dependence of the wavenumber. Poynting vector is used in describing the energy flow in anisotropic media (Auld 1990). This vector, which is parallel to the heading of the group velocity, is orientated normal to the curve obtained by plotting the wavenumber as a function of the wave heading. Thus, the heading of group velocity is different to the heading of wave propagation, except for some values. Figure 3.11 gives an illustration of this phenomenon.

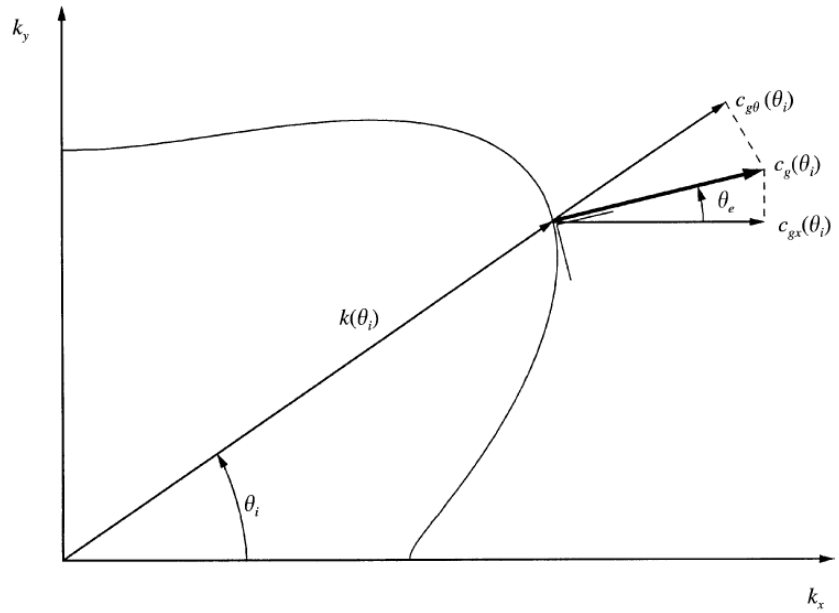

Figure 3.11 Wavenumber as a function of wave heading in the wavenumber plane

The x component of group velocity is expressed as c_{gx}, the component along the heading of wave propagation θ is expressed as $c_{g\theta}$. The angle between $c_{g\theta}$ and c_g is the heading of group velocity θ_e.

The following relations exist for the wave propagation:

$$c(\theta_i) = \frac{\omega}{k(\theta_i)} \tag{3.74}$$

$$c_{g\theta}(\theta_i) = \frac{\partial \omega}{\partial k(\theta_i)} \tag{3.75}$$

Now let's derive the group velocity for bending waves in composite laminate plates. For composite laminate plate, the bending wavenumber is expressed in equation (3.21) (Bosmans, Vermeir et al. 2002).

$$c_{gB\theta}(\theta_i) = \frac{\partial \omega}{\partial k_B(\theta_i)} = \frac{2\omega}{k_B} \tag{3.76}$$

The normal vector of the wavenumber curve can be expressed as:

$$\tan\theta_e = \frac{\partial k_{Bx}/\partial\theta_i}{-\partial k_{By}/\partial\theta_i} = \frac{\partial[k_B(\theta_i)\cos\theta_i]/\partial\theta_i}{-\partial[k_B(\theta_i)\sin\theta_i]/\partial\theta_i} = \frac{\frac{\partial k_B}{\partial\theta_i}\cos\theta_i - k_B\sin\theta_i}{-\frac{\partial k_B}{\partial\theta_i}\sin\theta_i - k_B\cos\theta_i} \tag{3.77}$$

where $\frac{\partial k_B}{\partial\theta_i}$ can be obtained from equation (3.21).

From Figure 3.11, the following relationship between $c_{gB\theta}$ and c_{gB} can be obtained:

$$c_{gB} = \frac{c_{gB\theta}}{\cos(\theta_i - \theta_e)} \tag{3.78}$$

The group velocity corresponding to the bending wave c_{gB} can be calculated from equation (3.78). The group velocity of the in-plane waves can also be calculated following the similar procedure.

3.7.2 Equivalent homogenized isotropic material for composite laminate plates

From Chapter 2, we know that the EFEA differential equation for isotropic material can be expressed as (Bouthier and Bernhard 1992):

$$-\frac{c_g^2}{\eta\omega}\nabla^2\langle \underline{e}\rangle + \eta\omega\langle \underline{e}\rangle = \langle \underline{\Pi}_{in}\rangle \tag{3.79}$$

$$c_g = 2\sqrt[4]{\frac{D\omega^2}{\rho h}} \tag{3.80}$$

The property of the material is taken into consideration in the group velocity c_g of the material. For the composite laminate plate, it is also possible to come up with a similar EFEA differential equation by using the averaged group velocity c_g^*. As described previously, the group velocity for composite laminate plate is a function of wave propagation angle θ. The averaged group velocity c_g^* removed the dependency to θ by taking the average of c_g from 0 to 2π.

$$c_g^* = \int_0^{2\pi} c_g d\theta \tag{3.81}$$

Using the averaged group velocity, we can express the EFEA differential equation for composite laminate plate as:

$$-\frac{c_g^{*2}}{\eta\omega}\nabla^2\langle \underline{e}\rangle + \eta\omega\langle \underline{e}\rangle = \langle \underline{\Pi}_{in}\rangle \tag{3.82}$$

At element level, the EFEA differential equation can be expressed as:

$$[K^e]\{e^e\} = \{F^e\} + \{Q^e\} \tag{3.83}$$

where $\{e^e\}$ is the vector of nodal values for the time and space averaged energy density, $[K^e]$ is the system matrix for each element, $\{F^e\}$ is the excitation vector, it represents the energy input at each node, $\{Q^e\}$ is the power flow across the element boundary.

From the averaged group velocity c_g^* for composite laminate plate, we can find its equivalent isotropic material property using equation (3.80).

$$D_{eq} = \frac{{c_g^*}^4 \rho h}{16\omega^2} \tag{3.84}$$

3.7.3 Validation of alternative approach

The two-layer general composite laminate plate used in 3.6.2 is used to implement the validation. In the calculation, the energy density distribution of plate is calculated using EFEA differential equation derived for both the composite laminate plate and the equivalent isotropic plate. The results for the frequency 1000 Hz and 5000 Hz are plotted in Figure 3.12. In both plots, good correlation is observed between these two methods.

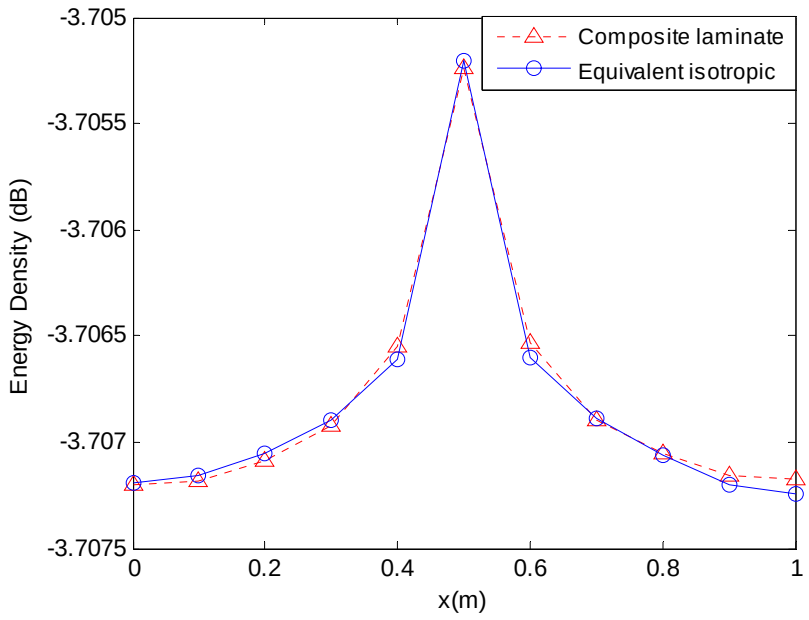

(a) f =1000 Hz

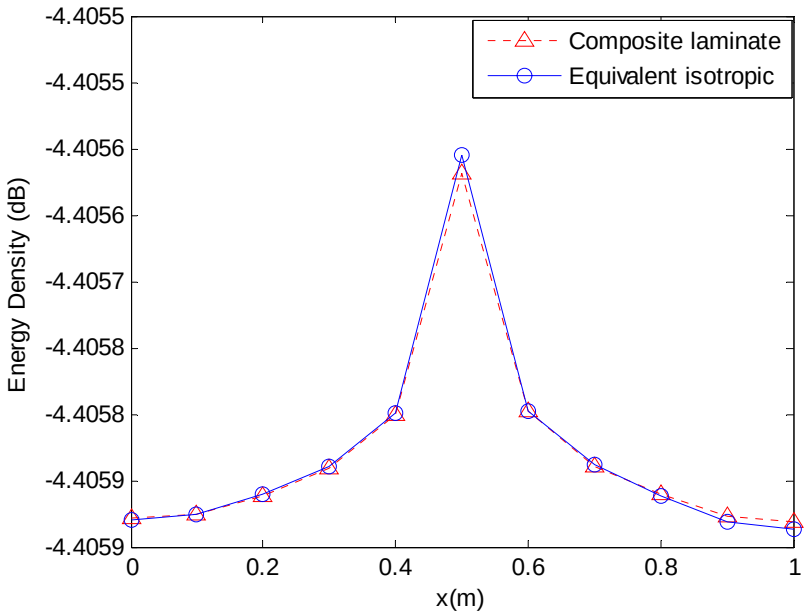

(b) f =5000 Hz

Figure 3.12 Energy density distribution comparison between composite laminate plate and its equivalent isotropic plate

Chapter 4

POWER TRANMISSION THROUGH COUPLED ORTHOTROPIC PLATES

4.1 Introduction

In order to analyze the power transmitted from the excitation location to the other components within the structure at high frequency, it is necessary to calculate the vibrational energy transmission at the plate junctions. The power transmission coefficients can be utilized to form the joint matrix at the structural junctions, where the energy density value is discontinuous. It is then possible to assemble the global system of matrix of EFEA differential equation and solve for the energy density throughout the entire system.

Approaches to calculate the power transmission coefficients include the methods for semi-infinite plates and finite-sized plates, but both methods are based on the proper formulation of the continuity and equilibrium conditions at the junction. In the past, this problem has been solved for thin (Langley and Heron 1990) and thick plates (Mccollum and Cuschieri 1990), for plate junction with beams (Langley and Heron 1990), junctions with elastic interlayer (Wohle, Beckmann et al. 1981; Mees and Vermeir 1993), junction of curved panels (Langley 1994).

In this chapter, the derivation of power transmission coefficients is introduced for orthotropic plates. As we know, many structures can be considered as orthotropic by virtue of their internal structure. This type of structures is commonly found in ship structures, building constructions (Bosmans, Mees et al. 1996; Bosmans and Nightinghale 1999) etc., as long as they have different stiffness in two mutual perpendicular directions.

The approach that has been adopted in this chapter is to consider the vibrations of the structure in terms of elastic waves (Langley and Heron 1990). The elastic waves propagate from the excited plate towards the plate junction and are partially reflected and partially transmitted at the junctions. The "wave dynamic stiffness matrix" can be derived for each plate from the expressions of wave solution of displacement and the resultant forces and moments. All the wave dynamic stiffness matrices for the plates can then be assembled into a global equation by applying the appropriate equilibrium and compatibility conditions at the junction. The displacement of each plate can then be solved from this global equation and the power transmission coefficients can be solved.

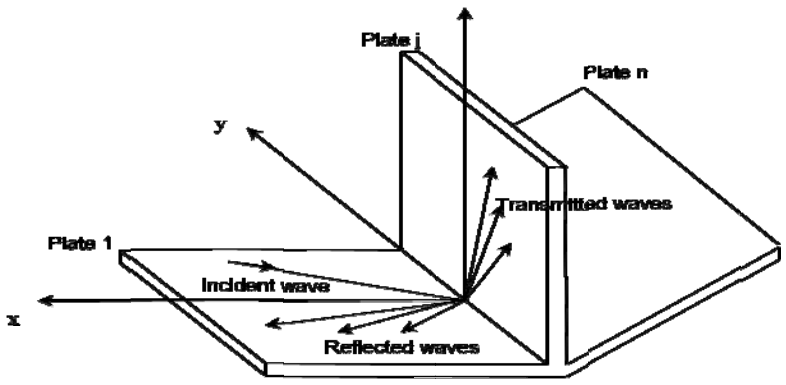

Figure 4.1 Schematic of plate junction

Figure 4.1 gives a schematic plot of a junction that consists of an arbitrary number of coupled plates. There are three types of waves involved in the plate junction problem: bending, longitudinal and shear waves.

This chapter is organized as follows. First, the equations of motion that govern the wave propagation in orthotropic plates are presented. The solutions for the equations are introduced, including the derivation of in-plane wavenumbers for orthotropic plates. Second, the wave dynamic stiffness matrix is derived, the global equation is assembled and the power transmission coefficients are solved. Third, the joint matrix is formed in terms of the power transmission coefficients and the global matrix of EFEA differential equation is form to solve for the energy density distribution within the structure. Finally, numerical examples are presented using the L-junction of two orthotropic plates with different orientations and the results obtained from EFEA formulation are compared with the results from very dense FEA model.

4.2 Derivation of Power Transmission Coefficients for Orthotropic Plate Junction

4.2.1 Governing equations

The deformation of each plate is defined with respect to the local coordinate system, which has the x-axis along the connection edge, as shown in Figure 4.2. The equations of motion that govern the deflections of the j th plate can be written in the form (Whitney and Ashton 1987) :

$$D_{11j}\frac{\partial^4 w}{\partial x^4} + 2\left(D_{12j} + 2D_{66j}\right)\frac{\partial^4 w}{\partial x^2 \partial y^2} + D_{22j}\frac{\partial^4 w}{\partial y^4} + \rho_j \frac{\partial^2 w}{\partial t^2} = 0 \tag{4.1}$$

$$A_{11j}\frac{\partial^2 u}{\partial x^2} + A_{66j}\frac{\partial^2 u}{\partial y^2} + \left(A_{12j} + A_{66j}\right)\frac{\partial^2 v}{\partial x \partial y} - \rho_j \frac{\partial^2 u}{\partial t^2} = 0 \tag{4.2}$$

$$A_{66j}\frac{\partial^2 v}{\partial x^2}+A_{22j}\frac{\partial^2 v}{\partial y^2}+\left(A_{12j}+A_{66j}\right)\frac{\partial^2 u}{\partial x\partial y}-\rho_j\frac{\partial^2 v}{\partial t^2}=0 \tag{4.3}$$

where D_{11j}, A_{11j} etc. are the coefficients of bending and extensional stiffness matrices of j th plate.

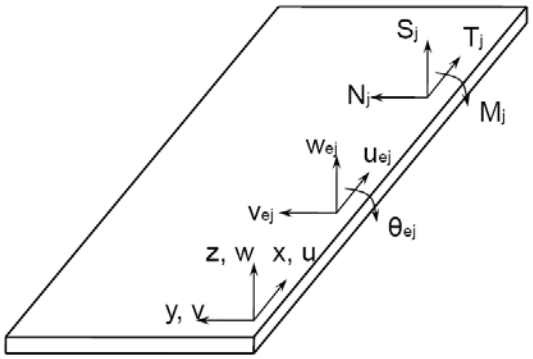

Figure 4.2 Coordinate system, displacements, forces and moments for plate j

The relationship between the displacements and the traction that act at the connected edge of the plate can be expressed as follows (Ashton and Whitney 1970).

$$M_j=D_{22j}\frac{\partial^2 w}{\partial y^2}+D_{12j}\frac{\partial^2 w}{\partial x^2} \tag{4.4}$$

$$S_j=-\left[\left(D_{12j}+2D_{66j}\right)\frac{\partial^3 w}{\partial x^2\partial y}+D_{22j}\frac{\partial^3 w}{\partial y^3}\right] \tag{4.5}$$

$$N_j=A_{12j}\frac{\partial u}{\partial x}+A_{22j}\frac{\partial v}{\partial y} \tag{4.6}$$

$$T_j=A_{66j}\left(\frac{\partial u}{\partial y}+\frac{\partial v}{\partial x}\right) \tag{4.7}$$

The tractions that act on the common edge of the plates are evaluated at $y=0$.

The forces and moments per unit length that are applied to the junction by the semi-infinite plates can be expressed as (Langley and Heron 1990):

$$Q=\sum_{j=1}^{N}R_jF_j \tag{4.8}$$

where $F = \left(T_j \;\; N_j \;\; S_j \;\; M_j\right)^T$ represents the tractions on the connected edge of plate j, and the transformation matrix R_j is given by (Langley and Heron 1990):

$$R_j = \begin{bmatrix} 1 & 0 & 0 & 0 \\ 0 & \cos\emptyset_j & -\sin\emptyset_j & 0 \\ 0 & \sin\emptyset_j & \cos\emptyset_j & 0 \\ 0 & 0 & 0 & 1 \end{bmatrix} \tag{4.9}$$

where $\emptyset_j$ is the angle of the local coordinate in plate j with respect to the global coordinate system.

The compatibility conditions between the common junction displacement a, and the edge displacement of plate j b_j, require that

$$b_j = R_j^T a \tag{4.10}$$

where $a = (u \;\; v \;\; w \;\; \theta)^T$, $b_j = \left(u_{ej} \;\; v_{ej} \;\; w_{ej} \;\; \theta_{ej}\right)^T$, and $u,\ v,\ w$ are the displacements of the junction in x, y, z directions respectively, θ is the rotation of the junction with respect to the x axis, $u_{ej}, v_{ej},\ w_{ej},\ \theta_{ej}$ are the corresponding displacements and moments for plate j.

4.2.2 Derivation of in-plane wavenumbers for orthotropic plates

The in-plane equations of motion for orthotropic plates can be expressed in equation (4.2) and (4.3). In the case of isotropic materials, these two equations predict two modes of propagation – longitudinal and shear modes. However, in the case of orthotropic material, because of the anisotropy, the modes are not pure longitudinal and pure shear except when they are propagating along directions of material symmetry. In general, these two modes are referred as quasi-longitudinal and quasi-shear modes (Prosser 1991).

The dispersion relationship for the orthotropic case is much more complicated than the isotropic case. Because of the anisotropy, the velocity of the mode is dependent on the direction of wave propagation. The dispersion relationship will again be obtained by assuming a plane wave form of the displacement and substituting into the equations of motion. The in-plane displacements are given by (Prosser 1991):

$$u = A_0\alpha_x exp[i(\omega t - k\cos\varphi x - k\sin\varphi y)] \tag{4.11}$$

$$v = A_0\alpha_y exp[i(\omega t - k\cos\varphi x - k\sin\varphi y)] \tag{4.12}$$

where $A_0\alpha_x$ and$A_0\alpha_y$ are the amplitudes of the two in-plane motions, k is the in-plane wavenumber, φ is the angle of wave propagation.

Substituting these displacements into the equations of motion yields the following relationship:

$$\begin{bmatrix} A_{11}k^2\cos^2\varphi + A_{66}k^2\sin^2\varphi - \rho h\omega^2 & (A_{12}+A_{66})k^2\cos\varphi\sin\varphi \\ (A_{12}+A_{66})k^2\cos\varphi\sin\varphi & A_{66}k^2\cos^2\varphi + A_{22}k^2\sin^2\varphi - \rho h\omega^2 \end{bmatrix}\begin{bmatrix}\alpha_x \\ \alpha_y\end{bmatrix} = 0 \tag{4.13}$$

The non-trivial solution for this equation will be obtained only when the determinant of the matrix is equal to zero. Setting the determinant equal to zero will yield a quadratic equation of k^2. The two solutions of wavenumber correspond to the quasi-longitudinal and quasi-shear modes respectively. Generally, the quasi-longitudinal mode is faster and thus corresponds to the smaller root.

For the wave propagation along the x axis or the 0 degree direction of the laminate, we have $\cos\varphi = 1, \sin\varphi = 0$. Thus, equation (4.13) becomes:

$$\begin{bmatrix} A_{11}k^2 - \rho h\omega^2 & 0 \\ 0 & A_{66}k^2 - \rho h\omega^2 \end{bmatrix}\begin{Bmatrix}\alpha_x \\ \alpha_y\end{Bmatrix} = 0 \tag{4.14}$$

The non-trivial solution requires:

$$det\begin{vmatrix} A_{11}-\rho hc^2 & 0 \\ 0 & A_{66}-\rho hc^2 \end{vmatrix} = 0 \tag{4.15}$$

where $c = \omega/k$ is the phase velocity.

The two solutions can be solved:

$$c_1 = \sqrt{\frac{A_{11}}{\rho h}} \tag{4.16}$$

$$c_2 = \sqrt{\frac{A_{66}}{\rho h}} \tag{4.17}$$

In this case, $\begin{Bmatrix} \alpha_x \\ \alpha_y \end{Bmatrix} = \begin{Bmatrix} 1 \\ 0 \end{Bmatrix}$ or $\begin{Bmatrix} 0 \\ 1 \end{Bmatrix}$, which correspond to a pure longitudinal wave mode or a pure shear wave mode.

4.2.3 Derivation of dynamic stiffness matrix

The wave dynamic stiffness matrix is derived by considering a plane wave propagating through one of the semi-infinite plates towards the plate junctions and being partly reflected to the plate and partly transmitted to other plates.

Assume the incident wave have a form of exp $(-ikx + i\mu y + i\omega t)$, the Snell's law requires that the response in all the plates must have the same x dependency exp $(-ikx + i\omega t)$, the y dependency will be determined from the plate equation of motion.

Assume the out-of-plane displacement of plate j has the form of exp $(-ikx + i\mu_B y + i\omega t)$, μ_B can be expressed as:

$$\mu_B^2 = k^2 \pm k_B^2 \tag{4.18}$$

where $k_B = \left[\frac{m\omega^2}{D_{11}\cos^4\varphi + 2(D_{12}+2D_{66})\cos^2\varphi\sin^2\varphi + D_{22}\sin^4\varphi}\right]^{1/4}$ is the bending wavenumber, it depends on the direction of wave propagation φ.

If $k > k_B$, equation (4.18) will have four real roots, in this case, only the two negative roots are physically significant because the response must decay as $y \to \infty$. In the case that $k < k_B$, equation (4.18) will have two real roots and two imaginary roots. In this case, only the negative real root and the negative imaginary root should be selected, because the response must either decay as $y \to \infty$ or propagate away from the junction (Langley and Heron 1990). After selecting the right y component of wavenumber μ_B, the out-of-plane response of the plate can be written in the form:

$$w = \sum_{n=1}^{2} \alpha_{Bn} \exp(-ikx + \mu_{Bn} y + i\omega t) \tag{4.19}$$

where μ_{B1} and μ_{B2} are the two valid roots from equation (4.18), α_{B1} and α_{B2} are the complex amplitudes associated with two roots.

The rotation can be expressed as:

$$\theta_j = \frac{\partial w}{\partial y} \tag{4.20}$$

From equation (4.19) and (4.20), the displacement and rotation at the edge of the plate j can be evaluated at $y = 0$, they can be expressed in terms of μ_{B1}, μ_{B2} α_{B1} and α_{B2} (Langley and Heron 1990):

$$\begin{Bmatrix} w_{ej} \\ \theta_{ej} \end{Bmatrix} = \begin{bmatrix} 1 & 1 \\ \mu_{B1} & \mu_{B2} \end{bmatrix} \begin{Bmatrix} \alpha_{B1} \\ \alpha_{B2} \end{Bmatrix} \exp(-ikx + i\omega t) \tag{4.21}$$

From equations (4.4) and (4.5) and equation (4.19), the edge tractions M_j and S_j can be expressed in terms of α_{B1} and α_{B2} as:

$$\begin{Bmatrix} S_j \\ M_j \end{Bmatrix} = \begin{bmatrix} k^2(D_{12} + 4D_{66})\mu_{B1} - D_{22}\mu_{B1}^3 & k^2(D_{12} + 4D_{66})\mu_{B2} - D_{22}\mu_{B2}^3 \\ D_{22}\mu_{B1}^2 - k^2 D_{12} & D_{22}\mu_{B2}^2 - k^2 D_{12} \end{bmatrix} \begin{Bmatrix} \alpha_{B1} \\ \alpha_{B2} \end{Bmatrix} \times$$

$$\exp(-ikx + i\omega t) \tag{4.22}$$

From equation (4.21), we can express α_{B1} and α_{B2} in terms of w_{ej} and θ_{ej} as:

$$\begin{Bmatrix}\alpha_{B1}\\ \alpha_{B2}\end{Bmatrix} = \begin{bmatrix}1 & 1\\ \mu_{B1} & \mu_{B2}\end{bmatrix}^{-1}\begin{Bmatrix}w_{ej}\\ \theta_{ej}\end{Bmatrix}\exp(ikx - i\omega t) \tag{4.23}$$

Eliminate $\alpha_{B1}$and α_{B2} from equation (4.22) using equation (4.23), we can get the following relationship between the edge displacements w_{ej}, $\theta_{ej}$and the edge tractions S_j andM_j:

$$\begin{Bmatrix}S_j\\ M_j\end{Bmatrix} = \frac{1}{\mu_{B1}-\mu_{B2}}\times$$

$$\begin{bmatrix}D_{22}\mu_{B1}\mu_{B2}(\mu_{B1}^2-\mu_{B2}^2) & k^2(D_{12}+4D_{66})(\mu_{B1}-\mu_{B2})+D_{22}(\mu_{B2}^3-\mu_{B1}^3)\\ D_{22}\mu_{B1}\mu_{B2}(\mu_{B2}-\mu_{B1})+k^2D_{12}(\mu_{B2}-\mu_{B1}) & D_{22}(\mu_{B1}^2-\mu_{B2}^2)\end{bmatrix}\begin{Bmatrix}w_{ej}\\ \theta_{ej}\end{Bmatrix} \tag{4.24}$$

Similar procedure can be used to determine the in-plane behavior of the plate. In order to simplify the derivation calculation, we assume the in-plane motions in the following expressions instead of equations (4.11) and (4.12) (Bosmans, Mees et al. 1996):

$$u = A_0 exp(i\omega t - ikx + \mu y) \tag{4.25}$$

$$v = VA_0 exp(i\omega t - ikx + \mu y) \tag{4.26}$$

where V is the ratio between the amplitudes of the two displacements.

Substituting equations (4.25) and (4.26) into the in-plane equations of motion (4.2) and (4.3), we can get the following expression:

$$\begin{bmatrix}A_{11}k^2 - A_{66}\mu^2 - \rho h\omega^2 & i(A_{12}+A_{66})k\mu\\ i(A_{12}+A_{66})k\mu & A_{66}k^2 - A_{22}\mu^2 - \rho h\omega^2\end{bmatrix}\begin{Bmatrix}1\\ V\end{Bmatrix} = \begin{Bmatrix}0\\ 0\end{Bmatrix} \tag{4.27}$$

Take the determinant equal to zero yield a polynomial equation of μ . Among the four roots of μ only the real and negative or imaginary and negative roots are selected. They are the corresponding y components of longitudinal and shear wavesnumbers respectively. Associated with each root is a mode shape which governs the relationship

between the two in-plane displacements. The two mode shapes can be obtained as $\begin{Bmatrix}1\\V_1\end{Bmatrix}$ and $\begin{Bmatrix}1\\V_2\end{Bmatrix}$.

Thus, the in-plane response can be written in the form:

$$\begin{Bmatrix}u\\v\end{Bmatrix} = \left\{\alpha_L \begin{pmatrix}1\\V_1\end{pmatrix} e^{\mu_L y} + \alpha_S \begin{pmatrix}1\\V_2\end{pmatrix} e^{\mu_S y}\right\} \exp(-ikx + i\omega t) \tag{4.28}$$

where α_L and α_S are the complex amplitudes of the associated complementary functions. Thus, the edge displacements u_{ej} and v_{ej} can be also expressed in terms of α_L and α_S as:

$$\begin{Bmatrix}u_{ej}\\v_{ej}\end{Bmatrix} = \begin{bmatrix}1 & 1\\V_1 & V_2\end{bmatrix}\begin{Bmatrix}\alpha_L\\\alpha_S\end{Bmatrix} \exp(-ikx + i\omega t) \tag{4.29}$$

Similarly, we can express the edge tractions T_j and N_j in terms of α_L and α_S as:

$$\begin{Bmatrix}T_j\\N_j\end{Bmatrix} = \begin{bmatrix}A_{66}(\mu_L - ikV_1) & A_{66}(\mu_S - ikV_2)\\-ikA_{12} + \mu_L V_1 A_{22} & -ikA_{12} + \mu_S V_2 A_{22}\end{bmatrix}\begin{Bmatrix}\alpha_L\\\alpha_S\end{Bmatrix} \tag{4.30}$$

Eliminate α_L and α_S from equation (4.30) using equation (4.29), we can get the following relationship between the edge displacements u_{ej}, v_{ej} and the edge tractions T_j and N_j:

$$\begin{Bmatrix}T_j\\N_j\end{Bmatrix} = \frac{1}{V_1 - V_2}\begin{bmatrix}A_{66}(\mu_S V_1 - \mu_L V_2) & A_{66}(\mu_L - \mu_S) + ikA_{66}(V_2 - V_1)\\V_1 V_2 A_{22}(\mu_s - \mu_L) & A_{22}(V_2\mu_s - V_1\mu_L)\end{bmatrix}\begin{Bmatrix}u_{ej}\\v_{ej}\end{Bmatrix} \tag{4.31}$$

Equations (4.24) and (4.31) can be combined to produce a relationship between the complete set of edge displacements b_j and tractions F_j of the form:

$$F_j = K_j b_j \tag{4.32}$$

where $b_j = \begin{pmatrix}u_{ej} & v_{ej} & w_{ej} & \theta_{ej}\end{pmatrix}^T$ and $F_j = \begin{pmatrix}T_j & N_j & S_j & M_j\end{pmatrix}^T$

$$K_j = \begin{bmatrix}K_{11} & K_{12} & K_{13} & K_{14}\\K_{21} & K_{22} & K_{23} & K_{24}\\K_{31} & K_{32} & K_{33} & K_{34}\\K_{41} & K_{42} & K_{43} & K_{44}\end{bmatrix} \tag{4.33}$$

where the entries of matrix K_j have been derived and can be found from equation (4.24) and (4.31).

$$K_{11} = \frac{1}{V_1 - V_2}[A_{66}(\mu_S V_1 - \mu_L V_2)]$$

$$K_{12} = \frac{1}{V_1 - V_2}[A_{66}(\mu_L - \mu_S) + ikA_{66}(V_2 - V_1)]$$

$$K_{21} = \frac{1}{V_1 - V_2}[V_1 V_2 A_{22}(\mu_s - \mu_L)]$$

$$K_{22} = \frac{1}{V_1 - V_2}[A_{22}(V_2 \mu_s - V_1 \mu_L)]$$

$$K_{33} = \frac{1}{\mu_{B1} - \mu_{B2}}\left[D_{22}\mu_{B1}\mu_{B2}\left(\mu_{B1}^2 - \mu_{B2}^2\right)\right]$$

$$K_{34} = \frac{1}{\mu_{B1} - \mu_{B2}}\left[k^2(D_{12} + 4D_{66})\left(\mu_{B1} - \mu_{B2}\right) + D_{22}\left(\mu_{B2}^3 - \mu_{B1}^3\right)\right]$$

$$K_{43} = \frac{1}{\mu_{B1} - \mu_{B2}}\left[D_{22}\mu_{B1}\mu_{B2}\left(\mu_{B2} - \mu_{B1}\right) + k^2 D_{12}\left(\mu_{B2} - \mu_{B1}\right)\right]$$

$$K_{44} = \frac{1}{\mu_{B1} - \mu_{B2}}\left[D_{22}\left(\mu_{B1}^2 - \mu_{B2}^2\right)\right]$$

$$K_{13} = K_{14} = K_{23} = K_{24} = K_{31} = K_{32} = K_{41} = K_{42} = 0$$

This matrix K_j is called the dynamic stiffness matrix of the semi-infinite plate j.

If the incident wave is carried by plate j, then equation (4.32) needs to be modified as (Langley and Heron 1990):

$$F_j = K_j b_j - f_j \tag{4.34}$$

$$f_j = K_j b_j' - F_j' \tag{4.35}$$

where b_j' and F_j' are the edge displacements and tractions caused by the incident wave.

The b_j' vectors can be expressed as the followings for the incident wave as bending wave, longitudinal wave and shear wave respectively (Langley and Heron 1990).

For bending incident wave:

$$b_j' = \begin{Bmatrix} 0 \\ 0 \\ \alpha \\ \alpha\mu \end{Bmatrix} \tag{4.36}$$

where $\mu = ik_B \sin\varphi$, $k = k_B \cos\varphi$.

For longitudinal incident wave:

$$b_j' = \begin{Bmatrix} \alpha \\ \alpha V_1 \\ 0 \\ 0 \end{Bmatrix} \tag{4.37}$$

For shear incident wave:

$$b_j' = \begin{Bmatrix} \alpha \\ \alpha V_2 \\ 0 \\ 0 \end{Bmatrix} \tag{4.38}$$

The F_j' vector can be expressed as product of the dynamic stiffness caused by the incident wave K_{in} and b_j'. K_{in} is calculated by using the same coefficient in the matrix but with the opposite sign of μ, which corresponds to the incident wave instead of the reflected wave.

4.2.4 Assembly of the complete equations and the calculation of transmission coefficients

Equation (4.8) gives the forces and moments per unit length that are acted on the junction by all the *N* semi-infinite plates. With equation (4.32) and equation (4.10), we can get the following equation (Langley and Heron 1990):

$$\left\{\sum_{j=1}^{N} R_j K_J R_j^T\right\} a = R_m f_m \tag{4.39}$$

where m is the plate that carries the incident wave.

Equation (4.39) can be solved to get the displacement a at the junction; it is also the common displacements of at the plate edge of all the semi-infinite plates. Equation (4.10) can be used to obtain the displacement of each plate. Equations (4.21) and (4.29)

can then be used to calculate the corresponding wave amplitudes of bending, shear and longitudinal waves.

The power associated with each wave can be calculated using the corresponding wave amplitudes. The power transmission coefficients associated with each of the generated waves can then be calculated as the ratio of the transmitted power to the total incident power on the junction. The transmission coefficients for the junction can be written in the form $\tau_{pr}^{ij}(\omega, \varphi)$, where i, p, ω and φ represent the incident plate, wave type, frequency and the heading of the incident wave, j and r represent the carrier plate and wave type of the generated wave. $\tau_{pr}^{ij}(\omega, \varphi)$ is also often referred as $r_{pr}^{ij}(\omega, \varphi)$ as the reflection coefficients for $i = j$.

From the law of conservation of energy, we can prove that the transmission and reflection coefficient sum equal to unity, since the total power that is incident on the junction must equal the total power which is carried away by the generated waves.

$$\sum_r \sum_j \tau_{pr}^{ij}(\omega, \varphi) = 1 \tag{4.40}$$

During the derivation of power transmission coefficients, the bending and in-plane wavenumbers are dependent on the angle of incident wave. Thus, the above expression of transmission coefficients is also the function of the incident angle φ. The averaged coefficient values are selected for the analysis. The averaged power transmission coefficient $\tau_{pr}^{ij}(\omega)$ can be obtained by integration as:

$$\tau_{pr}^{ij}(\omega) = \frac{1}{2}\int_0^{\pi} \tau_{pr}^{ij}(\omega, \varphi) \sin\varphi d\phi \tag{4.41}$$

4.3 Derivation of Joint Matrix

4.3.1 Power flow relationship of two systems through a lossless joint

In this section the, some background of forming the joint matrix between two systems are introduced first. The joint matrix is derived by considering the energy flow between two structures (Bitsie and Bernhard 1996). The conservation of energy flow requires the net outward energy flow for a single wave across the boundary of one system must be equal and opposite to the energy flow across the boundary of the other system. The conservation of energy flow relationship can be expressed as:

$$\int_{S=S_1+S_2} \vec{I} \cdot \vec{n} ds = \int_{S_1} \vec{I}_1 \cdot \vec{n} dS_1 + \int_{S_2} \vec{I}_2 \cdot \vec{n} dS_2 = 0 \qquad (4.42)$$

where subscripts 1 and 2 denote the individual subsystems 1 and 2.

Figure 4.3 gives a schematic plot of energy flow between two subsystems through a lossless joint for a single wave. The surface normal $\vec{n}$ defines the positive direction of power flow out of the lossless joint.

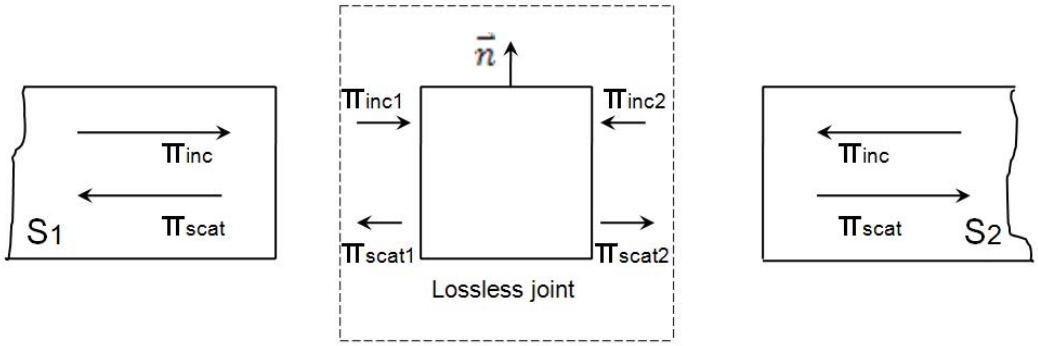

Figure 4.3 Schematic plot of energy flow between two subsystems for a single wave

The expression of energy flow across the lossless joint are (Bitsie and Bernhard 1996):

$$\int_{S_1} \vec{I}_1 \cdot \vec{n} dS_1 = \int_{S_1} \vec{I}_{inc1} \cdot \vec{n} dS_1 + \int_{S_1} \vec{I}_{scat1} \cdot \vec{n} dS_1 \tag{4.43}$$

$$\int_{S_2} \vec{I}_2 \cdot \vec{n} dS_2 = \int_{S_2} \vec{I}_{inc2} \cdot \vec{n} dS_2 + \int_{S_2} \vec{I}_{scat2} \cdot \vec{n} dS_2 \tag{4.44}$$

where $\vec{I}_{inc1}$ and $\vec{I}_{inc2}$ are incident energy flows in subsystems 1 and 2, $\vec{I}_{scat1}$ and $\vec{I}_{scat2}$ are the scattered energy flows from the discontinuity in each subsystem. The energy flow is denoted as positive when it flows out of the system.

The scattered energy flows can be expressed in terms of the incidents waves, power transmission and power reflection coefficients:

$$\int_{S_1} (|I_{scat1}|)\, dS_1 = -\int_{S_1} r_{11} (|I_{inc1}|)\, dS_1 - \int_{S_2} \tau_{12} (|I_{inc2}|)\, dS_2 \tag{4.45}$$

$$\int_{S_2} (|I_{scat2}|)\, dS_2 = -\int_{S_1} \tau_{21} (|I_{inc1}|)\, dS_1 - \int_{S_2} r_{22} (|I_{inc2}|)\, dS_2 \tag{4.46}$$

where r_{ij} and τ_{ij} are the reflection and transmission coefficients in subsystem i due to the incident wave in subsystem j.

After substituting equations (4.45) and (4.46) into equations (4.43) and (4.44), we find the following relationship between the energy flow and the incident energy intensities:

$$\begin{Bmatrix} \int_{S_1} \vec{I}_1 \cdot \vec{n} dS_1 \\ \int_{S_2} \vec{I}_2 \cdot \vec{n} dS_2 \end{Bmatrix} = \begin{bmatrix} 1 - r_{11} & -\tau_{12} \\ -\tau_{21} & 1 - r_{22} \end{bmatrix} \begin{Bmatrix} \int_{S_1} |I_{inc1}|\, dS_1 \\ \int_{S_2} |I_{inc2}|\, dS_2 \end{Bmatrix} = [P] \begin{Bmatrix} \int_{S_1} |I_{inc1}|\, dS_1 \\ \int_{S_2} |I_{inc2}|\, dS_2 \end{Bmatrix} \tag{4.47}$$

The energy superposition relationship for energy field requires:

$$e_1 = e_{inc1} + e_{scat1} \tag{4.48}$$

$$e_2 = e_{inc2} + e_{scat2} \tag{4.49}$$

Integrate equations (4.48) and (4.49) and using the relationship $ce = |I|$, we can get the following expressions:

$$\int_{S_1} c_1 e_1\, dS_1 = -\int_{S_1} |I_{inc1}|\, dS_1 + \int_{S_1} |I_{scat1}|\, dS_1 \tag{4.50}$$

$$\int_{S_2} c_2 e_2 \, dS_1 = -\int_{S_2} |I_{inc2}| \, dS_2 + \int_{S_2} |I_{scat2}| \, dS_2 \tag{4.51}$$

Substituting equations (4.45) and (4.46) into equations (4.50) and (4.51) yields the following expressions (Bitsie and Bernhard 1996):

$$\begin{Bmatrix} \int_{S_1} c_1 e_1 \, dS_1 \\ \int_{S_2} c_2 e_2 \, dS_1 \end{Bmatrix} = -\begin{bmatrix} 1 + r_{11} & \tau_{12} \\ \tau_{21} & 1 + r_{22} \end{bmatrix} \begin{Bmatrix} \int_{S_1} |I_{inc1}| \, dS_1 \\ \int_{S_2} |I_{inc2}| \, dS_2 \end{Bmatrix} = [E] \begin{Bmatrix} \int_{S_1} |I_{inc1}| \, dS_1 \\ \int_{S_2} |I_{inc2}| \, dS_2 \end{Bmatrix} \tag{4.52}$$

Combining equations (4.47) and (4.52) yield the relationship between energy density to the intensities:

$$\begin{Bmatrix} \int_{S_1} \vec{I}_1 \cdot \vec{n} dS_1 \\ \int_{S_2} \vec{I}_2 \cdot \vec{n} dS_2 \end{Bmatrix} = [J] \begin{Bmatrix} \int_{S_1} c_1 e_1 \, dS_1 \\ \int_{S_2} c_2 e_2 \, dS_1 \end{Bmatrix} = [P][E]^{-1} \begin{Bmatrix} \int_{S_1} c_1 e_1 \, dS_1 \\ \int_{S_2} c_2 e_2 \, dS_1 \end{Bmatrix} \tag{4.53}$$

where $[J]$ is the joint matrix.

For the two subsystems connected, the joint matrix can be expressed as:

$$[J] = [P][E]^{-1} = -\begin{bmatrix} 1 - r_{11} & -\tau_{12} \\ -\tau_{21} & 1 - r_{22} \end{bmatrix} \begin{bmatrix} 1 + r_{11} & \tau_{12} \\ \tau_{21} & 1 + r_{22} \end{bmatrix}^{-1}$$

$$= \frac{\begin{bmatrix} (1-r_{11})(1+r_{22})+\tau_{12}\tau_{21} & -2\tau_{12} \\ -2\tau_{21} & (1+r_{11})(1-r_{22})+\tau_{12}\tau_{21} \end{bmatrix}}{(1+r_{11})(1+r_{22})-\tau_{12}\tau_{21}} \tag{4.54}$$

Conservation of energy requires:

$$r_{11} + \tau_{21} = 1 \tag{4.55}$$

$$r_{22} + \tau_{12} = 1 \tag{4.56}$$

Thus the joint matrix for two subsystems can be simplified as (Bitsie and Bernhard 1996):

$$[J] = \frac{\begin{bmatrix} \tau_{21} & -\tau_{12} \\ -\tau_{21} & \tau_{12} \end{bmatrix}}{2-\tau_{12}-\tau_{21}} \tag{4.57}$$

4.3.2 Joint matrix for two coupled plates

The derivation of joint matrix for coupled plates has the similar formula as described in equation (4.54). First, the transmission coefficients matrix between two plates can be expressed as in a matrix $[T]$ as:

$$[T]_{6\times6} = \begin{bmatrix} r_{11,11} & r_{12,11} & r_{13,11} & \tau_{21,11} & \tau_{22,11} & \tau_{23,11} \\ r_{11,12} & r_{12,12} & r_{13,12} & \tau_{21,12} & \tau_{22,12} & \tau_{23,12} \\ r_{11,13} & r_{12,13} & r_{13,13} & \tau_{21,13} & \tau_{22,13} & \tau_{23,13} \\ \tau_{11,21} & \tau_{12,21} & \tau_{13,21} & r_{21,21} & r_{22,21} & r_{23,21} \\ \tau_{11,22} & \tau_{12,22} & \tau_{13,22} & r_{21,22} & r_{22,22} & r_{23,22} \\ \tau_{11,23} & \tau_{12,23} & \tau_{13,23} & r_{21,23} & r_{22,23} & r_{23,23} \end{bmatrix} \tag{4.58}$$

where $r_{ij,il}$ represents the l (=1, 2, 3, where 1 indicates the bending wave, 2 indicates the in-plane longitudinal wave, and 3 indicates the in-plane shear wave) wave type power reflection coefficient in plate i(=1,2) due to the incident j wave type in plate i, $\tau_{ij,kl}$ represents the l wave type power transmission coefficient in plate k due to the incident j wave type in plate i.

Let $[I]_{6\times6}$ be the unit matrix, and

$$[P]_{6\times6} = [I]_{6\times6} - [T]_{6\times6} \tag{4.59}$$

$$[E]_{6\times6} = [I]_{6\times6} + [T]_{6\times6} \tag{4.60}$$

Similar to equation (4.54), the matrix $[C]_{6\times6}$ can be expressed as:

$$[C]_{6\times6} = [P]_{6\times6} \cdot [E]_{6\times6}^{-1} \tag{4.61}$$

Then the joint matrix $[J]$ can be calculated by:

$$[J]_{12\times12} = \begin{bmatrix} C_{11}[L]_{2\times2} & C_{12}[L]_{2\times2} & C_{13}[L]_{2\times2} & C_{14}[L]_{2\times2} & C_{15}[L]_{2\times2} & C_{16}[L]_{2\times2} \\ C_{21}[L]_{2\times2} & C_{22}[L]_{2\times2} & C_{23}[L]_{2\times2} & C_{24}[L]_{2\times2} & C_{25}[L]_{2\times2} & C_{26}[L]_{2\times2} \\ C_{31}[L]_{2\times2} & C_{32}[L]_{2\times2} & C_{33}[L]_{2\times2} & C_{34}[L]_{2\times2} & C_{35}[L]_{2\times2} & C_{36}[L]_{2\times2} \\ C_{41}[L]_{2\times2} & C_{42}[L]_{2\times2} & C_{43}[L]_{2\times2} & C_{44}[L]_{2\times2} & C_{45}[L]_{2\times2} & C_{46}[L]_{2\times2} \\ C_{51}[L]_{2\times2} & C_{52}[L]_{2\times2} & C_{53}[L]_{2\times2} & C_{54}[L]_{2\times2} & C_{55}[L]_{2\times2} & C_{56}[L]_{2\times2} \\ C_{61}[L]_{2\times2} & C_{62}[L]_{2\times2} & C_{63}[L]_{2\times2} & C_{64}[L]_{2\times2} & C_{65}[L]_{2\times2} & C_{66}[L]_{2\times2} \end{bmatrix} \tag{4.62}$$

where $[L]_{2\times2}$ is calculated by the integral along the joint line in the form same as that for a consistent mass matrix.

4.4 Assembly of Global Matrix for Coupled Orthotropic Plates

From Chapter 2, the matrix expression of EFEA differential equation at the element level can be expressed as:

$$[K^e]\{e^e\} = \{F^e\} + \{Q^e\} \tag{4.63}$$

where $\{e^e\}$ is the vector of nodal values for the time and space averaged energy density, $[K^e]$ is the system matrix for each element, $\{F^e\}$ is the excitation vector, it represents the energy input at each node, $\{Q^e\}$ is the power flow across the element boundary.

The power flow can be expressed in terms of energy density and power transmission coefficients.

$$\begin{Bmatrix} Q_n^i \\ Q_{n+1}^i \\ Q_m^j \\ Q_{m+1}^j \end{Bmatrix} = [JC]_j^i \begin{Bmatrix} e_n^i \\ e_{n+1}^i \\ e_m^j \\ e_{m+1}^j \end{Bmatrix} \tag{4.64}$$

where n and $n+1$ represents the two nodes of the i element at the joint, m and $m+1$ represents the two nodes of the j element at the joint, the joint matrices $[JC]_j^i$ define the power transfer across elements at the joints and is expressed in equation (4.62).

The final assembled system of EFEA equations can be expressed as:

$$\left(\begin{bmatrix} [K^e]_i & \\ & [K^e]_j \end{bmatrix} + [JC]_j^i\right)\begin{Bmatrix} \{e^i\} \\ \{e^j\} \end{Bmatrix} = \begin{Bmatrix} \{F^e\}_i \\ \{F^e\}_j \end{Bmatrix} \tag{4.65}$$

where $[K^e]_i$ and $[K^e]_j$ are the element matrix for the i and j element, $\{e^i\}$ and $\{e^j\}$ are the vectors containing all the nodal degrees of freedom for elements i and j.

4.5 Numerical Examples and Validation

In this section, numerical calculation will be presented for the case of L-junction of two identical orthotropic plates connected with different orientations. The EFEA results are validated by comparing with results obtained from conventional FEA models.

The dimensions and the material properties of the orthotropic plates can be expressed as:

$$h = 0.01m, L_x = 1m, L_y = 1m$$

$$E_L = 40.0Gpa, E_T = 20.0Gpa, G_{LT} = 11.54Gpa, \nu_{LT} = 0.3 \quad (4.66)$$

$$\rho = 2500kg/m^3, \eta_d = 0.01$$

Four cases of the L-junction are considered in the calculation based on the different orientations of the two orthotropic plates. Figure 4.4 gives the explanation of the four different cases of the L-junction. The arrows on each plate indicate the stiffest principal material direction. In cases 1 and 4, the two plates have identical orientations while in cases 2 and 3; the two plates have different orientations.

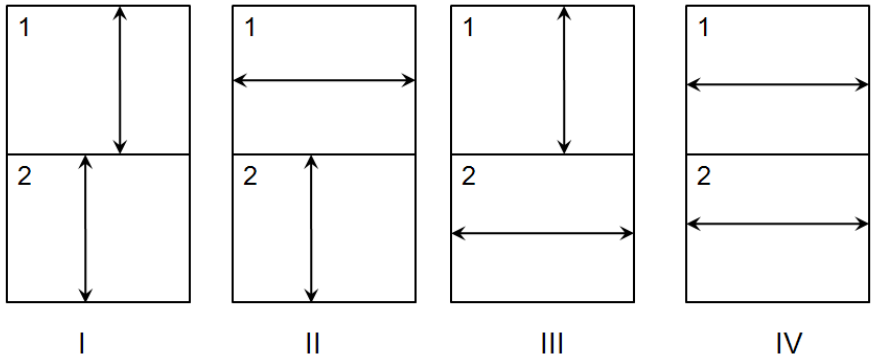

Figure 4.4 Four different orientations for two orthotropic plate L-junctions

The calculation in conventional FEA is implemented using NASTRAN finite element program. Plate 1 is given excitation at three randomly selected positions and the

velocities of both plates are calculated from dynamic analysis. The bending wave energy density of two plates can then be calculated and compared with the energy density calculated using EFEA formulation.

First, the transmission loss for bending wave is calculated using the procedure stated in section 4.2. Transmission loss is calculated as (Bosmans, Mees et al. 1996):

$$R_{12} = -10\log(\overline{\tau}_{12}) \tag{4.67}$$

where $\overline{\tau}_{12}$ is the averaged bending transmission coefficient from plate 1 to plate 2, it is obtained by integrating the power transmission coefficient $\tau_{12}(\theta)$ over all the angles of incidence θ.

The transmission loss for the four different orientations of L-junction has been calculated and plotted in Figure 4.5. From the plot we can see that the transmission loss for the similar orientation (case 1 and case 4) is smaller than the transmission loss of the dissimilar orientation (case 2 and case 3). It can also be observed from the plot that the transmission loss of the four cases lie within a range of 1 dB, which means that the model for the semi-infinite plate is not very sensitive to the Young's modulus of the plates.

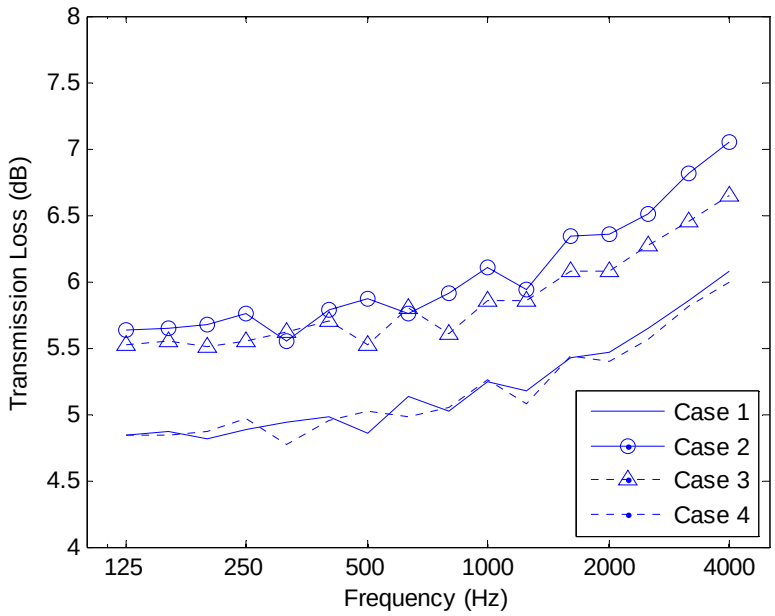

Figure 4.5 The transmission loss for the four cases of orthotropic L-junction

The energy density of plate 1 and plate 2 is calculated using conventional FEA model and the EFEA formulation. The models in the conventional FEA and EFEA formulation are shown in Figure 4.6 (a) and (b) respectively. The model in conventional FEA has 12,800 elements. The model in EFEA has only 32 elements.

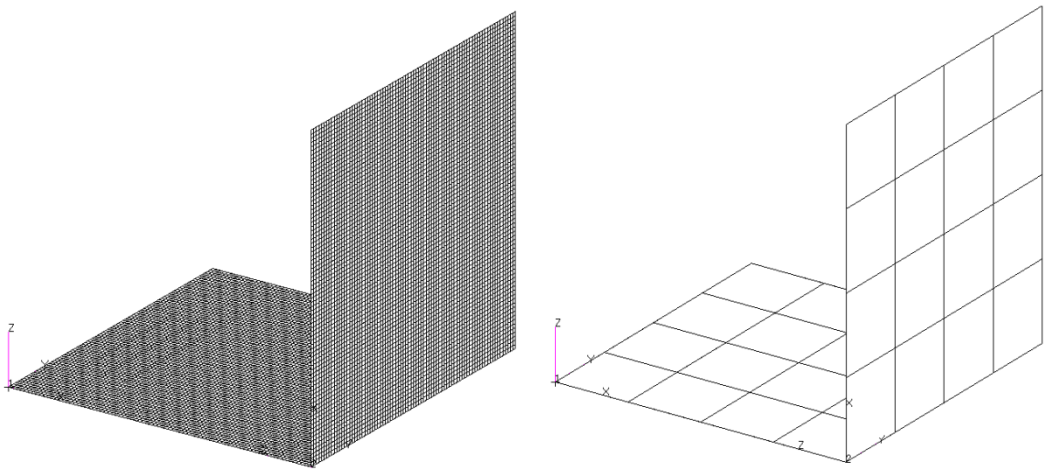

(a) (b)

Figure 4.6 The models of orthotropic L-junction in conventional FEA and EFEA

The energy density in two plates with properties described in equation (4.66) is calculated using conventional FEA and EFEA formulation respectively for the four different orientation cases and the results are shown in the following figures. First, in the conventional FEA model, the first plate is excited at three randomly selected locations and the input power at the three locations is computed using dynamic analysis. The computed input power at these locations serve as the excitations applied in the EFEA model. The velocity at each node in the FEA model is computed from NASTRAN program and the energy density can be calculated from the following equation:

$$e = \frac{1}{2}\rho|v|^2 \tag{4.68}$$

To compare the values of energy density with the results of EFEA model, the above value from equation (4.68) is averaged over the 1/3 octave band for the desired central frequencies.

The energy density value obtained from both conventional FEA and EFEA models are averaged over the entire plate in order to get the space-averaged energy density values. The energy density values of the two plates obtained from conventional FEA and EFEA models respectively are calculated for the four orientation of L-junction and are shown in Figure 4.7.

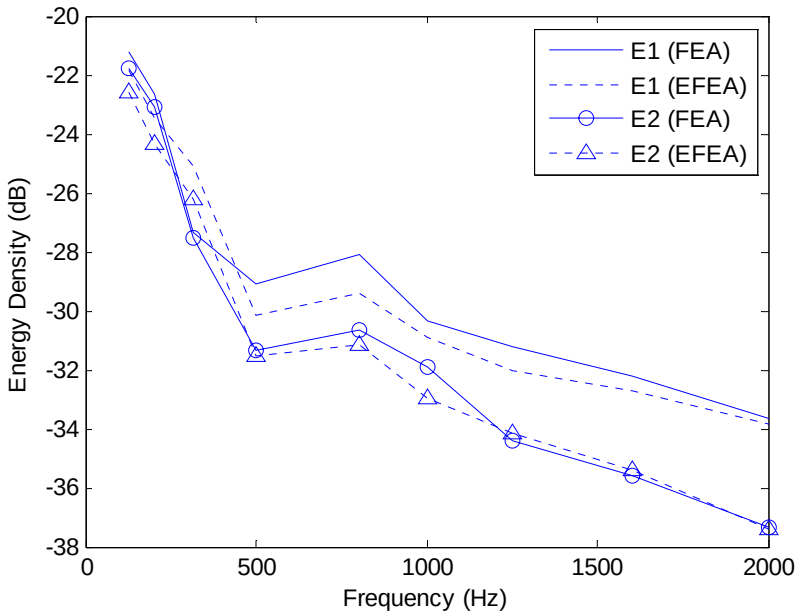

(a) Case 1

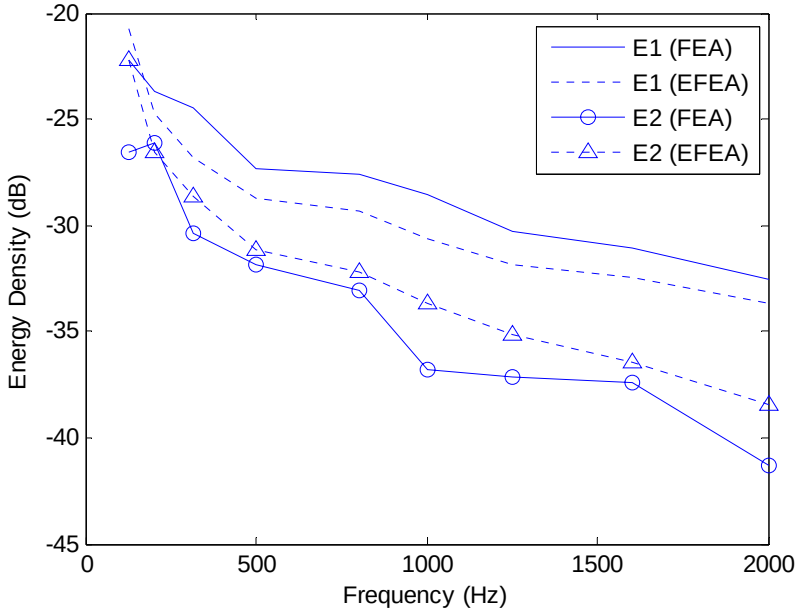

(b) Case2

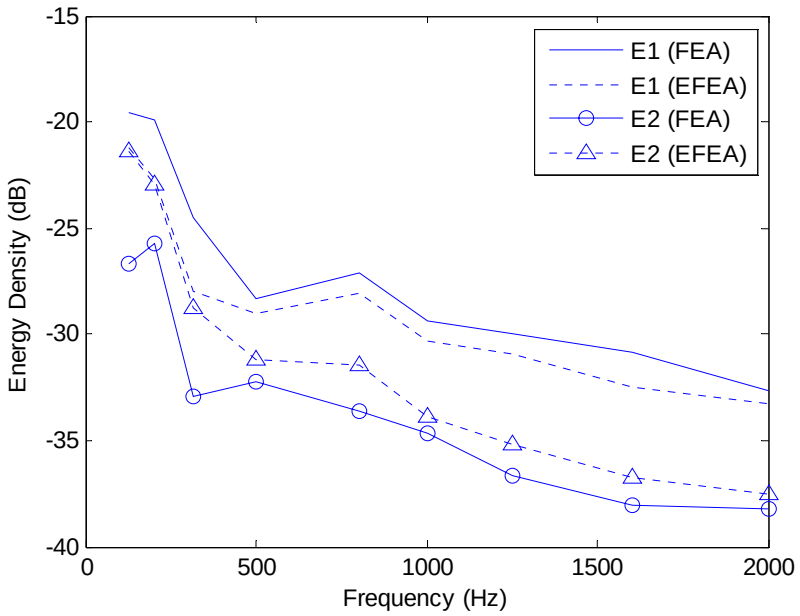

(c) Case 3

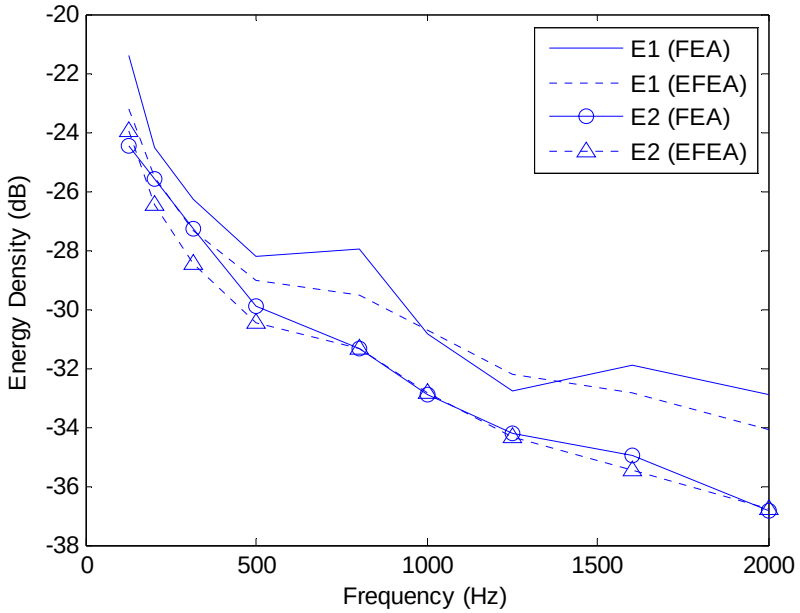

(d) Case 4

Figure 4.7 Energy density in two orthotropic plates (t=0.01m)

From Figure 4.7, we can see that for the similar orientation (case 1 and 4), the EFEA model matches well with the results from FEA. For the cases of dissimilar orientation (case 2 and 3), however, the EFEA model overestimates the bending wave transmission from plate 1 to plate 2. This phenomenon can be explained by the fact that the two models (EFEA model and FEA model) consider different coupling between eigenmodes (Bosmans, Mees et al. 1996). The FEA model predicts the actual coupling between the eigenmodes of the two plates; however, the EFEA model assumes that every mode of the first plate is evenly coupled to every mode of the second plate. This assumption is valid for the cases of similar orientation, because the eigenmodes have the same shape in two plates. For the cases of dissimilar orientation, the eigenmodes have different shapes in two plates; the assumption made by EFEA is no long valid.

To validate this explanation, we increase the modal density of the plates by reducing the thickness from 0.01m to 0.001m and increasing the frequency range to 5000 Hz. The results are shown in Figure 4.8.

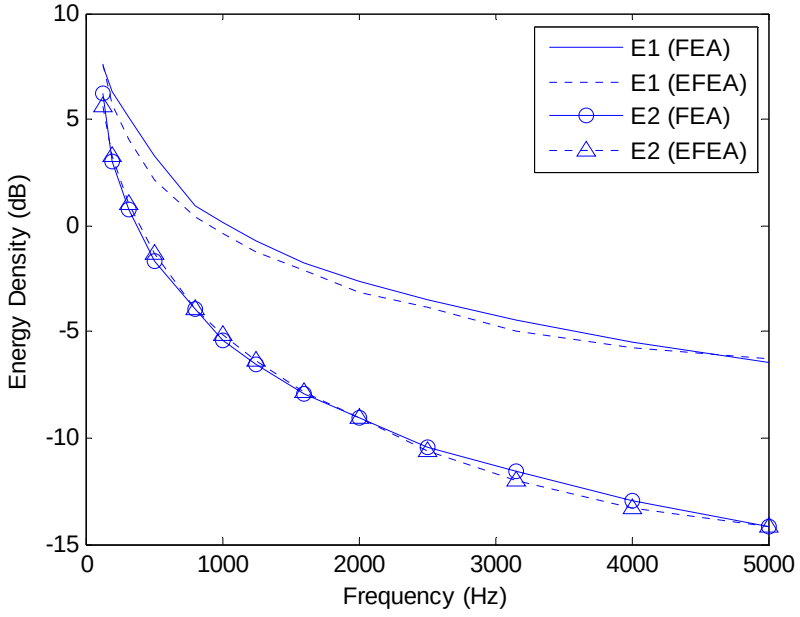

(a) Case 1

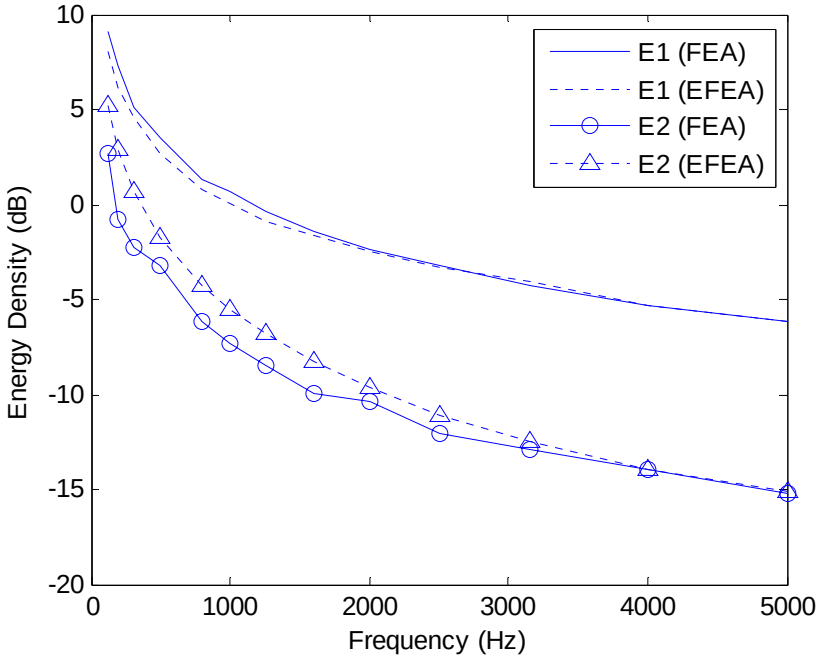

(b) Case 2

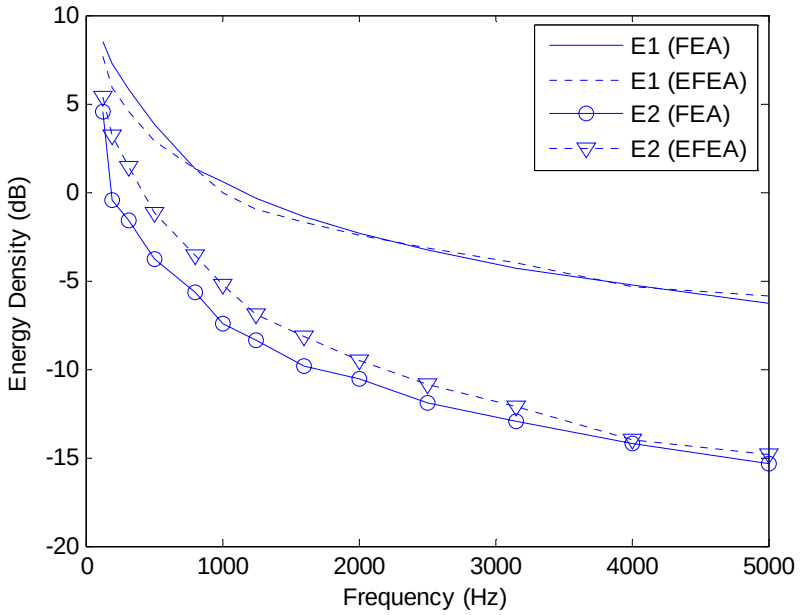

(c) Case 3

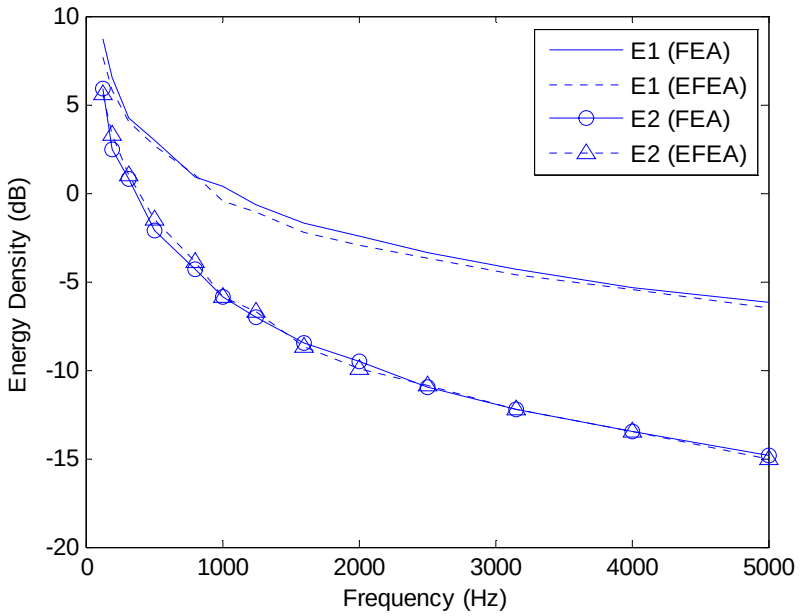

(d) Case 4

Figure 4.8 Energy density in two orthotropic plates (t=0.001m)

In Figure 4.8, much better agreements between FEA and EFEA models can be observed for all the four cases. Especially for the cases of dissimilar orientation (case 2 and 3), with the increasing frequency, the difference between FEA and EFEA results of energy density level of the two plates dropped from 3 dB to 0 dB. The reason for this better agreement is that with the increased modal density of the plates, the coupling between the modes also increased, especially for the differently orientated plates.

Chapter 5

POWER TRANMISSION THROUGH COUPLED COMPOSITE LAMINATE PLATES

5.1 Introduction

Composite laminate plates are increasingly used to construct structures or structural components because of their high specific mechanical properties and light weight. In order to evaluate the power flow within such structures at high frequency, the power transmission characteristic of the junctions where two or more composite laminate plates are connected together needs to be studied.

In Chapter 4, the power transmission coefficient and joint matrix for coupled orthotropic plates was derived. In this chapter, the power transmission mechanism at the junctions of general composite laminate plates is studied following the similar approach as discussed in Chapter 4. First, the governing equations for the bending and in-plane vibrations of composite laminate plate are presented. The solutions to the governing equations are derived, with emphasis on derivation of in-plane wavenumbers. Second, the expression of wave dynamic stiffness matrix is derived. Then, the complete equations at the junction, with contribution from each semi-infinite plate is formed and solved. The displacement in each plate can be found and the power transmission coefficients can be

calculated. Third, the joint matrix is formed and the global system of EFEA matrix is assembled. Finally, numerical examples are given and comparison between EFEA formulation and very dense FEA model is presented.

5.2 Derivation of Power Transmission Coefficients

5.2.1 Governing equations

Compared to the equations of motion for orthotropic plate, the equations of motion for the composite laminate plate have additional terms D_{16}, D_{26}, A_{16}, A_{26}. These terms gives the coupling between bending and torsion(Whitney and Ashton 1987).

$$D_{11j}\frac{\partial^4 w}{\partial x^4} + 4D_{16j}\frac{\partial^4 w}{\partial x^3 \partial y} + 2\left(D_{12j} + 2D_{66j}\right)\frac{\partial^4 w}{\partial x^2 \partial y^2} + 4D_{26j}\frac{\partial^4 w}{\partial x \partial y^3} + D_{22j}\frac{\partial^4 w}{\partial y^4} + \rho_j \frac{\partial^2 w}{\partial t^2} = 0 \tag{5.1}$$

$$A_{11j}\frac{\partial^2 u}{\partial x^2} + 2A_{16j}\frac{\partial^2 u}{\partial x \partial y} + A_{66j}\frac{\partial^2 u}{\partial y^2} + A_{16j}\frac{\partial^2 v}{\partial x^2} + \left(A_{12j} + A_{66j}\right)\frac{\partial^2 v}{\partial x \partial y} + A_{26j}\frac{\partial^2 v}{\partial y^2} - \rho_j \frac{\partial^2 u}{\partial t^2} = 0 \tag{5.2}$$

$$A_{66j}\frac{\partial^2 v}{\partial x^2} + 2A_{26j}\frac{\partial^2 v}{\partial x \partial y} + A_{22j}\frac{\partial^2 v}{\partial y^2} + A_{16j}\frac{\partial^2 u}{\partial x^2} + \left(A_{12j} + A_{66j}\right)\frac{\partial^2 u}{\partial x \partial y} + A_{26j}\frac{\partial^2 u}{\partial y^2} - \rho_j \frac{\partial^2 v}{\partial t^2} = 0 \tag{5.3}$$

where D_{11j} etc. are the coefficients of bending stiffness matrices of j th plate, A_{11j} etc. are the coefficients of extensional stiffness matrices of j th plate.

The relationship between the displacements and the traction that act at the connected edge of the plate can be expressed as follows (Whitney and Ashton 1987). The tractions that act on the common edge of the plates are evaluated at $y = 0$.

$$M_j = D_{22j}\frac{\partial^2 w}{\partial y^2} + D_{12j}\frac{\partial^2 w}{\partial x^2} + 2D_{26}\frac{\partial^2 w}{\partial x \partial y} \tag{5.4}$$

$$S_j = -\left[D_{16j}\frac{\partial^3 w}{\partial x^3} + \left(D_{12j} + 2D_{66j}\right)\frac{\partial^3 w}{\partial x^2 \partial y} + 3D_{26j}\frac{\partial^3 w}{\partial x \partial y^2} + D_{22j}\frac{\partial^3 w}{\partial y^3}\right] \tag{5.5}$$

$$N_j = A_{12j}\frac{\partial u}{\partial x} + A_{26j}\left(\frac{\partial u}{\partial y} + \frac{\partial v}{\partial x}\right) + A_{22j}\frac{\partial v}{\partial y} \tag{5.6}$$

$$T_j = A_{16j}\frac{\partial u}{\partial x} + A_{66j}\left(\frac{\partial u}{\partial y} + \frac{\partial v}{\partial x}\right) + A_{26j}\frac{\partial v}{\partial y} \tag{5.7}$$

The forces and moments per unit length at the junction can be expressed as the summation of the product of transformation matrix and the tractions at each plate (Langley and Heron 1990). It can be expressed as:

$$Q = \sum_{j=1}^{N} R_j F_j \tag{5.8}$$

where $F = \left(T_j \;\; N_j \;\; S_j \;\; M_j\right)^T$ represents the tractions that act at the connected edge of plate j, and the transformation matrix R_j is given by:

$$R_j = \begin{bmatrix} 1 & 0 & 0 & 0 \\ 0 & \cos\emptyset_j & -\sin\emptyset_j & 0 \\ 0 & \sin\emptyset_j & \cos\emptyset_j & 0 \\ 0 & 0 & 0 & 1 \end{bmatrix} \tag{5.9}$$

where $\emptyset_j$ is the angle of the local coordinate in plate j with respect to the global coordinate system.

Similar to Chapter 4, the compatibility conditions between the junction displacement a, and the edge displacement of plate j b_j, require that

$$b_j = R_j^T a \tag{5.10}$$

where $a = (u \;\; v \;\; w \;\; \theta)^T$, $b_j = \left(u_{ej} \;\; v_{ej} \;\; w_{ej} \;\; \theta_{ej}\right)^T$

5.2.2 Derivation of in-plane wavenumbers for composite laminate plates

Because of the anisotropy of composite laminate plate, the velocity of the mode is dependent on the direction of wave propagation (Bosmans, Mees et al. 1996; Bosmans, Vermeir et al. 2002). The dispersion relationship will again be obtained by assuming a plane wave form of the displacement and substituting into the equations of motion. Same

as the orthotropic case, the in-plane displacements for composite laminate plates are given by (Prosser 1991):

$$u = A_0\alpha_x exp[i(\omega t - k\cos\varphi x - k\sin\varphi y)] \tag{5.11}$$

$$v = A_0\alpha_y exp[i(\omega t - k\cos\varphi x - k\sin\varphi y)] \tag{5.12}$$

where $A_0\alpha_x$ and $A_0\alpha_y$ are the amplitudes of the two in-plane motions, φ is the direction of the wave propagation.

Substituting these displacements into the equations of motion yields:

$$\begin{bmatrix} A_{11}\,l_x^2 + 2A_{16}l_x l_y + A_{66}\,l_y^2 - \rho h c^2 & A_{16}l_x^2 + (A_{12}+A_{66})\,l_x\,l_y + A_{26}l_y^2 \\ A_{16}l_x^2 + (A_{12}+A_{66})\,l_x\,l_y + A_{26}l_y^2 & A_{66}\,l_x^2 + 2A_{26}l_x l_y + A_{22}\,l_y^2 - \rho h c^2 \end{bmatrix} \begin{bmatrix} \alpha_x \\ \alpha_y \end{bmatrix} = 0 \tag{5.13}$$

where $l_x = \cos\varphi$, $l_y = \sin\varphi$.

Setting the determinant equal to zero will yield a quadratic equation of c^2. The two solutions of group velocity correspond to the quasi-longitudinal and quasi-shear modes. Generally, the quasi-longitudinal mode is faster and thus corresponds to the smaller root.

5.2.3 Derivation of dynamic stiffness matrix

Assume the out-of-plane displacement of plate *j* has the form of exp $(-ikx + i\mu_B y + i\omega t)$, μ_B can be expressed as:

$$\mu_B^2 = k^2 \pm k_B^2 \tag{5.14}$$

where $k_B = \left[\frac{m\omega^2}{D_{11}\cos^4\varphi + 4D_{16}\sin\varphi\cos^3\varphi + 2(D_{12}+2D_{66})\cos^2\varphi\sin^2\varphi + 4D_{26}\cos\varphi\sin^3\varphi + D_{22}\sin^4\varphi}\right]^{1/4}$ is the bending wavenumber (Langley 1996), it depends on the direction of wave propagation φ.

The selection of μ_B follows the same rule as stated in Chapter 4. In the two cases of $k > k_B$ and $k < k_B$, equation (5.14) will have four real roots /two real roots and two imaginary roots. In both cases, only the negative roots are physical significant because the response must decay as $y \to \infty$ or propagate away from the junction (Langley and Heron 1990). After selecting the appropriate roots, the out-of-plane response of the plate can be written in the form:

$$w = \sum_{n=1}^{2} \alpha_{Bn} \exp(-ikx + \mu_{Bn} y + i\omega t) \tag{5.15}$$

where μ_{B1} and μ_{B2} are the two valid roots from equation (5.14), α_{B1} and α_{B2} are the complex amplitudes.

From equation (5.15), the displacement and rotation at the edge of the plate *j* can be expressed in terms of α_{B1} and α_{B2}:

$$\begin{Bmatrix} w_{ej} \\ \theta_{ej} \end{Bmatrix} = \begin{bmatrix} 1 & 1 \\ \mu_{B1} & \mu_{B2} \end{bmatrix} \begin{Bmatrix} \alpha_{B1} \\ \alpha_{B2} \end{Bmatrix} \exp(-ikx + i\omega t) \tag{5.16}$$

From equations (5.4) and (5.5), the edge tractions M_j and S_j can be expressed in terms of α_{B1} and α_{B2} as:

$$\begin{Bmatrix} S_j \\ M_j \end{Bmatrix} = [M_1] \begin{Bmatrix} \alpha_{B1} \\ \alpha_{B2} \end{Bmatrix} \tag{5.17}$$

where

$$M_1(1,1) = -ik^3 D_{16} + k^2(D_{12} + 4D_{66})\mu_{B1} + 3ikD_{26}\mu_{B1}^2 - D_{22}\mu_{B1}^3$$

$$M_1(1,2) = -ik^3 D_{16} + k^2(D_{12} + 4D_{66})\mu_{B2} + 3ikD_{26}\mu_{B2}^2 - D_{22}\mu_{B2}^3$$

$$M_1(2,1) = D_{22}\mu_{B1}^2 - k^2 D_{12} - 2ikD_{26}\mu_{B1}$$

$$M_1(2,2) = D_{22}\mu_{B2}^2 - k^2 D_{12} - 2ikD_{26}\mu_{B2}$$

Eliminate $\alpha_{B1}$and α_{B2} from equation (5.17) using equation (5.16), we can get the following relationship between the edge displacementsw_{ej}, $\theta_{ej}$and the edge tractions S_j and M_j:

$$\begin{Bmatrix} S_j \\ M_j \end{Bmatrix} = [N_1] \begin{Bmatrix} w_{ej} \\ \theta_{ej} \end{Bmatrix} \tag{5.18}$$

where

$$N_1(1,1) = \frac{1}{\mu_{B1}-\mu_{B2}} [ik^3 D_{16}(\mu_{B2}-\mu_{B1}) + 3ikD_{26}\mu_{B1}\mu_{B2}(\mu_{B2}-\mu_{B1}) + D_{22}\mu_{B1}\mu_{B2}(\mu_{B1}^2 - \mu_{B2}^2)]$$

$$N_1(1,2) = \frac{1}{\mu_{B1}-\mu_{B2}} [k^2(D_{12} + 4D_{66})(\mu_{B1}-\mu_{B2}) + 3ikD_{26}(\mu_{B1}^2 - \mu_{B2}^2) + D_{22}(\mu_{B2}^3 - \mu_{B1}^3)]$$

$$N_1(2,1) = \frac{1}{\mu_{B1}-\mu_{B2}} [D_{22}\mu_{B1}\mu_{B2}(\mu_{B2}-\mu_{B1}) + k^2 D_{12}(\mu_{B2}-\mu_{B1})]$$

$$N_1(2,2) = \frac{1}{\mu_{B1}-\mu_{B2}} [D_{22}(\mu_{B1}^2 - \mu_{B2}^2) + 2ikD_{26}(\mu_{B2}-\mu_{B1})]$$

Similar procedure can be used to determine the in-plane behavior of the plate. Assuming the in-plane motions are in the following expressions:

$$u = A_0 exp(i\omega t - ikx + \mu y) \tag{5.19}$$

$$v = VA_0 exp(i\omega t - ikx + \mu y) \tag{5.20}$$

where V is the ratio between the amplitudes of the two displacements.

Substituting equation (5.19) and (5.20) into the in-plane equations of motion, we can get the following expression:

$$\begin{bmatrix} A_{11}k^2 - 2iA_{16}k\mu - A_{66}\mu^2 - \rho h\omega^2 & A_{16}k^2 - i(A_{12}+A_{66})k\mu - A_{26}\mu^2 \\ A_{16}k^2 - i(A_{12}+A_{66})k\mu - A_{26}\mu^2 & A_{66}k^2 - 2iA_{26}k\mu - A_{22}\mu^2 - \rho h\omega^2 \end{bmatrix} \begin{Bmatrix} 1 \\ V \end{Bmatrix} = \begin{Bmatrix} 0 \\ 0 \end{Bmatrix} \tag{5.21}$$

Take the determinant equal to zero yield a polynomial equation of μ. Again, among the four roots of μ only the real and negative or imaginary and negative roots are selected. They are the corresponding y components of longitudinal and shear wavesnumbers respectively. Associated with each root is a mode shape which governs

the relationship between the two in-plane displacements. The two mode shapes can also be obtained as $\begin{Bmatrix}1\\V_1\end{Bmatrix}$ and $\begin{Bmatrix}1\\V_2\end{Bmatrix}$.

Thus, the in-plane response can be written in the form:

$$\begin{Bmatrix}u\\v\end{Bmatrix} = \left\{\alpha_L \begin{pmatrix}1\\V_1\end{pmatrix} e^{\mu_L y} + \alpha_S \begin{pmatrix}1\\V_2\end{pmatrix} e^{\mu_S y}\right\} \exp(-ikx + i\omega t) \tag{5.22}$$

where α_L and α_S are the complex amplitudes of the associated complementary functions. Thus, the edge displacements u_{ej} and v_{ej} can be also expressed in terms of α_L and α_S as:

$$\begin{Bmatrix}u_{ej}\\v_{ej}\end{Bmatrix} = \begin{bmatrix}1 & 1\\V_1 & V_2\end{bmatrix}\begin{Bmatrix}\alpha_L\\\alpha_S\end{Bmatrix} \exp(-ikx + i\omega t) \tag{5.23}$$

Similarly, we can express the edge tractions T_j and N_j in terms of α_L and α_S as:

$$\begin{Bmatrix}T_j\\N_j\end{Bmatrix} = [M_2]\begin{Bmatrix}\alpha_L\\\alpha_S\end{Bmatrix} \tag{5.24}$$

where

$$M_2(1,1) = A_{66}(\mu_L - ikV_1) - ikA_{16} + V_1\mu_L A_{26}$$

$$M_2(1,2) = A_{66}(\mu_S - ikV_2) - ikA_{16} + V_2\mu_S A_{26}$$

$$M_2(2,1) = -ikA_{12} + \mu_L V_1 A_{22} + \mu_L A_{26} - ikV_2 A_{26}$$

$$M_2(2,2) = -ikA_{12} + \mu_S V_2 A_{22} + \mu_S A_{26} - ikV_2 A_{26}$$

Eliminate α_L and α_S from equation (5.24) using equation (5.23), we can get the following relationship between the edge displacements u_{ej}, v_{ej} and the edge tractions T_j and N_j:

$$\begin{Bmatrix}T_j\\N_j\end{Bmatrix} = [N_2]\begin{Bmatrix}u_{ej}\\v_{ej}\end{Bmatrix} \tag{5.25}$$

where

$$N_2(1,1) = \frac{1}{V_1 - V_2}[A_{66}(\mu_S V_1 - \mu_L V_2) + ikA_{16}(V_2 - V_1) + A_{26}V_1V_2(\mu_S - \mu_L)]$$

$$N_2(1,2) = \frac{1}{V_1 - V_2}[A_{66}(\mu_L - \mu_S) + ikA_{66}(V_2 - V_1) + A_{26}(\mu_L V_1 - \mu_S V_2)]$$

$$N_2(2,1) = \frac{1}{V_1 - V_2}[V_1 V_2 A_{22}(\mu_s - \mu_L) + A_{26}(\mu_S V_1 - \mu_L V_2)]$$

$$N_2(2,2) = \frac{1}{V_1 - V_2}[A_{22}(V_2 \mu_s - V_1 \mu_L) + A_{26}(\mu_L - \mu_S) + ik(V_2 - V_1)]$$

Equations (5.18) and (5.25) can be combined to produce a relationship between the complete set of edge displacements b_j and tractions F_j of the form:

$$F_j = K_j b_j \tag{5.26}$$

where

$$b_j = \left(u_{ej} \;\; v_{ej} \;\; w_{ej} \;\; \theta_{ej}\right)^T,$$

$$F_j = \left(T_j \;\; N_j \;\; S_j \;\; M_j\right)^T,$$

The entries of dynamic stiffness matrix K_j have been derived and can be found from equation (5.18) and (5.25) as:

$$K_j = \begin{bmatrix} N_2(1,1) & N_2(1,2) & 0 & 0 \\ N_2(2,1) & N_2(2,2) & 0 & 0 \\ 0 & 0 & N_1(1,1) & N_1(1,2) \\ 0 & 0 & N_1(2,1) & N_1(2,2) \end{bmatrix} \tag{5.27}$$

5.2.4 Assembly of the complete equations and the calculation of transmission coefficients

The assembly of the complete equations and the calculation of transmission coefficients of the composite laminate plate follows the same procedure as described in Chapter 4. The averaged power transmission coefficient $\tau_{pr}^{ij}(\omega)$ can be obtained by integrating the angle of incidence from 0 to π.

$$\tau_{pr}^{ij}(\omega) = \frac{1}{2}\int_0^{\pi} \tau_{pr}^{ij}(\omega, \phi) \sin\phi d\phi \tag{5.28}$$

5.3 Derivation of Joint Matrix

The derivation of joint matrix for composite laminate plates will also follow the same procedure as in Chapter 4. The joint matrix expression for the coupled composite laminate plates appears same as equation (4.62), but the entries of the joint matrix is calculated using the power transmission coefficients derived in this Chapter.

5.4 Assembly of Global EFEA Equations for Coupled Composite Laminate Plates

The matrix expression of EFEA differential equation for single composite laminate plate at the element level is obtained in Chapter 3 and it can be expressed as:

$$[K^{1,2}]\langle \underline{e} \rangle_{1,2} = \{F^e\}_{1,2} + \{Q^e\}_{1,2} \tag{5.29}$$

where subscript 1 corresponds to the stiffness coefficients $D_{11}, D_{22}, D_{12}, D_{66}$, which correspond to the orthotropic plate, and the subscripts 2 corresponds to the stiffness $D_{16}$and D_{26}.

Using the alternative approach for developing the EFEA differential equation for composite laminate plate by finding the equivalent isotropic material, the EFEA differential equation at element level can be expressed as:

$$[K^e]\{e^e\} = \{F^e\} + \{Q^e\} \tag{5.30}$$

The power flow can be expressed in terms of energy density and power transmission coefficients.

$$\begin{Bmatrix} Q_n^i \\ Q_{n+1}^i \\ Q_m^j \\ Q_{m+1}^j \end{Bmatrix} = [JC]_j^i \begin{Bmatrix} e_n^i \\ e_{n+1}^i \\ e_m^j \\ e_{m+1}^j \end{Bmatrix} \tag{5.31}$$

where n and $n+1$ represents the two nodes of the i element at the joint, m and $m+1$ represents the two nodes of the j element at the joint, the joint matrices $[JC]_j^i$ define the power transfer across elements at the joints.

The final assembled system of EFEA equations can be expressed as:

$$\left(\begin{bmatrix}[K^e]_i & \\ & [K^e]_j\end{bmatrix} + [JC]_j^i\right)\begin{Bmatrix}\{e^i\}\\ \{e^j\}\end{Bmatrix} = \begin{Bmatrix}\{F^e\}_i\\ \{F^e\}_j\end{Bmatrix} \tag{5.32}$$

where $[K^e]_i$ and $[K^e]_j$ are the element matrix for the i and j element, $\{e^i\}$ and $\{e^j\}$ are the vectors containing all the nodal degrees of freedom for elements i and j.

5.5 Numerical Examples and Validation

In this section, an L-junction of two composite laminate plates is modeled using EFEA and conventional FEA and the results of energy distribution in two plates from both methods are compared.

The properties of the fiber composites that are used to compose the laminate plates are:

Carbon/Epoxy:

$$E_L = 138Gpa, E_T = 8.96Gpa, G_{LT} = 7.10Gpa, \nu_{12} = 0.30, \rho = 1600kg/m^3 \tag{5.33}$$

E-glass/Epoxy:

$$E_L = 39Gpa, E_T = 8.6Gpa, G_{LT} = 3.8Gpa, \nu_{12} = 0.28, \rho = 2100kg/m^3 \tag{5.34}$$

The first composite laminate plate is composed of three layers of carbon/epoxy fiber composites. The thickness of each layer is 1mm. The orientation of the composite is shown in Figure 5.1.

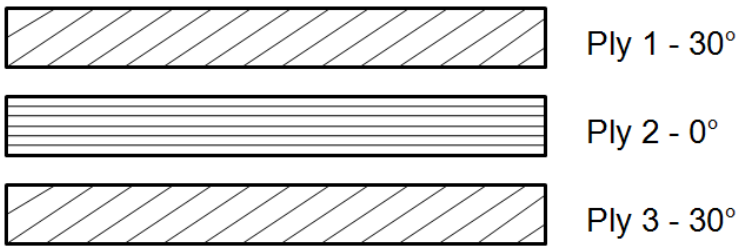

Figure 5.1 The orientation of the first composite laminate plate

The extensional and bending stiffness matrices of the first plate can be obtained from the orientation and properties of each ply and can be expressed as:

$$A_1 = \begin{bmatrix} 30.9 & 5.09 & 8.09 \\ 5.09 & 4.92 & 3.15 \\ 8.09 & 3.15 & 6.41 \end{bmatrix} \times 10^7 N/m \tag{5.35}$$

$$D_1 = \begin{bmatrix} 196 & 52.4 & 87.6 \\ 52.4 & 44.3 & 34.1 \\ 87.6 & 34.1 & 62.3 \end{bmatrix} N \cdot m \tag{5.36}$$

The second composite laminate plate is composed of two layers of e-glass/epoxy fiber composites. The orientation of the composite is shown in Figure 5.2.

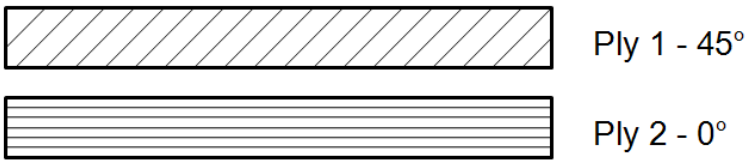

Figure 5.2 The orientation of the second composite laminate plate

The extensional and bending stiffness matrices of the first plate can be obtained from the orientation and properties of each ply and can be expressed as:

$$A_2 = \begin{bmatrix} 28.4 & 5.99 & 3.87 \\ 5.99 & 12.9 & 3.87 \\ 3.87 & 3.87 & 7.34 \end{bmatrix} \times 10^6 N/m \tag{5.37}$$

$$D_2 = \begin{bmatrix} 2.37 & 0.499 & 0.322 \\ 0.499 & 1.08 & 0.322 \\ 0.322 & 0.322 & 0.612 \end{bmatrix} N \cdot m \tag{5.38}$$

For this L-junction of two composite laminate plates, two cases are calculated. In these two cases, the second plate is connected to the different edges of the first plate. In the first case, the second plate is connected to first plate at the edge with 0 degree to the reference coordinate; in the second case, the second plate is connected to the first plate at the edge with 90 degree to the reference coordinate.

The models in the conventional FEA and EFEA formulation are shown in Figure 5.3 (a) and (b) respectively. The model in conventional FEA has 12,800 elements. The model in EFEA has only 32 elements.

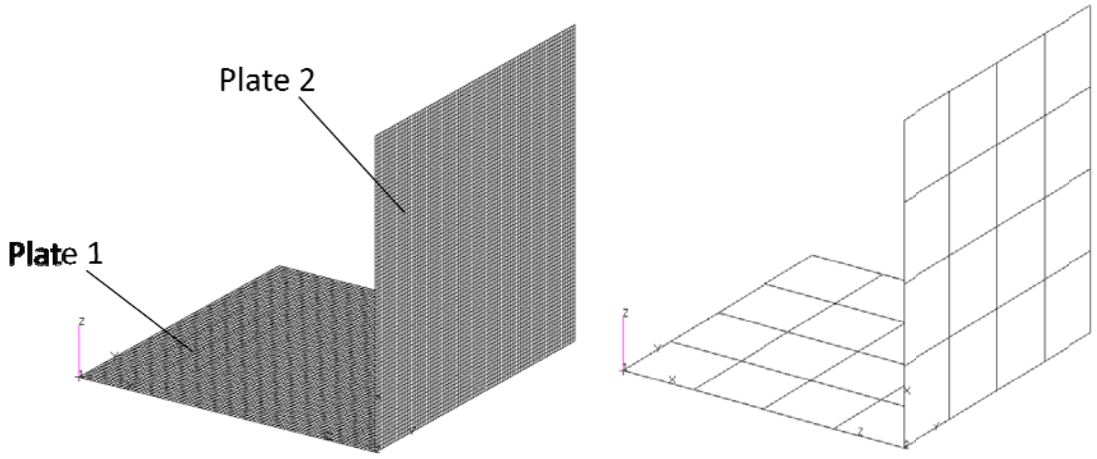

(a) (b)

Figure 5.3 The models of orthotropic L-junction in conventional FEA and EFEA

In the calculation, plate 1 is given excitation on three randomly selected locations, the energy density of plate 1 and plate 2 in two cases is calculated using conventional FEA model and the EFEA formulations respectively. The power transmission mechanism

derived for composite laminate plates is used in the calculation. For the conventional finite element analysis, the velocity at each node within the plate is obtained through dynamic analysis. First, the input power can be computed from FEA model at the excitation locations and the computed input power serve as the excitation applied in the EFEA model at the corresponding locations. Then, the energy density level of the plate is computed from the velocity value and then averaged over the entire plate (spatial average) and over the 1/3 octave band (frequency average). The averaged energy density level obtained from FEA model is then compared with the energy density computed from EFEA formulation. The comparison is shown in Figure 5.4 – 5.5.

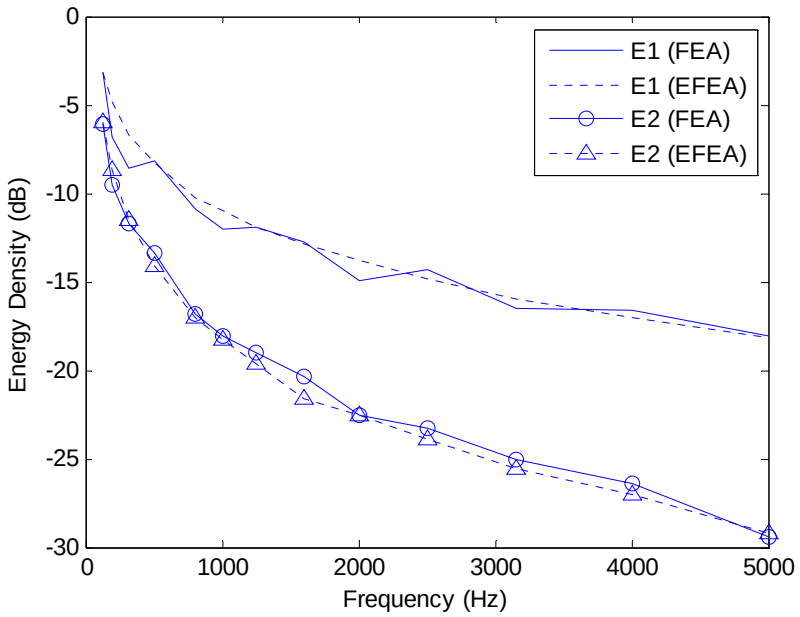

Figure 5.4 Comparison of energy density between EFEA and conventional FEA (case 1)

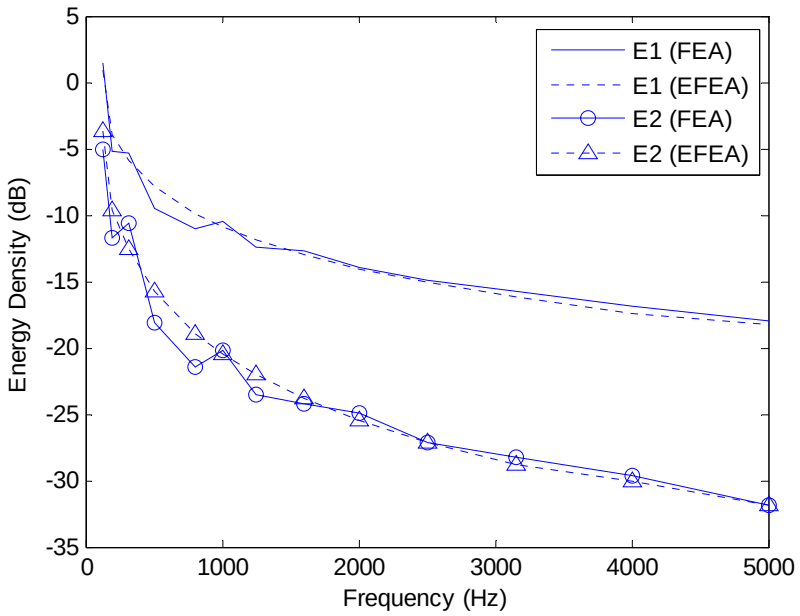

Figure 5.5 Comparison of energy density between EFEA and conventional FEA (case 2)

The velocity difference between these two plates is also calculated using two models. The velocity difference is defined as (Bosmans, Mees et al. 1996):

$$L_{vp} = 10\log\left(v_1^2/v_2^2\right) \tag{5.39}$$

The velocity difference between the two plates is computed using two methods and is shown in Figure 5.6 and 5.7.

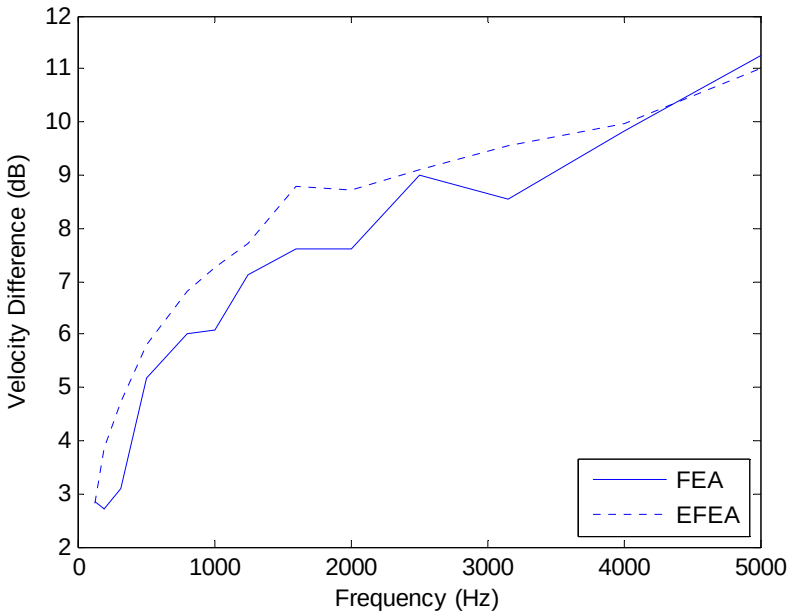

Figure 5.6 Comparison of velocity difference between two plates (case 1)

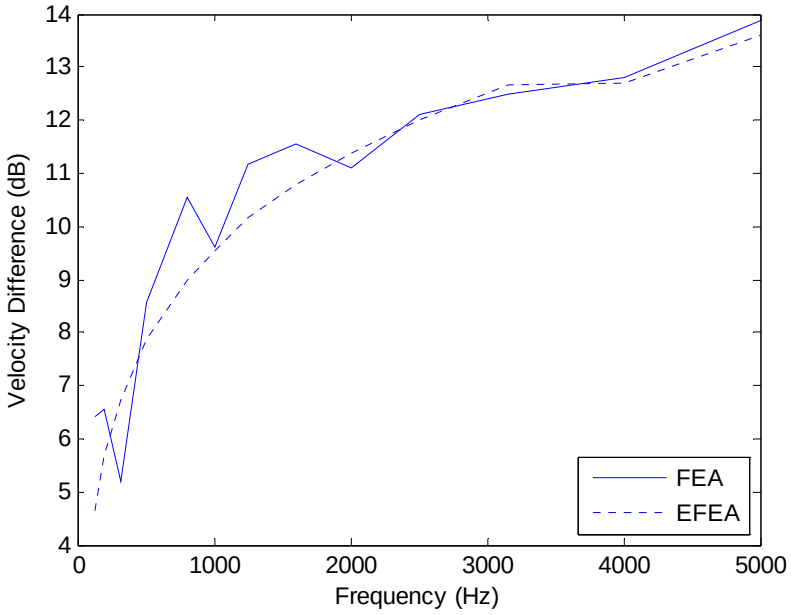

Figure 5.7 Comparison of velocity difference between two plates (case 2)

From the comparison plots, we find good agreements between the EFEA results and the results from very dense FEA model. The difference of the results obtained from

two models is within 1.5 dB. For the two different cases when the second plate is connected to the different edges of the first plate, the energy density level and velocity difference level have about 3 dB difference. This phenomenon is expected because of the anisotropy of the composite laminate plate.

Chapter 6

CONCLUSIONS AND RECOMMENDATIONS FOR FUTURE WORK

6.1 Conclusions

EFEA has been proven to be an effective and reliable tool for high frequency vibration analysis. It uses the averaged energy variable as the primary variable to form the governing differential equations and provides a practical approach to evaluate the structural response at high frequencies, which is hard to reach with conventional finite element analysis because of the computational cost. In the past, EFEA has been applied successfully to different structures, such as beams, rods, plates, curved panels etc. Until recently, however, not much work has been done in the field of composite structures.

The new developments of EFEA formulations in composite laminate plates are presented in this dissertation. The EFEA governing differential, with the time- and space- averaged energy density as the primary variable, is developed for general composite laminate plates. The power transmission characteristics at plate junctions of non-isotropic materials, including orthotropic plates and composite laminate plates are studied in order to assemble to global system of EFEA equations for complex structures.

The major work of this dissertation is:

1. The EFEA differential equation for single composite laminate plate is derived. The equations of motions that govern the vibration of composite laminate plate are presented. Convergence study is proceeded to prove the fact that the coupling terms between bending and in-plane motions become insignificant in high frequency range. The out-of-plane and in-plane equations of motions are thus considered uncoupled in our derivation. The wave solutions for the out-of-plane and in-plane displacements and the corresponding dispersion relationships are obtained. The expressions of energy density and energy intensities are derived and the relationship between the time- and space- averaged energy density and intensities is found, this relation, together with the power balance in a differential control volume of the plate, are utilized to form the EFEA differential equation with the energy density as the primary variable. The EFEA differential equation is derived for both bending and in-plane wave motion of the plate. Some numerical examples are presented where the EFEA model is validated by comparing with very dense FEA model. Finally, an alternative approach of forming the EFEA differential equation for composite laminate plates is introduced by using its equivalent isotropic plate and some validation is presented.
2. The power transmission for coupled orthotropic plates is studied. In the model, an arbitrary number of orthotropic plates are connected at a common edge. The power transmission coefficients are derived using the wave propagation approach. It assumes the wave propagates in the semi-infinite plate and is partially reflected and partially transmitted to other plates through the junction. The wave dynamic stiffness matrix is derived for each semi-infinite plate and the appropriate equilibrium and compatibility conditions at the junction are utilized to form the complete equation at

the junction. This equation is solved to obtain the displacements in each plate and the wave amplitudes of each type of waves that has been reflected or transmitted. The power transmission coefficients can then be computed. The power transmission coefficients are dependent on the angle of incident wave, thus, the final coefficients are averaged over all the angles of incidence. The joint matrix is then derived and the global system of EFEA equations are formed for coupled orthotropic plates. Finally, some numerical examples are studied to validate the derivation.

3. The power transmission for coupled composite laminate plates is also studied. The derivation of power transmission coefficients is also based on the same procedure assuming the propagation of elastic waves in semi-infinite composite laminate plates. Numerical example of two general composite laminate plates connected at junction is studied and the EFEA formulation is validate through comparing the results with the results from very dense FEA model.

6.2 Recommendations for Future Work

This dissertation summarized the work regarding to the application of energy finite element analysis to composite laminate plates. There are several possible developments for future work:

1. In the development of energy finite element formulations in composite laminate plates, classical laminate theory is used. This theory, however, is not accurate enough for thick composite plates, in which the shear resultants cannot be neglected. Thus, some other theories, such as shear deformation theory and layer by layer theory can be used for thick composite plates by accounting for the transverse shear deformation and the shear discontinuity through the plate thickness.

2. The main part of the derivation that has been done in this dissertation is written in MATLAB program. A FORTRAN program is needed in order to make this part of EFEA formulation work effectively with the main EFEA program. This will enable us to model the complex structures using finite element pre-processor and solve for the energy density distribution using the EFEA program effectively.
3. There are other forms of composite structures that are also widely used in the industries. The application of EFEA formulation to these types of structures, such as composite sandwich plate, thick composite plates, composite beams, composite panels etc. is very necessary and important.
4. Stiffeners are often used at junctions in the construction of composite structures. The EFEA formulation can be extended to account for the presence of stiffeners at the junction between composite panels.
5. The high frequency vibration analysis of composite structures under heavy fluid loading. Previously, this analysis has been done in thin isotropic plates and the extension of this research to the field of composite plates is meaningful for the NVH analysis of composite marine structures.
6. The development of hybrid finite element formulation for composite structures. The hybrid finite element method provides an approach for evaluating the vibration in the mid-frequency range. This development will give valuable significance to assess the response of composite structures at mid-frequencies.

APPENDIX

Derivation of Time- and Space- averaged Energy Density and Intensities for Composite Laminate Plates

A.1 Derivation of Time- and Space- averaged Energy Density

In equation (3.24), the time-averaged energy density for composite laminate plates can be expressed as:

$$\langle e\rangle = \frac{1}{4}Re\left\{D_{11c}\frac{\partial^2 w}{\partial x^2}\left(\frac{\partial^2 w}{\partial x^2}\right)^* + 2D_{12c}\frac{\partial^2 w}{\partial x^2}\left(\frac{\partial^2 w}{\partial y^2}\right)^* + D_{22c}\frac{\partial^2 w}{\partial y^2}\left(\frac{\partial^2 w}{\partial y^2}\right)^* + 4D_{66c}\frac{\partial^2 w}{\partial x\partial y}\left(\frac{\partial^2 w}{\partial x\partial y}\right)^* + 4D_{16c}\frac{\partial^2 w}{\partial x^2}\left(\frac{\partial^2 w}{\partial x\partial y}\right)^* + 4D_{26c}\frac{\partial^2 w}{\partial y^2}\left(\frac{\partial^2 w}{\partial x\partial y}\right)^* + m\frac{\partial w}{\partial t}\left(\frac{\partial w}{\partial t}\right)^*\right\} \quad \text{(A.1)}$$

The far-field displacement solution for the bending vibration of the plate can be expressed as:

$$w_{ff}(x,y,t) = \left\{Ae^{-i(k_x x+k_y y)} + Be^{i(k_x x-k_y y)} + Ce^{-i(k_x x-k_y y)} + De^{i(k_x x+k_y y)}\right\}e^{i\omega t} \quad \text{(A.2)}$$

Substituting (A.2) into (A.1), we get the following expression:

$$\langle e\rangle = \frac{1}{4}Re\{(D_{11c}|k_x|^4 + 2D_{12c}k_x^2\left(k_y^2\right)^* + D_{22c}\left|k_y\right|^4 + m\omega^2) \times |[A]^{--} + [B]^{+-} + [C]^{-+} + [D]^{++}|^2 + 4D_{66c}|k_x|^2\left|k_y\right|^2 \times |[A]^{--} - [B]^{+-} - [C]^{-+} + [D]^{++}|^2 + (4D_{16c}k_x^2k_x^*k_y^* + 4D_{26c}k_y^2k_x^*k_y^*) \times ([A]^{--} + [B]^{+-} + [C]^{-+} + [D]^{++})([A]^{--} - [B]^{+-} - [C]^{-+} + [D]^{++})^*\} \quad \text{(A.3)}$$

where $[\,]^{\pm\pm}$ means $[\,] \times \exp(\pm ik_x x \pm ik_y y)$.

In equation (A.3), the term $|[A]^{--}+[B]^{+-}+[C]^{-+}+[D]^{++}|^2$ can be expanded as:

$$|[A]^{--}+[B]^{+-}+[C]^{-+}+[D]^{++}|^2 = |[A]^{--}|^2+|[B]^{+-}|^2+|[C]^{-+}|^2+|[D]^{++}|^2+$$
$$[A]^{--}([B]^{+-})^*+[B]^{+-}([A]^{--})^*+[A]^{--}([C]^{-+})^*+[C]^{-+}([A]^{--})^*+[A]^{--}([D]^{++})^*+$$
$$[D]^{++}([A]^{--})^*+[B]^{+-}([C]^{-+})^*+[C]^{-+}([B]^{+-})^*+[B]^{+-}([D]^{++})^*+[D]^{++}([B]^{+-})^*+$$
$$[C]^{-+}([D]^{++})^*+[D]^{++}([C]^{-+})^* \quad (A.4)$$

In order to get the space-averaged energy density, we need to average the energy density value over a half wavelength as:

$$\langle \underline{e} \rangle = \frac{k_{xl}k_{yl}}{\pi^2}\int_0^{\pi/k_{yl}}\int_0^{\pi/k_{xl}}\langle e\rangle dxdy \quad (A.5)$$

The integral for the first term in equation (A.4) becomes:

$$\int_0^{\pi/k_{yl}}\int_0^{\pi/k_{xl}}|[A]^{--}|^2dxdy = \int_0^{\pi/k_{yl}}\int_0^{\pi/k_{xl}}|A|^2e^{-\left(\frac{\eta}{2}\right)k_{xl}x-\left(\frac{\eta}{2}\right)k_{yl}y}dxdy \quad (A.6)$$

If the damping is very small ($\eta \ll 1$), the exponential function in (A.6) can be assumed to be constant on the interval (Park, Hong et al. 2003):

$$\int_0^{\pi/k_{yl}}\int_0^{\pi/k_{xl}}|A|^2e^{-\left(\frac{\eta}{2}\right)k_{xl}x-\left(\frac{\eta}{2}\right)k_{yl}y}dxdy \approx |A|^2e^{--}\int_0^{\pi/k_{yl}}\int_0^{\pi/k_{xl}}dxdy = \frac{\pi^2}{k_{xl}k_{yl}}|A|^2e^{--} \quad (A.7)$$

The other similar terms $|[B]^{+-}|^2, |[C]^{-+}|^2, |[D]^{++}|^2$ can also be integrated similarly and get similar results as in (A.7).

The integral for the other terms such as $[A]^{--}([B]^{+-})^*$ can be obtained as:

$$\int_0^{\pi/k_{yl}}\int_0^{\pi/k_{xl}}[A]^{--}([B]^{+-})^*dxdy = AB^*\int_0^{\pi/k_{yl}}e^{-\left(\frac{\eta}{2}\right)k_{yl}y}\int_0^{\pi/k_{xl}}e^{-\left(\frac{\eta}{2}\right)k_{xl}x}dxdy = 0 \quad (A.8)$$

Thus, the time- and space- averaged energy density can be expressed as:

$$\langle \underline{e} \rangle =$$
$$\frac{1}{4}Re\{\left(D_{11c}|k_x|^4+2D_{12c}k_x^2\left(k_y^2\right)^*+D_{22c}\left|k_y\right|^4+4D_{66c}|k_x|^2\left|k_y\right|^2+m\omega^2\right)(|A|^2e^{--}+$$

$$|B|^2e^{+-} + |C|^2e^{-+} + |D|^2e^{++}) + \left(4D_{16c}k_x^2k_x^*k_y^* + 4D_{26c}k_y^2k_x^*k_y^*\right)(|A|^2e^{--} -$$

$$|B|^2e^{+-} - |C|^2e^{-+} + |D|^2e^{++})\} \quad \text{(A.9)}$$

Substituting $k_x = k_{xl}\left(1 - i\frac{\eta}{4}\right), k_y = k_{yl}\left(1 - i\frac{\eta}{4}\right)$ and $D_{11c} = D_{11}(1 + i\eta), D_{22c} = D_{22}(1 + i\eta)$ etc. into equation (A.9), and neglecting all the second and higher order terms of the damping loss factor, the terms can be simplified as:

$$Re\left(D_{11c}|k_x|^4 + 2D_{12c}k_x^2\left(k_y^2\right)^* + D_{22c}\left|k_y\right|^4 + 4D_{66c}|k_x|^2\left|k_y\right|^2 + m\omega^2\right) =$$

$$D_{11}k_{xl}^4(1 + \tfrac{\eta^2}{16})^2 + 2D_{12}k_{xl}^2k_{yl}^2\left[(1 - \tfrac{\eta^2}{16})^2 + \tfrac{\eta^2}{4}\right] + D_{22}k_{yl}^4(1 + \tfrac{\eta^2}{16})^2 + 4D_{66}k_{xl}^2k_{yl}^2(1 +$$

$$\tfrac{\eta^2}{16})^2 + m\omega^2 \approx D_{11}k_{xl}^4 + 2(D_{12} + 2D_{66})k_{xl}^2k_{yl}^2 + D_{22}k_{yl}^4 + m\omega^2 \quad \text{(A.10)}$$

$$Re\left(4D_{16c}k_x^2k_x^*k_y^* + 4D_{26c}k_y^2k_x^*k_y^*\right) = 4\left(D_{16}k_{xl}^3k_{yl} + D_{26}k_{yl}^3k_{xl}\right)\left[(1 - \tfrac{\eta^2}{16})^2 + \tfrac{\eta^2}{4}\right] \approx$$

$$4\left(D_{16}k_{xl}^3k_{yl} + D_{26}k_{xl}k_{yl}^3\right) \quad \text{(A.11)}$$

Thus, the time- and space- averaged energy density can be expressed as:

$$\langle \underline{e} \rangle = \frac{1}{4}\left(D_{11}k_{xl}^4 + 2(D_{12} + 2D_{66})k_{xl}^2k_{yl}^2 + D_{22}k_{yl}^4 + m\omega^2\right)(|A|^2e^{--} + |B|^2e^{+-}$$

$$+ |C|^2e^{-+} + |D|^2e^{++})$$

$$+ \left(D_{16}k_{xl}^3k_{yl} + D_{26}k_{xl}k_{yl}^3\right)(|A|^2e^{--} - |B|^2e^{+-} - |C|^2e^{-+} + |D|^2e^{++}) \quad \text{(A.12)}$$

where $e^{\pm\pm}$ represents $exp\left\{\pm\frac{\eta}{2}k_{xl}^*x \pm \frac{\eta}{2}k_{yl}^*y\right\}$.

A.2 Derivation of Time- and Space- averaged Energy Intensities

The x and y components of the time-averaged intensity of a laminated plate can be expressed as:

$$\langle I_x \rangle = \frac{1}{2} Re\left\{-Q_{xz}\left(\frac{\partial w}{\partial t}\right)^* + M_x\left(\frac{\partial^2 w}{\partial x \partial t}\right)^* + M_{xy}\left(\frac{\partial^2 w}{\partial y \partial t}\right)^*\right\} \quad \text{(A.13)}$$

$$\langle I_y \rangle = \frac{1}{2} Re\left\{-Q_{yz}\left(\frac{\partial w}{\partial t}\right)^* + M_y\left(\frac{\partial^2 w}{\partial y \partial t}\right)^* + M_{yx}\left(\frac{\partial^2 w}{\partial x \partial t}\right)^*\right\} \quad \text{(A.14)}$$

Substituting the forces and moments into equation (A.13) yields the expression for the x component of the energy intensity as:

$$\langle I_x \rangle = \frac{1}{2} Re\left\{\left[D_{11c}\frac{\partial^3 w}{\partial x^3} + (D_{12c} + 2D_{66c})\frac{\partial^3 w}{\partial x \partial y^2} + 3D_{16c}\frac{\partial^3 w}{\partial x^2 \partial y} + D_{26c}\frac{\partial^3 w}{\partial y^3}\right]\left(\frac{\partial w}{\partial t}\right)^* - \left(D_{11c}\frac{\partial^2 w}{\partial x^2} + D_{12c}\frac{\partial^2 w}{\partial y^2} + 2D_{16c}\frac{\partial^2 w}{\partial x \partial y}\right)\left(\frac{\partial^2 w}{\partial x \partial t}\right)^* - \left(D_{16c}\frac{\partial^2 w}{\partial x^2} + D_{26c}\frac{\partial^2 w}{\partial y^2} + 2D_{66c}\frac{\partial^2 w}{\partial x \partial y}\right)\left(\frac{\partial^2 w}{\partial y \partial t}\right)^*\right\} \quad \text{(A.15)}$$

Substituting the far-field solution into equation (A.15), and taking the space average of the energy intensity by integrating it over a half wavelength, we get the time- and space- averaged energy intensity as:

$$\langle \underline{I_x} \rangle = \frac{\omega}{2} Re\{\left[D_{11c}(k_x^3 + k_x^2 k_x^*) + (D_{12c} + 2D_{66c})k_x k_y^2 + D_{12c}k_y^2 k_x^* + 2D_{66c}k_x k_y k_y^*\right](|A|^2 e^{--} - |B|^2 e^{+-} + |C|^2 e^{-+} - |D|^2 e^{++}) + \left(3D_{16c}k_x^2 k_y + D_{26c}k_y^3 + 2D_{16c}k_x k_x^* k_y + D_{16c}k_x^2 k_y^* + D_{26c}k_y^2 k_y^*\right)(|A|^2 e^{--} + |B|^2 e^{+-} - |C|^2 e^{-+} - |D|^2 e^{++})\} \quad \text{(A.16)}$$

Again, substituting $k_x = k_{xl}\left(1 - i\frac{\eta}{4}\right), k_y = k_{yl}\left(1 - i\frac{\eta}{4}\right)$ and $D_{11c} = D_{11}(1 + i\eta), D_{22c} = D_{22}(1 + i\eta)$ etc. into equation (A.16), and neglecting all the second and higher order terms of the damping loss factor, the terms can be simplified as:

$$Re\left[D_{11c}(k_x^3 + k_x^2 k_x^*) + (D_{12c} + 2D_{66c})k_x k_y^2 + D_{12c}k_y^2 k_x^* + 2D_{66c}k_x k_y k_y^*\right] \approx 2D_{11}k_{xl}^3 + 2(D_{12} + 2D_{66})k_{xl}k_{yl}^2 \quad \text{(A.17)}$$

$$Re\left(3D_{16c}k_x^2k_y + D_{26c}k_y^3 + 2D_{16c}k_xk_x^*k_y + D_{16c}k_x^2k_y^* + D_{26c}k_y^2k_y^*\right) \approx 6D_{16}k_{xl}^2k_{yl} + 2D_{26}k_{yl}^3 \quad \text{(A.18)}$$

Thus, the x component of the time- and space- averaged energy intensity can be expressed as:

$$\langle \underline{I}_x \rangle = \omega\left[D_{11}k_{xl}^3 + (D_{12} + 2D_{66})k_{xl}k_{yl}^2\right](|A|^2e^{--} - |B|^2e^{+-} + |C|^2e^{-+} - |D|^2e^{++}) + \omega\left[3D_{16}k_{xl}^2k_{yl} + D_{26}k_{yl}^3\right](|A|^2e^{--} + |B|^2e^{+-} - |C|^2e^{-+} - |D|^2e^{++}) \quad \text{(A.19)}$$

Similarly, the y component of the time- and space- averaged energy intensity can be expressed as:

$$\langle \underline{I}_y \rangle = \omega\left[D_{22}k_{yl}^3 + (D_{12} + 2D_{66})k_{xl}^2k_{yl}\right](|A|^2e^{--} + |B|^2e^{+-} - |C|^2e^{-+} - |D|^2e^{++}) + \omega\left[3D_{26}k_{xl}k_{yl}^2 + D_{16}k_{xl}^3\right](|A|^2e^{--} - |B|^2e^{+-} + |C|^2e^{-+} - |D|^2e^{++}) \quad \text{(A.20)}$$

REFERENCES

1. Agarwal, B. D. and L. J. Broutman (1990). Analysis and Performance of Fiber Composites. New York, Wiley.
2. Ashton, J. E. and J. M. Whitney (1970). Theory of Laminated Plates. Stamford, Conn., Technomic.
3. Auld, B. A. (1990). Acoustic Fields and Waves in Solids. Malabar, Fla., R.E. Krieger.
4. Bernhard, R. J. and J. E. Huff (1999). "Structural-Acoustic Design at High Frequency using the Energy Finite Element Method." Journal of Vibration and Acoustics-Transactions of the ASME **121**(3): 295-301.
5. Bitsie, F. and R. J. Bernhard (1996). The Structural-Acoustic Energy Finite Element Method and Energy Boundary Element Method. West Lafayette, Purdue Univeristy.
6. Bosmans, I., P. Mees, et al. (1996). "Structure-borne sound transmission between thin orthotropic plates: Analytical solutions." Journal of Sound and Vibration **191**(1): 75-90.
7. Bosmans, I. and T. R. T. Nightinghale (1999). Structure-borne Sound Transmission in Rib-stiffened Plate Structures Typical of Wood Frame Buildings.

Ontario, National Research Council Canada, Institute for Research in Construction Acoustics.

8. Bosmans, I., G. Vermeir, et al. (2002). "Coupling Loss Factors for Coupled Anisotropic Plates." Journal of Sound and Vibration **250**(2): 351-355.
9. Bouthier, O. M. (1992). Energetics of Vibrating Systems. Mechanical Engineering Department. West Lafayette, Purdue University. Ph.D. Dissertation.
10. Bouthier, O. M. and R. J. Bernhard (1992). "Models of Space-Averaged Energetics of Plates." AIAA Journal **30**(3): 616-623.
11. Bouthier, O. M. and R. J. Bernhard (1995). "Simple-Models of Energy-Flow in Vibrating Membranes." Journal of Sound and Vibration **182**(1): 129-147.
12. Bouthier, O. M. and R. J. Bernhard (1995). "Simple-Models of the Energetics of Transversely Vibrating Plates." Journal of Sound and Vibration **182**(1): 149-166.
13. Chakraborty, A., D. R. Mahapatra, et al. (2002). "Finite Element Analysis of Free Vibration and Wave Propagation in Asymmetric Composite Beams with Structural Discontinuities." Composite Structures **55**(1): 23-36.
14. Cho, P. E. (1993). Energy Flow Analysis of Coupled Structures. Mechanical Engineering Department. West Lafayette, Purdue University. Ph. D. Dissertation.
15. Cho, P. E. and R. J. Bernhard (1998). "Energy Flow Analysis of Coupled Beams." Journal of Sound and Vibration **211**(4): 593-605.
16. Crandali, S. H. and R. Lotz (1971). "On the Coupling Loss Factor in Statistical Energy Analysis." The Journal of the Acoustical Society of America **49**(1): 354-356.

17. Craven, P. G. and B. M. Gibbs (1981). "Sound-Transmission and Mode-Coupling at Junctions of Thin Plates .1. Representation of the Problem." Journal of Sound and Vibration **77**(3): 417-427.
18. Cremer, L., M. Heckl, et al. (1973). Structure Born Sound, Springer-Verlag.
19. DeLanghe, K., P. Sas, et al. (1997). "The Use of Wave-Absorbing Elements for the Evaluation of Transmission Characteristics of Beam Junctions." Journal of Vibration and Acoustics-Transactions of the ASME **119**(3): 293-303.
20. Fahy, F. J. (1982). Noise and Vibration, Chichester: Ellis Horwood.
21. Fahy, F. J. (1994). "Statistical Energy Analysis - a Critical Overview." Philosophical Transactions of the Royal Society of London Series a-Mathematical Physical and Engineering Sciences **346**(1681): 431-447.
22. Fredo, C. R. (1997). "A SEA-like Approach for the Derivation of Energy Flow Coefficients with a Finite Element Model." Journal of Sound and Vibration **199**(4): 645-666.
23. Gibbs, B. M. and P. G. Craven (1981). "Sound-Transmission and Mode-Coupling at Junctions of Thin Plates .2. Parametric Survey." Journal of Sound and Vibration **77**(3): 429-435.
24. Heckl, M. (1962). "Vibrations of Point-Driven Cylindrical Shells." Journal of the Acoustical Society of America **34**(10): 1553-1557.
25. Her, S. C. and Y. C. Liang (2004). "The Finite Element Analysis of Composite Laminates and Shell Structures subjected to Low Velocity Impact." Composite Structures **66**(1-4): 277-285.

26. Horner, J. L. and R. G. White (1990). "Prediction of Vibrational Power Transmission through Jointed Beams." International Journal of Mechanical Sciences **32**(3): 215-223.
27. Iannucci, L. and J. Ankersen (2006). "An Energy Based Damage Model for Thin Laminated Composites." Composites Science and Technology **66**(7-8): 934-951.
28. Jones, R. M. (1999). Mechanics of Composite Materials. Philadelphia, PA, Taylor & Francis.
29. Kim, H. S., H. J. Kang, et al. (1994). "A Vibration Analysis of Plates at High-Frequencies by the Power-Flow Method." Journal of Sound and Vibration **174**(4): 493-504.
30. Koh, C. G., K. K. Ang, et al. (2003). "Dynamic Analysis of Shell Structures with Application to Blast Resistant Doors." Shock and Vibration **10**(4): 269-279.
31. Krishnamurthy, K. S., P. Mahajan, et al. (2003). "Impact Response and Damage in Laminated Composite Cylindrical Shells." Composite Structures **59**(1): 15-36.
32. Langley, R. S. (1989). "A General Derivation of the Statistical Energy Analysis Equations for Coupled Dynamic-Systems." Journal of Sound and Vibration **135**(3): 499-508.
33. Langley, R. S. (1990). "A Derivation of the Coupling Loss Factors Used in Statistical Energy Analysis." Journal of Sound and Vibration **141**(2): 207-219.
34. Langley, R. S. (1994). "Elastic-Wave Transmission Coefficients and Coupling Loss Factors for Structural Junctions between Curved Panels." Journal of Sound and Vibration **169**(3): 297-317.

35. Langley, R. S. (1996). "The Modal Density of Anisotropic Structural Components." Journal of the Acoustical Society of America **99**(6): 3481-3487.
36. Langley, R. S. and P. Bremner (1999). "A Hybrid Method for the Vibration Analysis of Complex Structural-acoustic Systems." Journal of the Acoustical Society of America **105**(3): 1657-1671.
37. Langley, R. S. and K. H. Heron (1990). "Elastic Wave Transmission through Plate Beam Junctions." Journal of Sound and Vibration **143**(2): 241-253.
38. Langley, R. S., J. R. D. Smith, et al. (1997). "Statistical Energy Analysis of Periodically Stiffened Damped Plate Structures." Journal of Sound and Vibration **208**(3): 407-426.
39. Lyon, R. (1975). Statistical Energy Analysis of Dynamical Systems: Theory and Application. Cambridge, The MIT Press.
40. Lyon, R. H. and E. Eichler (1964). "Random Vibration of Connected Structures." Journal of the Acoustical Society of America **36**(7): 1344-1356.
41. Lyon, R. H. and G. Maidanik (1962). "Power Flow between Linearly Coupled Oscillators." Journal of the Acoustical Society of America **34**(5): 623-630.
42. Mahapatra, D. R. and S. Gopalakrishnan (2004). "Spectral Finite Element Analysis of Coupled Wave Propagation in Composite Beams with Multiple Delaminations and Strip Inclusions." International Journal of Solids and Structures **41**(5-6): 1173-1208.
43. Maidanik, G. (1962). "Response of Ribbed Panels to Reverberant Acoustic Fields." Journal of the Acoustical Society of America **34**(6): 809-815.

44. Manning, J. E. and G. Maidanik (1964). "Radiation Properties of Cylindrical Shells." Journal of the Acoustical Society of America **36**(9): 1691-1700.

45. Mccollum, M. D. and J. M. Cuschieri (1990). "Thick Plate Bending Wave Transmission Using a Mobility Power Flow Approach." Journal of the Acoustical Society of America **88**(3): 1472-1479.

46. Mees, P. and G. Vermeir (1993). "Structure-Borne Sound-Transmission at Elastically Connected Plates." Journal of Sound and Vibration **166**(1): 55-76.

47. Meo, M., R. Vignjevic, et al. (2005). "The Response of Honeycomb Sandwich Panels under Low-velocity Impact Loading." International Journal of Mechanical Sciences **47**(9): 1301-1325.

48. Nayakl, A. K., R. A. Shenoi, et al. (2006). "Dynamic Response of Composite Sandwich Plates subjected to Initial Stresses." Composites Part A-Applied Science and Manufacturing **37**(8): 1189-1205.

49. Nefske, D. J. and S. H. Sung (1989). "Power Flow Finite-Element Analysis of Dynamic-Systems - Basic Theory and Application to Beams." Journal of Vibration Acoustics Stress and Reliability in Design-Transactions of the ASME **111**(1): 94-100.

50. Oguibe, C. N. and D. C. Webb (1999). "Finite-element Modelling of the Impact Response of a Laminated Composite Plate." Composites Science and Technology **59**(12): 1913-1922.

51. Park, D. H., S. Y. Hong, et al. (2003). "Power Flow Model of Flexural Waves in Finite Orthotropic Plates." Journal of Sound and Vibration **264**(1): 203-224.

52. Park, D. H., S. Y. Hong, et al. (2001). "Power Flow Models and Analysis of In-plane Waves in Finite Coupled Thin Plates." Journal of Sound and Vibration **244**(4): 651-668.

53. Pierre, C., N. Vlahopoulos, et al. (2004). "Advanced Structure Methodologies for Next-generation Ground Vehicles, Part 1: Basic Theories." International Journal of Heavy Vehicle Systems **11**(3-4): 257-281.

54. Pierre, C., N. Vlahopoulos, et al. (2004). "Advanced Structure Methodologies for Next-generation Ground Vehicles, Part 2: Case Study." International Journal of Heavy Vehicle Systems **11**(3-4): 282-302.

55. Prosser, W. H. (1991). The Propagation Characteristics of the Plate Modes of Acoustic Emission Waves in Thin Aluminum Plates and Thin Graphite/epoxy Composite Plates and Tubes, The Johns Hopkins Univsersity. Ph.D. Dissertation.

56. Qiu, X., V. S. Deshpande, et al. (2003). "Finite Element Analysis of the Dynamic Response of Clamped Sandwich Beams subject to Shock Loading." European Journal of Mechanics **22**(6): 801-814.

57. Reddy, J. N. (1997). Mechanics of Laminated Composite Plates : Theory and Analysis. Boca Raton, CRC Press.

58. Reddy, J. N. (2004). Mechanics of Laminated Composite Plates and Shells : Theory and Analysis. Boca Raton, CRC Press.

59. Renji, K., P. S. Nair, et al. (1996). "Modal Density of Composite Honeycomb Sandwich Panels." Journal of Sound and Vibration **195**(5): 687-699.

60. Rostam-Abadi, F., C. M. Chen, et al. (2000). "Design Analysis of Composite Laminate Structures for Light-weight Armored Vehicle by Homogenization Method." Computers & Structures **76**: 319-335.
61. Sablik, M. J. (1982). "Coupling Loss Factors at a Beam L-Joint Revisited." Journal of the Acoustical Society of America **72**(4): 1285-1288.
62. Simmons, C. (1991). "Structure-Borne Sound-Transmission through Plate Junctions and Estimates of Sea Coupling Loss Factors Using the Finite-Element Method." Journal of Sound and Vibration **144**(2): 215-227.
63. Smith, P. W. (1962). "Response and Radiation of Structural Modes Excited by Sound." Journal of the Acoustical Society of America **34**(5): 640-650.
64. Steel, J. A. and R. J. M. Craik (1994). "Statistical Energy Analysis of Structure-Borne Sound-Transmission by Finite-Element Methods." Journal of Sound and Vibration **178**(4): 553-561.
65. Szecheny, E. (1971). "Modal Densities and Radiation Efficiencies of Unstiffened Cylinders Using Statistical Methods." Journal of Sound and Vibration **19**(1): 65-81.
66. Vaziri, R., X. Quan, et al. (1996). "Impact Analysis of Laminated Composite Plates and Shells by Super Finite Elements." International Journal of Impact Engineering **18**(7-8): 765-782.
67. Vlahopoulos, N., L. O. Garza-Rios, et al. (1999). "Numerical Implementation, Validation, and Marine Applications of an Energy Finite Element Formulation." Journal of Ship Research **43**(3): 143-156.

68. Vlahopoulos, N. and X. Zhao (1999). "Basic Development of Hybrid Finite Element Method for Midfrequency Structural Vibrations." AIAA Journal **37**(11): 1495-1505.

69. Vlahopoulos, N. and X. Zhao (2001). "An Investigation of Power Flow in the Mid-frequency Range for Systems of Co-linear Beams based on a Hybrid Finite Element Formulation." Journal of Sound and Vibration **242**(3): 445-473.

70. Vlahopoulos, N., X. Zhao, et al. (1999). "An Approach for Evaluating Power Transfer Coefficients for Spot-welded Joints in an Energy Finite Element Formulation." Journal of Sound and Vibration **220**(1): 135-154.

71. Whitney, J. M. and J. E. Ashton (1987). Structural Analysis of Laminated Anisotropic Plates. Lancaster, Pa., U.S.A., Technomic Pub. Co.

72. Wilkinson, J. P. (1968). "Modal Densities of Certain Shallow Structural Elements." Journal of the Acoustical Society of America **43**(2): 245-256.

73. Wohle, W., T. Beckmann, et al. (1981). "Coupling Loss Factors for Statistical Energy Analysis of Sound-Transmission at Rectangular Structural Slab Joints .1." Journal of Sound and Vibration **77**(3): 323-334.

74. Wohle, W., T. Beckmann, et al. (1981). "Coupling Loss Factors for Statistical Energy Analysis of Sound-Transmission at Rectangular Structural Slab Joints .2." Journal of Sound and Vibration **77**(3): 335-344.

75. Wohlever, J. C. (1988). Vibrational Power Flow Analysis of Rods and Beams. Mechanical Engineering Department. West Lafayette, Purdue University. Ph.D. Dissertation.

76. Wohlever, J. C. and R. J. Bernhard (1992). "Mechanical Energy-Flow Models of Rods and Beams." Journal of Sound and Vibration **153**(1): 1-19.

77. Wu, H. Y. T. and F. K. Chang (1989). "Transient Dynamic Analysis of Laminated Composite Plates subjected to Transverse Impact." Computers & Structures **31**(3): 453-466.

78. Zhang, W. G., N. Vlahopoulos, et al. (2005). "An Energy Finite Element Formulation for High-frequency Vibration Analysis of Externally Fluid-loaded Cylindrical Shells with Periodic Circumferential Stiffeners subjected to Axi-symmetric Excitation." Journal of Sound and Vibration **282**(3-5): 679-700.

79. Zhang, W. G., A. M. Wang, et al. (2003). "High-frequency Vibration Analysis of Thin Elastic Plates under Heavy Fluid Loading by an Energy Finite Element Formulation." Journal of Sound and Vibration **263**(1): 21-46.

80. Zhang, W. G., A. M. Wang, et al. (2005). "A Vibration Analysis of Stiffened Plates under Heavy Fluid Loading by an Energy Finite Element Analysis Formulation." Finite Elements in Analysis and Design **41**(11-12): 1056-1078.

81. Zhao, X. and N. Vlahopoulos (2000). "A Hybrid Finite Element Formulation for Mid-frequency Analysis of Systems with Excitation Applied on Short Members." Journal of Sound and Vibration **237**(2): 181-202.

82. Zhao, X. and N. Vlahopoulos (2004). "A Basic Hybrid Finite Element Formulation for Mid-frequency Analysis of Beams Connected at an Arbitrary Angle." Journal of Sound and Vibration **269**(1-2): 135-164.